Lateral organization of the transmembrane domain and cytoplasmic tail of influenza virus hemagglutinin revealed by time resolved imaging

Dissertation

zur Erlangung des akademischen Grades
doctor rerum naturalium
(Dr. rer. nat.)
in Fach Biologie

eingereicht an der
Mathematisch-Naturwissenschaftlichen Fakultät I
der Humboldt-Universität zu Berlin

von
Dottore in Biotecnologie
Silvia Scolari
geb. 12.05.1981 in Padova, Italien

Präsident der Humboldt-Universität zu Berlin
Prof. Dr. Dr. h.c. Christoph Markschies

Dekan der Mathematisch-Naturwissenschaftlichen Fakultät I
Prof. Dr. Lutz-Helmut Schön

Gutachter: 1. Prof. Andreas Herrmann
2. PD Michael Veit
3. Prof. Manuel Prieto

Tag der mündlichen Prüfung: 24.07.09

Alla mia famiglia

Zusammenfassung

Die Freisetzung vieler Hüllviren findet an der Plasmamembran (PM) statt. Der Viruspartikelzusammenbau hängt von der Anreicherung viraler Untereinheiten in spezifischen Domänen der PM ab. Es wird vorgeschlagen, dass Membran-Rafts – geordnete, Sphingomyelin- und Cholesterin-reiche Mikrodomänen in der PM – als lokale Rekrutierungsstellen dienen. Hämagglutinin (HA) ist ein homotrimeres Glykoprotein in der Hülle des Influenzavirus. Es vermittelt die Bindung an die Wirtszelle und die Fusion mit der endosomalen Membran. Es wird angenommen, dass HA eine wichtige Rolle bei der Abschnürung neuer Viruspartikel von der Zelle spielt. Zwei Hauptbeobachtungen führten zu der Hypothese, dass sich HA in Lipid-Mikrodomänen einlagert: HA wurde biochemisch in Detergens-resistenten Membranen nachgewiesen und die Virushülle ist mit Lipiden angereichert, die Rafts bilden. Um die Rolle der HA-Transmembrandomäne für die Lipid-Raft-Inkorporation aufzuklären, wurde ein Konstrukt entwickelt, das den C-Terminus von HA, mit dem gelb fluoreszierenden Protein YFP fusioniert, und die Transmembrandomäne, nicht aber die N-terminale Ektodomäne von HA enthält. In transfizierten Säugetierzellen wurde der Förster-Resonanz-Energie-Transfer (FRET) zwischen diesem Konstrukt und einem GPI-verankerten cyan fluoreszierenden Protein CFP (Raft-Marker) durch Fluoreszenz-Lebenszeit-Mikroskopie (FLIM) gemessen. Die Ergebnisse zeigen, dass sich HA-Konstrukte in Cholesterin-abhängigen Lipiddomänen anreichern, was durch eine erhöhte FRET-Effizienz nachgewiesen wurde. Zudem führen der Entzug von Cholesterin aus der PM und die Deletion der drei hochkonservierten Palmitylierungsstellen von HA zu einer signifikanten Verringerung der FRET-Effizienz. Schließlich wurde ein sehr stark verringerter Energietransfer zwischen dem HA-Konstrukt und einem Marker für Nicht-Raft-Bereiche gemessen. Darüber hinaus konnte mit Hilfe von ortsspezifischer Mutagenese gezeigt werden, dass die verwendeten HA-Konstrukte Disulfidbrücken-verbundene Oligomere bilden und dass dies eine Voraussetzung für den Transport der Konstrukte an die PM ist. Zeitaufgelöste Anisotropiemessungen ergaben für diese ein starkes Homo-FRET-Signal, welches für eine lokale Anhäufung spricht und somit die Oligomerisierungshypothese bestätigt.

Schlagwörter: Influenzavirus, Hämagglutinin, FLIM-FRET, Lipid Rafts, Zusammenbau.

Abstract

Numerous enveloped viruses bud from the host cell plasma membrane (PM). The assembly of the new viral particles depends on the accumulation of the viral subunits at specific sites of the cell membrane. Lipid domains or “rafts” enriched of sphingomyelin and cholesterol have been suggested as sites for local recruitment of viral components. Hemagglutinin (HA) is a homotrimeric glycoprotein embedded in the envelope of influenza virus. It mediates binding of the virus to the host cell as well as fusion between the viral envelope and the endosomal membrane. HA might play an important role in budding of the new viral particles from the host cell. Two main observations led to the suggestion that HA entraps in lipid microdomains. First, HA was rescued in DRM fractions, second the viral envelope was found to be enriched in lipids generally forming rafts.

To elucidate the role of the HA transmembrane domain in lipid raft localization we expressed constructs harboring the transmembrane domain and the cytoplasmic tail but lacking the N-terminal ectodomain of HA in the PM of mammalian cells (CHO-K1). We studied energy transfer (FRET) between these constructs and a GPI anchored CFP as a raft marker by fluorescence lifetime imaging microscopy (FLIM). Our results suggest that HA constructs are indeed sorted and enriched into cholesterol-dependent lipid domains indicated by enhanced FRET efficiency. This is supported by the observation that cholesterol depletion of the PM caused a significant decrease of FRET. Likewise, deletion of the three highly conserved palmitoylation sites of HA is also accompanied by a reduction of FRET efficiency. Finally, very low energy transfer was measured upon coexpression of the HA construct with a non-raft marker protein.

In addition, site directed mutagenesis demonstrated that TMD-HA constructs form disulfide linked oligomers and that oligomerization is a prerequisite for the transport to the plasma membrane. This result was corroborated by time resolved anisotropy measurements that revealed strong homoFRET between TMD-HA-YFP molecules, thus indicating protein clustering. Oligomerization of TMD-HA contructs is in agreement with the observation that the trimerization of full length HA is fundamental for the stability of the glycoprotein and the subsequent delivery of the protein to the cell surface.

Key Words: influenza virus, hemagglutinin, FLIM-FRET, lipid rafts, assembly.

Abbreviations

A	Alanin	HIV	Human immunodeficiency virus
C, Cys	Cystein	IRF	Instrument response function
CFP, mCFP	Cyan fluorescent protein, monomeric cyan fluorescent protein	K	Lysin
CHO-K1	Chinese hamster ovary	lo	Liquid ordered
CT	Cytoplasmic tail	ld	Liquid disordered
Cyt D	Cytochalasin D	K	Lysin
DAF	Decay accelerationg factor	LPH	Lactase phlorizin hydrolase
DRM	Detergent resistant membranes	mCer	Monomeric cerulean
DTT	Dithiothreitol	MDCK-II	Madin-Darby canine kidney
E	FRET efficiency	Myr	Myristoylation
EndoH	Endoglycosidase H	MβCD	Methyl-β-Cylodextrin
ER	Endoplasmic reticulum	NNT	Glycosylation site
FLIM	Fluorescence lifetime imaging microscopy	Pal	Palmitoylation
FPALM	Fluorescence photoactivation localization microscopy	Rw	Reverse primer
FRET	Förster resonance energy transfer	S	Serin
Fw	Forward primer	SEM	Standard error of the mean
GPI	Glycosylphosphatidylinositol	SFV	Semliki forest virus
GPMV	Giant plasma membrane vesicle	SD	Standard deviation
HA	Hemagglutinin	TCSPC	Time correlated single photon counting
HA_0	Hemagglutinin precursor	TMD	Transmembrane domain
HA_1, HA_2	Hemagglutinin subunits	YFP, mYFP	Yellow fluorescent protein, monomeric yellow fluorescent protein

Index

1 INTRODUCTION

Influenza is one of the most studied viruses with respect to its structure and pathogenicity. However whereas the mechanism of infection has been elucidated in details, the assembly of the new viral progeny still remains a controversial topic. Several studies suggested that cholesterol-enriched lipid microdomains or "rafts", might recruit viral subunits, e.g. the spike protein hemagglutinin (HA), at specific site of the plasma membrane. In this study FLIM-FRET and time resolved anisotropy measurements were employed to investigate *in vivo* the lateral organization of HA. Since these are not conventional techniques, our approach will be extensively elucidated in the following section.

1.1 Influenza Virus

Every 30 to 40 years an aggressive flu virus emerges, one that has changed just enough that people natural defences are caught totally unprepared. First worldwide pandemics of influenza were reported already in 1889 and 1898 but the largest outbreak occurred in 1918 (Spanish influenza), infecting 500 million people and killing about 40 millions. Extensive studies on tissues isolated from victims of the 1918 epidemic, demonstrated that this virus (H1N1) was an avian influenza virus, able to adapt itself enough to replicate in human cells. Indeed this virus had a high level of similarity to the first human influenza A virus isolated (A/WSN/33), placing the 1918 virus amongst the Influenza A swine or human viruses. Other pandemics have followed in 1957 and 1968. More recently, in 1997, an avian influenza A virus (H5N1) was recovered in the samples derived from victims of a small influenza episode in Hong Kong. This event raised not only the fear for a new mortal pandemic of influenza, but also evidenced the possibility that avian influenza viruses could break through the species barrier and infect humans [1].

Influenza is an enveloped virus that belongs to the family of *Orthomyxoviridae*. This family includes the three influenza subtypes, A, B and C and the Thogotovirus and Isavirus. The most studied and widespread among animal species is the Influenza A subtype, while Influenza B and C represent only a minor population of circulating viruses and normally cause very mild respiratory diseases. Influenza virus is highly pleiomorphic even if generally it presents a spherical shape with a diameter of about 100 nm. Influenza A and B contain eight single strands of RNA with negative polarity that encode all the proteins of the virus. Influenza C virus contains only seven ssRNAs. Ribonucleoproteins (RNPs) are helical-shaped complexes that comprise the genomic RNA segments in association with a trimeric polymerase (PB1, PB2 and PA subunits) and several copies of nucleoproteins (NP). NPs form a proteinaceous core around which the RNA is wrapped. Underlying the membrane is the matrix protein M1, the major structural component of the virion, which is thought to act as an adaptor between the lipid envelope and the internal RNP particles. Embedded into the envelope are three proteins, two glycoproteins, hemagglutinin (HA) and neuraminidase

(NA) involved in cell entry and exit, respectively, and a low abundance ion channel, the protein M2, involved in uncoating and HA maturation [2] (**Figure 1**). Whereas the internal components of the different influenza subtypes are very similar, the envelope presents a quite different composition. Indeed in the influenza C virus, the hemagglutinin-esterase-fusion glycoprotein (HEF) supersedes both HA and NA and an alternative form of the M2 ion channel, named CM2 [3], is present. In the influenza B virus this channel is substituted by the protein NB, a protein much smaller than M2 [4] but with the same function. Finally, the proteins NS1 and NS2 are produced by alternative splicing of the eight gene fragment. NS1 plays a critical role in mRNA splicing and translation, while NS2 mediates the export of newly synthesized RNPs from the nucleus [5,6].

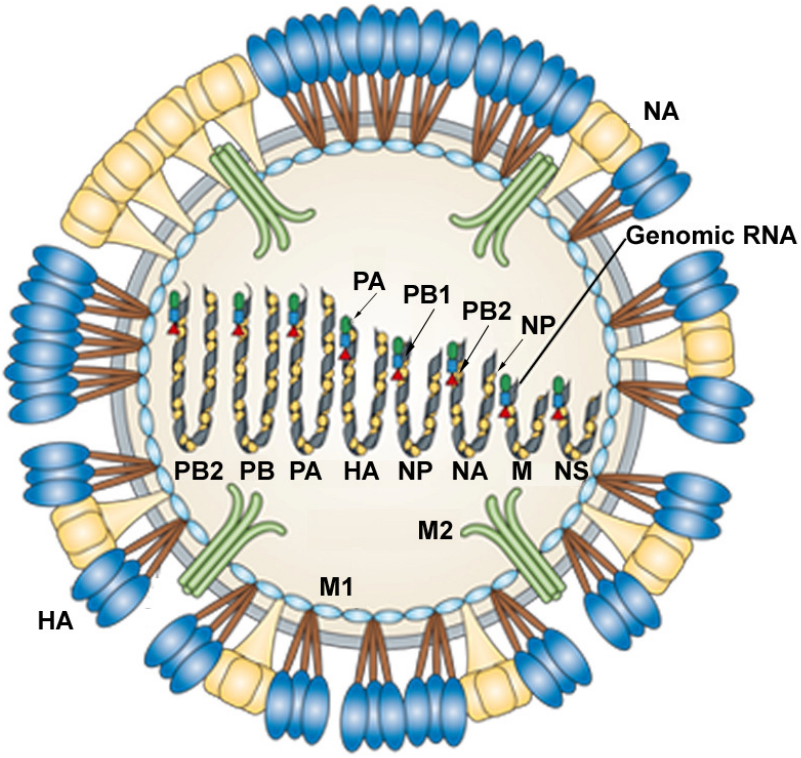

Figure 1: Influenza A virus structure. Influenza is an enveloped virus whose genome is constituted of 8 ssRNAs with negative polarity, encoding for all the viral proteins (indicated as PB2, PB, PA, HA, NP, N, M, NS).The RNA segments are complexed with the 3 subunits of a polymerase (PA, PB1 and PB2) and with nucleoproteins (NP) to form ribonucleoproteins (RNP). The proteins NS1 and NS2 are involved in mRNA splicing and in export of RNPs from the nucleus, respectively. Embedded into the envelope of the virus are two glycoproteins, hemagglutinin (HA) and neuraminidase (NA) and an ion channel, the protein M2. Finally, the protein M1 forms a proteinaceous shell under the envelope. Adapted from [7].

Influenza type A viruses are classified based on the antigenic properties of both the glycoproteins, HA and NA. In avian viruses 15 subtypes of HA and 9 subtypes of NA have been identified, of these viruses subtype H1, H2 and H3 infect humans. The amino acidic sequence can vary from 30 to 70% between different subtypes and up to 20% within the same subtype.

1.1.1 Influenza Virus replication

Influenza virus infections in humans are caused by inhalation of the aerolized virus in droplets. The inhaled viruses replicate in the respiratory epithelium and the new viral progeny buds into the airway lumen. Since the respiratory epithelium is polarized, entry of the virus as well as the release, takes place only at the apical membrane of the cells, precluding in this way the systemic spread of the virus [8]. The infection cycle begins with the receptor-mediated endocytosis of the virus, followed by the fusion between the endosomal and viral envelope (Figure 2). Both these events are accomplished by HA (see 1.1.3.3). The endosomal acidic environment is fundamental not only for triggering the fusion of the membranes, but the ionic flux into the viral envelope through the ion channel M2, allows also the disruption of the M1-vRNPs complexes. The viral genome is then imported into the nucleus through nuclear pores by dint of nuclear localization signals (NLS) localized on the NPs [9]. Both, NP and polymerase, accompany the RNA into the nucleus where they are essential for transcription and replication. The synthesis of positive-sense antigenomic RNAs (or cRNAs) and the subsequent transcription of the cRNAs into the gene segments (vRNAs), as well as the transcription into mRNAs are controlled by the three subunits of the polymerase [10]. Likewise eukaryotic mRNAs, the viral mRNA contains a 5' cap (a 7-methylguanosin added to the 5' and necessary for recognition by the ribosomes and protection from RNases) and the termination of the transcription is due to the presence of a poly-A signal (polyadenylation) [11]. New incapsidated vRNPs and mRNAs are then exported out of the nucleus. In the cytosol mRNA undergoes translation, while the viral genome migrates directly to the plasma membrane where assembly takes place. In particular, NP and M1 are produced in the cytosol whereas HA, NA and M2 are synthesized in the rough endoplasmic reticulum and transported to the cell surface via the Golgi apparatus.

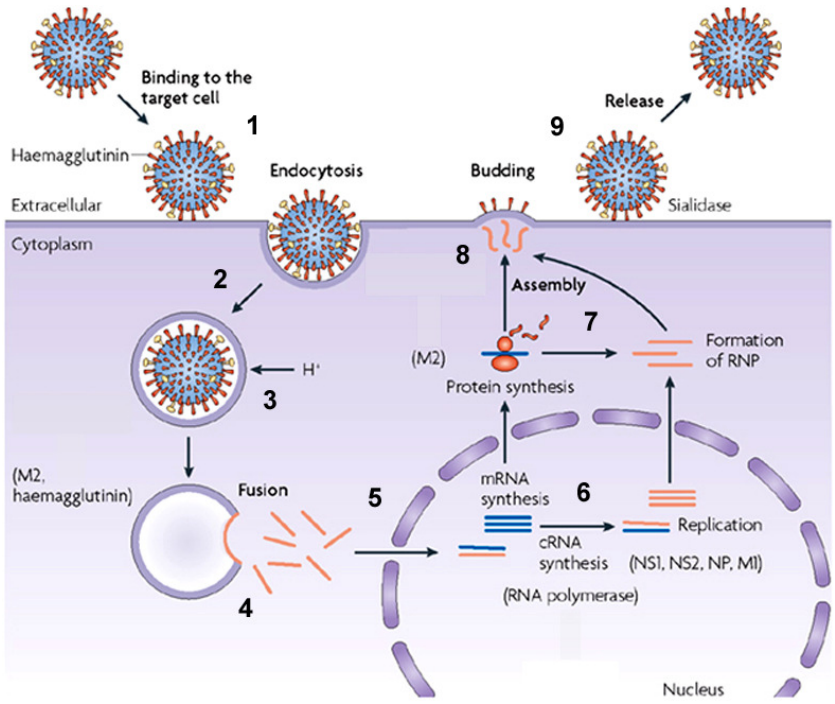

Figure 2: Influenza virus replication. The binding of influenza virus to the host cell (1) is mediated by the spike protein hemagglutinin (HA). The internalization of the virus occurs in endosomes (2) where, upon acidification (3), HA undergoes a conformational change which leads to the fusion between the viral envelope and the endosomal membrane (4). Thus the viral genome enters the nucleus (5) where it is both replicated and duplicated (6). Despite of HA, NA and M2, whose synthesis occurs in the ER, the other viral components are synthesized in the cytosol, where also RNPs are formed (7). The viral subunits accumulate at the budding site for the subsequent assembly and release of the new viral progeny (9). Adapted from [12].

1.1.2 The glycoprotein Neuraminidase

Neuraminidase is a homotetrameric glycoprotein forming mushroom-like projections on the surface of influenza virus. To date, nine antigenic subtypes of NA have been characterized. NA plays an important role in facilitating the spread of the viral infection since it cleaves the terminal sialic acid from different glycoconjugates, particularly abundant in the mucosal secretions. Therefore it helps the penetration of the virus into the respiratory epithelium. Furthermore, Neuraminidase assists the release of the new viral progeny avoiding the aggregation mediated by the interaction between hemagglutinin and sialic acid on the surface of the host cells and on the particle envelope (**Figure 7**) [13].

1.1.3 The glycoprotein Hemagglutinin

Fifteen different subtypes of Hemagglutinin, the most abundant spike protein on the virus surface, have been described. This cylindrical homotrimeric glycoprotein has a length of about 135 Å and a diameter varying between 35 and 70 Å [14]. The three identical monomers, each consisting of about 560 amino acids, are non-covalently linked and they are constituted of a globular head (HA_1, globular domain, **Figure 3**) connected to a stem-like domain (HA_2, fibrous domain, **Figure 3**) by

two disulfide bonds. HA_1 and HA_2 subunits originate upon proteolytical cleavage of the non-fusogenic precursor HA_0 (**Figure 4** A) [15].

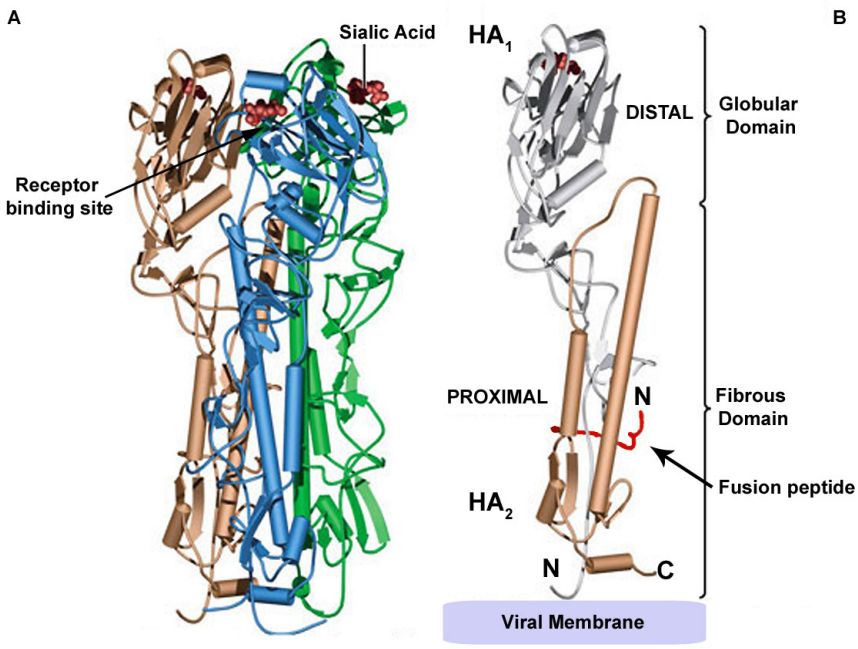

Figure 3: Hemagglutinin structure. Hemagglutinin is a homotrimeric glycoprotein formed of three identical monomers (A). Each monomer (B) is divided in two domains, HA1, the globular domain and HA2, the fibrous domain. HA1 and HA2 are connected by two disulfide bonds. In red the fusion peptide is indicated.

The cleavage of HA_0 is essential for triggering HA fusion properties, thus it determines the infectivity of the viral strain. In highly pathogenic avian influenza strains the cleavage site (**Figure 4** A) is constituted of several basic residues located in the linker between HA_1 and HA_2. These residues form the consensus sequence R-X-K/R-R (**Figure 4** B), which is recognized by intracellular proteases in a broad range of host cells [16]. In contrast, mammalian and apathogenic avian viruses present HA subtypes with only an arginine as cleavage site between the two HA subunits (**Figure 4** B). Due to this, few extracellular proteases, secreted by a restricted range of cells, are able to recognize the cleavage site of the HA_0 precursor. Therefore these viruses cause usually only local infections.

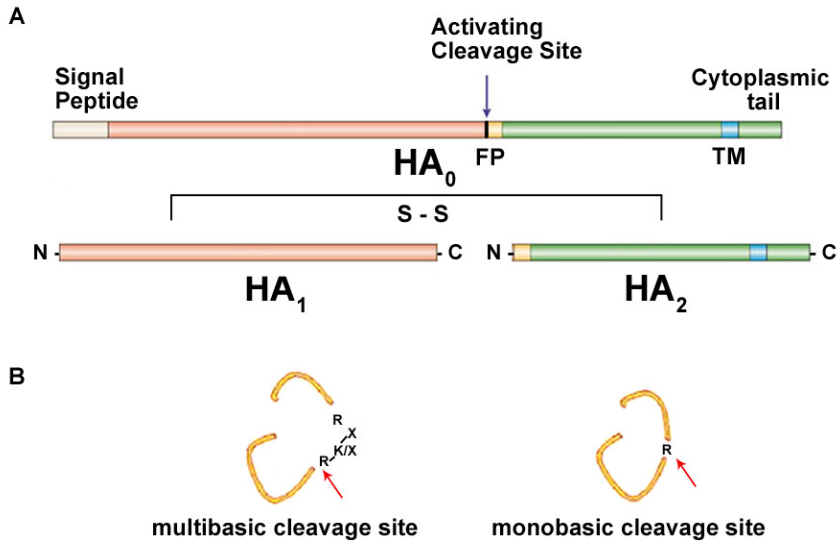

Figure 4: HA_0 cleavage. A) The cleavage of HA_0, the HA precursor, leads to the formation of the HA_1 and HA_2 subunits that remain disulfide linked. In this process the fusion peptide (FP in yellow) is also generated as N-terminus of the HA_2 subunit. TM indicates the transmembrane domain. B) Intracellular proteases responsible of the HA_0 cleavage recognize specific sequences, either consisting of few amino acids (left side) or of a single residue (right side).

The antigenic properties of HA reside into the HA_1 domain where the receptor binding site, formed by Tyr 98, His 183, Glu 190, Trp 153 and Leu 194, is localized (**Figure 3** A). These highly conserved amino acids build a pocket whose perimeter is surrounded by several other residues responsible for the antigenic variation of the protein. The globular head consists of about 340 residues and contains at the N-terminus a hydrophobic sequence referred to as signal peptide (**Figure 4**). This signal is necessary for the translation of the protein occurring on ER-bound ribosomes and it mediates the subsequent transfer of the polypeptide across the membrane [17]. About 220 amino acids form the HA_2 domain, the most highly conserved sequence in hemagglutinin. The proteolytical cleavage, by which HA_1 and HA_2 are separated, forms a new hydrophobic amino-terminus on the HA_2 subunit, the fusion peptide (**Figure 3** and **Figure 4** A). The transmembrane domain, anchoring the glycoprotein to the plasma membrane is also part of HA_2 (**Figure 5**). Finally the C-terminal cytoplasmic tail is about 11 amino acids long. Hemagglutinin undergoes extensive post-translational modifications during the transport through the Golgi apparatus to the plasma membrane, indeed despite of proteolytical cleavage, the protein becomes also glycosylated and palmitoylated. Glycosylation occurs at seven asparagine residues, four in the globular head and three localized in the stem region (see 1.1.3.1). Three cysteine residues (Cys-551, Cys-559 and Cys-562) are palmitoylated: two resides in the cytoplasmic tail and the third at the border between transmembrane domain and cytoplasmic tail (see 1.1.3.1).

Hemagglutinin plays a central role in virus entry since it recognizes the sialic acid residues covering the surface of the target cells. After internalization and acidification of the endosomes, HA

experiences a conformational change, which leads to the formation of the fusion peptide, essential for mediating the fusion between endosomal and viral membrane (see 1.1.3.3).

1.1.3.1 Folding, trimerization and transport of Hemagglutinin

The synthesis of HA takes place in the ER and the transport to the cell surface proceeds through the Golgi apparatus. The precursor HA_0 is synthesized on membrane-bound ribosomes and cotranslationally inserted into the ER where it is core glycosylated on five to seven sites and deprived of the signal peptide. Attachment of oligosaccharides to asparagine residues is important for promoting successive correct folding, maintenance of conformation and stability, protection against proteolysis or degradation and modulation of biological activities [18]. Three of these glycosylation sites, Asn-12, Asn-28 and Asn-478, localized in the stem region, are highly conserved and they act cooperatively to enhance the folding and trimerization rate. Loss of these carbohydrates affects stability, trimerization and transport of the protein [18,19]. Indeed oligomerization is a critical step, necessary for the transport of the glycoproteins from the ER to the Golgi complex [20]. During its transport through the Golgi apparatus to the cell surface, HA undergoes several posttranslational modifications including trimming of carbohydrate side chains and terminal glycosylation. Furthermore, in the H5 and H7 influenza virus subtypes, HA is proteolytically cleaved into the HA_1 and HA_2 subunits before integration into the plasma membrane [21], whereas tipically this cleavage takes place extracellularly by means of the protease CLARA [2]. Ester-bound fatty acids, in particular palmitic acid, are linked to the three cysteine residues localized in the HA transmembane domain and cytoplasmic tail (see 1.1.3). Palmitoylation occurs in the cis-Golgi and it is an irreversible post-translational modification [22]. Still, the role of palmitoylation has to be clarified; however it has been proposed that it might function as a signal for targeting HA to the cell surface. Furthermore, the insertion of these hydrocarbon chains into the membrane bilayer, it might be responsible of the HA association with lipid microdomains also named "rafts" (see 1.3) [23].

1.1.3.2 The Hemagglutinin anchor

The C-terminal peptide of Hemagglutinin, the transmembrane domain, is a predominantly hydrophobic peptide that anchors the glycoprotein to the membrane (**Figure 5**). This domain is probably α-helical and consists of 27 uncharged residues spanning the lipid bilayer. In particular, it has been reported that a 17 amino acid long transmembrane domain is strictly required in order for Hemagglutinin to mediate complete fusion [24]. Indeed, it has been demonstrated that HA mutants anchored to the plasma membrane by a lipid anchor spanning only the outer leaflet promote exclusively hemifusion. Thus, the transmembrane domain might function to stabilize the HA trimers surrounding the nascent fusion pore, or it might also be important in driving membrane hemifusion to full fusion [25]. Finally the transmembrane domain might stabilize the trimers interacting with

other transmembrane domains and it might also correctly orient the subunits in the membrane enhancing the stability of the final complex [20].

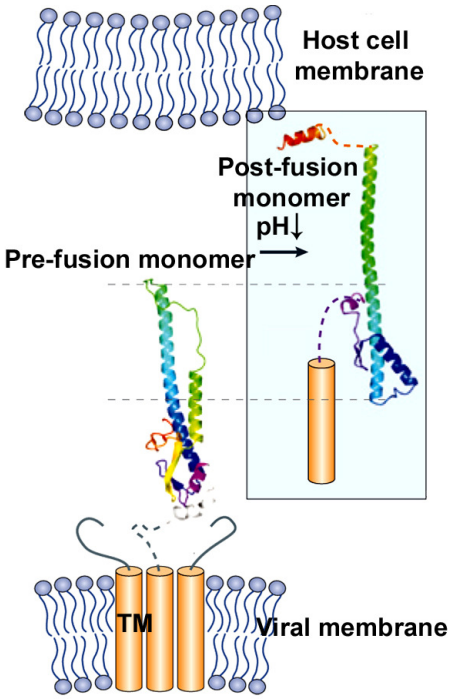

Figure 5: HA transmembrane domain. The HA transmembrane domain (TM) anchors the ectodomain spanning the viral envelope bilayer. Despite of mediating the binding to the host cell (pre-fusion conformation), the transmembrane domain cooperates with the fusion peptide (post-fusion conformation) to mediate fusion between the viral envelope and the endosomal membrane (see 1.1.3.3). Picture adapted from [26].

1.1.3.3 Hemagglutinin functions

An important determinant for influenza virus infection is the HA binding to the epithelial cells of the airway. Hemagglutinin interacts with glycoproteins and glycolipids containing oligosaccharides terminating in 5-N-acetyl-neuraminic acid (sialic acid) residues. Human influenza virus subtypes, whose HA contains a leucine at position 226, target preferentially sialic acid α-2,6-galactose β-1,4-*N*-acetyl glucosamine, avian and equine influenza viruses, having a glutamine at position 226, bind sialic acid α-2,3-galactose β-1,4-*N*-acetyl galactosamine, finally swine viruses appear to recognize both [27]. It has also been reported that in humans, where the influenza virus symptomatology is mainly confined to the respiratory tract, lung cells are abundant in α(2,6) linkage, while in pig intestine cells are enriched in α(2,3) linkages and influenza is normally associated to an enteric infection. The receptor binding site is a depression localized in the globular region at the top of the HA_1 subunit, formed by polar and non polar amino acids displaced to make direct contact with the receptors [28]. Mutation of specific amino acids surrounding the receptor binding site not only

influences the tropism and specificity of host infection, but might also contribute to the antigenic variation that is cause of new epidemics [15].

Besides receptor binding, Hemagglutinin is responsible for the fusion between viral and endosomal membranes (**Figure 6**). At neutral pH, HA is found to be in a metastable state, whose stability is maintained by electrostatic interactions between HA_1 and HA_2 monomers [29,30]. This conformation, referred to as native (**Figure 5**, pre-fusion monomer and **Figure 6**), is subjected to extensive changes upon acidification of the endosomal lumen to pH 5,5 (**Figure 5**, post-fusion monomer and **Figure 6**). In this form, the HA_2 subunit assumes the shape of a helical-hairpin structure, whose N-terminus, the fusion peptide, resembles a hook and it is buried within the coiled coil of the three HA_2 segments (**Figure 6** A) [31]. Due to acidification, the HA_1 subunit connected to HA_2 by a disulfide bond, dissociates from the top of the polypeptide and the fusion peptide is unleashed and boosted towards the target membrane where it inserts to promote fusion (**Figure 6** B) [31]. While the transmembrane α-helix spans the lipid bilayer almost perpendicular [32], the fusion peptide enters the target membrane with an oblique angle. The heptad-repeat regions (HR1 and HR2), linking the fusion peptide to the transmembrane domain, undertake an extensive refolding at acidic pH, forming a hairpin structure that brings the two membranes proximal (**Figure 6** A) [32]. The fusion is awaited by hemifusion [33], an intermediate step in which the lipids of the external leaflets of both, endosome and viral envelope, are pulled in proximity and bulged out due to the refolding and strong interactions between HR1 and HR2 (**Figure 6** C). In this process terminating with the coalescence of the two membranes, the TMD-homotrimer approaches the fusion peptide forming the TMD-FP complex (**Figure 6** C and D). In this way the FP is even more inserted into the membrane and destabilizes further the bilayer leading to the formation of a fusion pore and final fusion of the inner layers [32]. It has been proposed that clustering of at least six trimers is necessary to initiate fusion since their radial outward bending would force the interacting bilayers to bend as well [34]. Subsequently, the hemifusion diaphragm breaks due to the tension imposed by HA and the fusion pore opens irreversibly releasing the viral content into the cytoplasm [33].

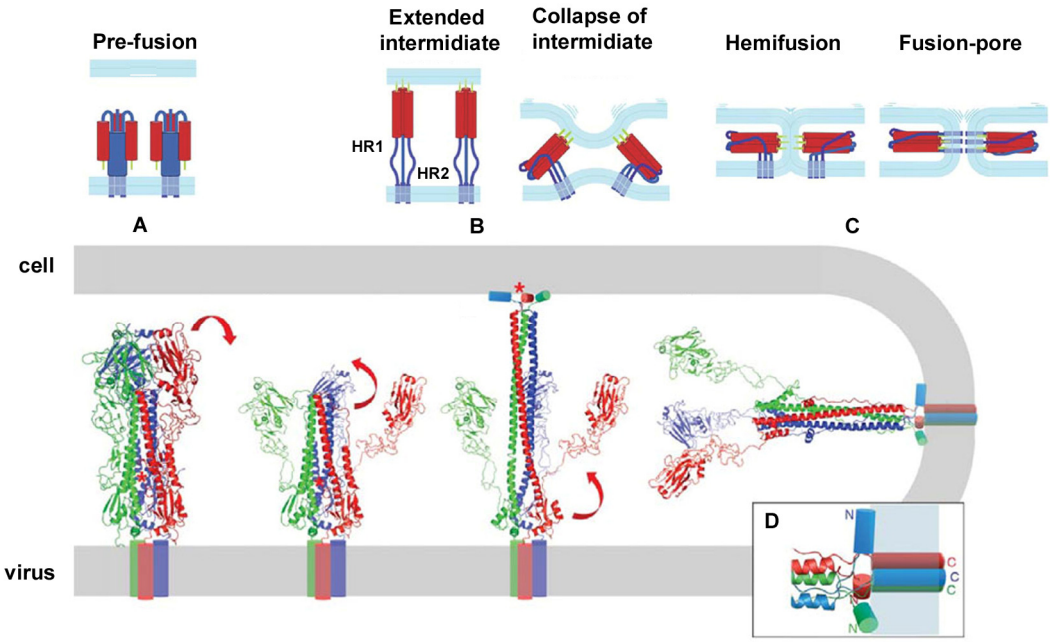

Figure 6: Fusion mechanism. In the pre-fusion conformation, the fusion peptide is buried within the three HA transmembrane domains (A). Upon endosomal acidification, HA undergoes an extensive rearrangement that leads to the insertion of the fusion peptide into the endosomal membrane bilayer (B). The heptad repeat regions HR1 and HR2 pull the two membranes together and mediate the hemifusion between the endosome and envelope external leaflets (C). This process terminates with the complete fusion of the apposing membranes and the generation of the fusion pore. This final step is due to the formation of the transmembrane domain-fusion pore (TMD-FP) complex (D). Adapted from [35].

1.1.3.4 Assembly and budding of influenza virus

After synthesis, all the viral components, namely, the envelope proteins HA, NA and M2, the matrix protein M1 and the viral genome, vRNPs, are delivered to the assembly site where they start interacting in order to form the new viral particles (**Figure 7**). Furthermore, viral proteins promote the outward bending of the plasma membrane, which terminates with the scission of the new viral progeny from the host plasma membrane and their release into the extracellular environment. The very first step in assembly is the delivery and accumulation of all the sub-viral constituents at the plasma membrane and specifically at the apical domain of the plasma membrane in polarized cells. The new synthesized genome, the vRNPs, is exported from the host nucleus via the Crm1-mediated nuclear export pathway [6,36,37], helped also by the viral proteins M1, NS1 and NP. However it still remains unclear how the vRNPs and M1 either together or separately reach the budding site. HA, NA and M2 posses different signals for the targeting to the apical membrane. A glycan attached to the ectodomain of both NA and HA has been identified as apical sorting determinant while the M2 sorting signal remains to be elucidated [18]. Furthermore, it has been demonstrated that the two glycoproteins interact with detergent resistant membranes (DRMs or lipid rafts, see 1.3) and that point mutations in the transmembrane domain or the deletion of the cytoplasmic tail resulted in

reduced raft affinity [38], thus it is likely that the determinant for lipid raft association is held into the transmembrane domain [39]. Still it remains controversial whether association of HA and NA with lipid microdomains occurs prior to the transport to the plasma membrane. However, there are evidences that the viral envelope is enriched of those lipids commonly found in lipid rafts [38,40] and since viral glycoproteins normally accumulate at the budding site, it has to be assumed that HA and NA determines the viral assembly and budding site. The role of lipid rafts in viral assembly and budding will be further discussed below. In order to produce infective and functional viral particles, eight (or seven) vRNAs need to be incorporated into the virions. One hypothesis suggests that vRNAs are randomly inserted given that viruses with more than eight genomic segments have been rescued [41]. Another hypothesis assumes that vRNAs contain specific structural features enabling the selective recruitment of the eight fragments into the nascent viral particles. Once accumulated, the viral envelope, the vRNPs and the protein M1 need to interact with each other. A major role in assembly is played by the matrix protein that not only forms a bridge between the envelope proteins and the vRNPs, thus associating with both of them, but it is also responsible for the recruitment of the viral components at the assembly site and it triggers the budding process. Indeed, mutant viruses lacking the protein M1 did not show any budding [42]. M1 might generate lipid asymmetry upon binding to the inner leaflet of the plasma membrane, therefore inducing outward bending of the membrane followed by bud formation. After assembly, bud formation and fission of the new particle from the plasma membrane, the virus employs NA for the complete release (**Figure 7**). Indeed this glycoprotein removes the sialic acid residues from the cell surface glycocalyx and from the glycoproteins of the viral particles, thus preventing self-aggregation and reattachment of the new progeny to the host cell [43].

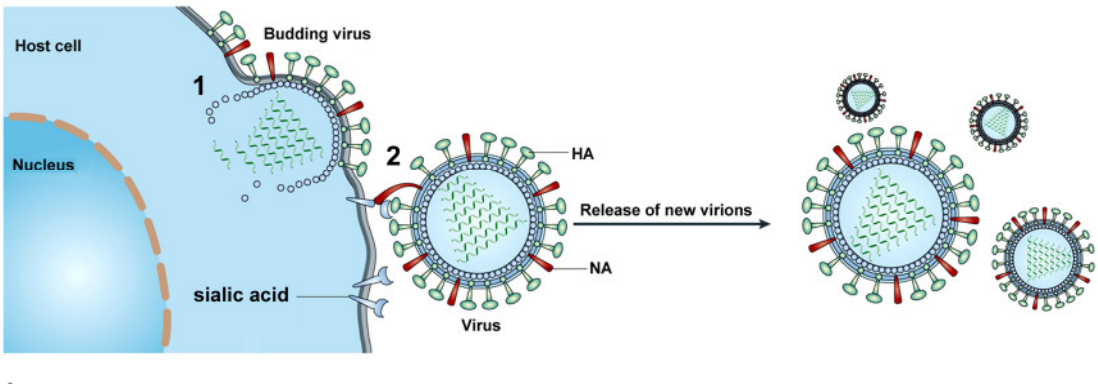

Figure 7: Influenza virus assembly and budding. The assembly of the new viral particles takes place at the plasma membrane of the host cell. The accumulation of the viral subunits promotes bending of the membrane and final budding of the viruses (1). The release of the virions is controlled by the glycoprotein neuraminidase (NA) that cleaves the sialic acid residues both from the particles and from the host cell (2). Thus NA prevents the self aggregation of the virions or even the attachment to the previous infected cell. Adapted from [44].

1.2 GPI Membrane anchors

Glycosylphosphatidylinositol anchors attach proteins to the external leaflet of the plasma membrane (**Figure 8** A). The addition of the GPI anchor to a protein is a posttranslational modification that occurs in the ER. GPI-anchored proteins display two signal sequences, one at the N-terminus, responsible of the targeting of the polypeptide to the ER and the second, the GPI signaling sequence (GSS) at the C-terminus, that directs the attachment of the GPI-anchor. In the ER, the transamidase enzyme complex (GPIT) recognizes those proteins containing the GPI signaling sequence and allows the attachment of the preformed GPI anchor to the C-terminus of the protein upon cleavage of GSS [45]. The mechanism is regulated by the translocon that discriminates between the stop transfer sequence of integral proteins and the GSS, which needs to be fully translocated into the lumen of the ER for recognition by the transamidase [46]. The new GPI-anchored proteins leave the ER in COPII coated vesicles, they travel through the *trans*-Golgi network and they are finally delivered to the plasma membrane. Normally GPI anchors are connected to the C-terminus of the protein (referred to as ω-residue) via a phosphoethanolamine group, followed by three mannose residues and a non-acetylated glucosamine attached to a phosphatidylinositol moiety, which interacts with the lipids of the plasma membrane through acyl or alkyl fatty acids, or ceramide residues (**Figure 8** B) [47].

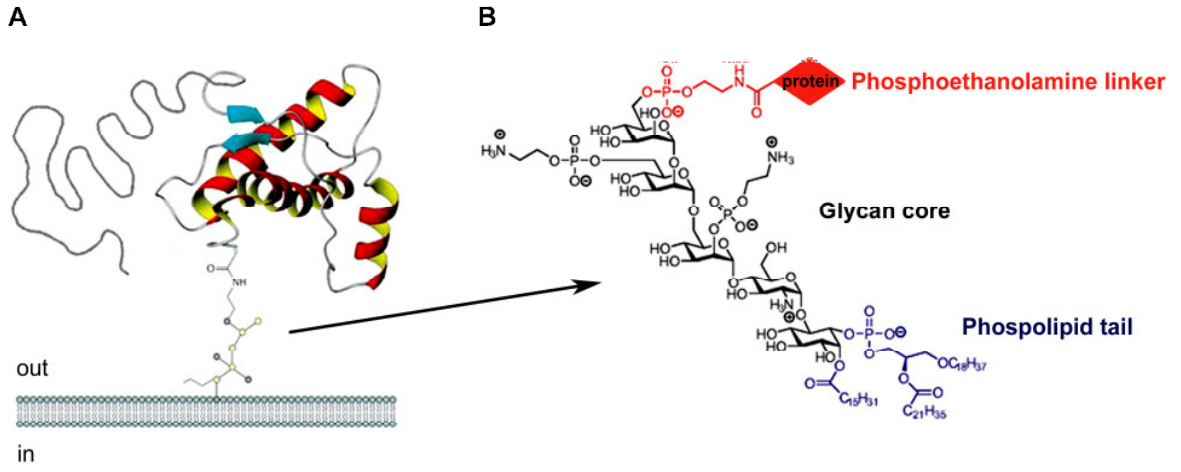

Figure 8: GPI-anchor structure. A wide variety of proteins are attached to the external leaflet of membranes through glycosylphosphatidylinositol (GPI)-anchors (A). A GPI-anchor is constituted of three main components, a phospholipid tail interacting with the lipids of the bilayer, a glycan core and a phosphoethanolamine that links the anchor to the protein C-terminus (B).

GPI-anchored proteins absolve many physiological functions, including transmembrane signalling, cell surface protection, cell adhesion and cell wall synthesis [45]. Examples of GPI-anchored proteins include hydrolases, like alkaline phosphatase, or 5´-Nucleotidase; cell surface receptors,

like the transferrin receptor, the folate receptor or CD14; complement regulatory proteins like the decay-accelerating factor DAF; cell adhesion proteins like NCAM or even prions like PrP^{C} or PrP^{Sc} [48]. The biosynthesis of the GPI-anchor occurring on the cytoplasmatic face of the ER, involves the action of about 20 proteins, whose exact mechanism has not been elucidated, yet [49]. In general, GPI-anchored proteins are apically sorted in several epithelial cell lines and they use their GPI anchor to associate with lipid microdomains or rafts (see 1.3). This association is probably due the saturated acyl chain of the GPI moiety that penetrate exclusively one leaflet of the membrane bilayer [50]. Since GPI-anchors can be extensively modified by the addition of phosphoethanolamine groups and other sugars to the phosphoinositol, glucosamine and mannose residues, it is likely that beside of a role in membrane attachment, apical sorting and lipid rafts partitioning, GPI-anchors might have many other biological and functional capabilities.

1.3 Lipid microdomains

In 1972 S. Jonathan Singer and Garth Nicholson proposed the "fluid mosaic model", a theory describing the biological membranes as a "sea" of lipids in which integral proteins are randomly distributed and move freely. Thus, the fluid mosaic model suggests that the lipid bilayer of biological membranes is simply a barrier between the extracellular environment and the cytosol or between the lumen of the different organelles and the cytoplasm. Therefore the role of membrane lipids was believed to be rather passive and aimed on acting just as a solvent for the embedded proteins [51]. However this simplistic model has been revised since not only a high variety of lipids constitute membranes, but lipids are also spatially organized and asymmetrically distributed within the two monolayers. Indeed cell membranes are formed by different amounts and kinds of lipids that define also their biological properties and functions [52]. Glycerolipids, sterols and sphingolipids are the most abundant lipids in biological membranes, distributed differently among the cellular membranes. As well as proteins, lipids can rapidly diffuse laterally in the plane of the membrane and they are also transported across the bilayer in a process named "flip-flop". Whereas diffusion is a spontaneous process, the latter is protein mediated. However no ATP is required in both mechanisms. Lipid flip-flop is a very slow movement since the polar head of the lipid needs to be translocated through the highly hydrophobic bilayer. Flippases (e.g. scramblases) might be responsible for the bidirectional lipid translocation across the membranes. Finally translocases use ATP hydrolysis to promote the unidirectional movement of lipids across the membranes. Tipically, aminophospholipid translocases and ABC transporters mediate the inward and outward translocation of phospholipids, respectively. In the plasma membrane of eukaryotic cells, almost all the glycerophospholipids such as phosphatidylinositol (PI), phosphatidylserine (PS) and phosphatidylethanolamine (PE) are predominantly localized in the inner leaflet, whereas lipids with large glycosylated headgroups such as sphingomyelin (SM) and phosphatidylcholine (PC), distribute

preferentially in the external leaflet. Finally, cholesterol has been described to be more abundant in the external leaflet since it has higher affinity for sphingolipids [53]. In 1988, Simons and van Meer [54] proposed that beside transverse lipid asymmetry, lipids might also present lateral asymmetry. This hypothesis arose from the observation that in epithelial cells apical and basolateral membranes have a different lipid composition and that proteins assigned to those two cell domains are selectively sorted. Indeed the redirection of the new glycoproteins either to the apical or to the basolateral membrane occurs in the trans-Golgi network, where also the synthesis of sphingolipids takes place. Therefore it was proposed that sorting of proteins and lipids might be correlated and that their transport to the cell surface might occur in common "carriers". These transporting vesicles may be formed by clustering of sphingolipids in the inner leaflet of the trans-Golgi network, followed by the association of the apical proteins. Vesicles destined to the basolateral domain might be the result of those membrane portions excluded from apical transport [54]. In agreement with this model, it has been reported that GPI-anchored proteins use their glycophospholipid anchor as an apical sorting signal [50]. These lipid domains, functioning as potential sorting centres, have been named microdomains or "membrane rafts" (**Figure 9**).

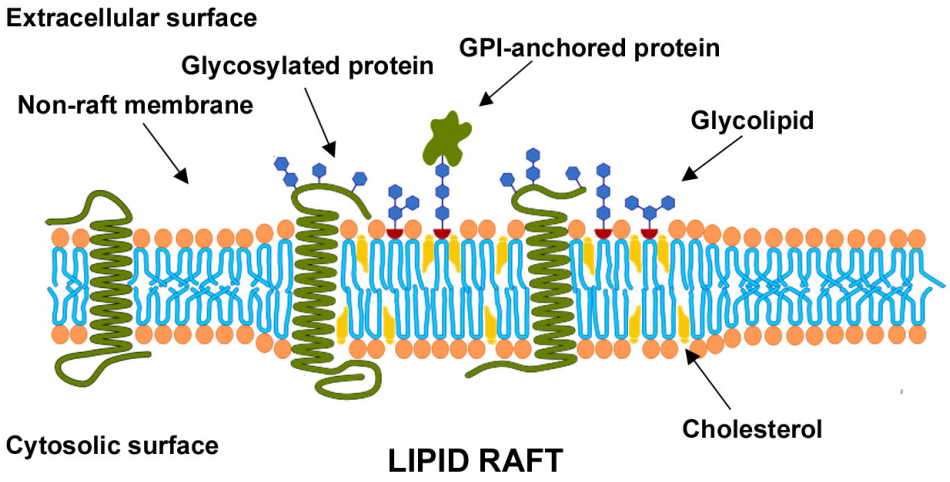

Figure 9: Lipid microdomains. In biological membranes saturated phospholipids, glycerosphingolipids and cholesterol are organized in small domains defined as "lipid rafts". The saturated acyl chain of these lipids, together with the presence of cholesterol is responsible not only of the high packaging of rafts, but it also increases the thickness of the lipid bilayer, with respect to the rest of the membrane. GPI-anchored proteins are in general enriched in those domains, but many other kind of transmembrane proteins (such as glycosylated proteins) have beend described to localize into rafts.

According to Simons and Ikonen [55], membrane raft organization is determined by the lateral association of sphingolipids and saturated PC, whose head groups exposed to the external environment interact rather weakly with each other, whereas the long saturated acyl chains forming the core of the bilayer are highly extended and more packed. Cholesterol functions as filler occupying the spaces between the sphingolipids. These highly packed domains are surrounded by

the more fluid regions formed by unsaturated phospholipids. Thus, membrane microdomains are defined as "small (10-200 nm), heterogeneous, highly dynamic, sterol- and sphingolipid-enriched domains that compartmentalize cellular processes. Small rafts can sometimes be stabilized to form larger platforms through protein-protein and protein-lipid interactions" [56]. Rafts have been reported to exist in both of the leaflets of the plasma membrane [57]; however since the two layers of the membrane are formed of different lipids, rafts in the inner and outer layer might differ not only in their composition but also in size and lifetime. Microdomains in the external leaflet are supposed to be small and very unstable, showing a very short lifetime; nevertheless they might merge in a bigger and more stable domain upon cell activation. Indeed, constitutive raft residents such as GPI-anchored proteins or transmembrane proteins might induce coalescence of unstable domains leading to the formation of a more lasting platform. This process might also trigger the recruitment of smaller rafts localized in the inner leaflet of the membrane. Anyway whether these microdomains are symmetrically distributed in the two leaflets still remains unclear [58,59]. Rafts are often considered to belong to the so called liquid ordered domains (lo), extensively characterized in model membranes [60,61,62]. Liquid ordered domains display properties normally associated to both the solid, gel (so) state and to the fluid, liquid disordered (ld) state. Indeed, on one side the tight packaging of the long stretched acyl chains resembles the behaviour of so, on the other, lateral diffusion of molecules in the lo state is as rapid as in ld. This intermediate state is due to the high amount of cholesterol in lo domains. Cholesterol induces higher compacting of the lipid acyl chains leading also to an increase bilayer thickness but at the same time allows the free movement of the lipids in the domain [63,64].

How the plasma membrane maintains its lateral organization still remains unclear. However it has been reported that the actin cytoskeleton might play a role in modulating this organization [65]. Actin filaments might either directly interact with lipid complexes or they could induce transient confinement of proteins and their subsequent clustering in response to extracellular signals [66]. The formation of such platforms has been proposed to play a central role in signal transduction. Indeed the coalescence of small rafts carrying specific proteins might create a suitable environment that would facilitate the action of kinases or phosphatases resulting in downstream signalling. The IgE signalling during an allergic immune response is only one of the many signalling pathways involving microdomains [67]. Rafts might also serve as carriers for proteins destined to the apical membrane in epithelial cells (see above and [55]), or they might be involved in the transport of proteins in the endocytotic pathway [68]. Finally, lipid rafts are apparently associated with viral infection [45]. Influenza as well as HIV virus engages lipid rafts during entry and budding. It has been reported that influenza virus buds from specific sites of apical membrane enriched in raft lipids. Furthermore the influenza virus envelope is constituted of lipids typically localized in lipid rafts

[40]. HIV virus uses lipid microdomains during entry and exit from the host cells and its envelope is enriched in raft lipids [69].

Caveolae represent perhaps the only tangible example of structurally defined domains isolated from biological membranes. These microdomains are composed mainly of sphingomyelin, glycosphyingolipids and cholesterol, they are resistant to extraction in cold, non-ionic detergent and they colocalize with the light-density fractions upon sucrose gradient centrifugation. Caveolae are mainly found in the endothelial cell plasma membrane, forming invaginations about 55 nm large and they are associated to the cytoplasmic surface through the interaction with caveolin -1 and -2. As well as membrane microdomains, caveolae might be involved in signalling or transport processes [70].

1.3.1 Methods for detecting membrane microdomains

Pioneering experiments demonstrating the existence of microdomains and microdomain-associated proteins were based on the insolubility of raft lipids and proteins in non-ionic detergents (typically, 1% Triton X-100 at 4 °C). This approach generated low-density detergent resistant membranes (DRMs), which were considered to resemble the lo phases in model membranes as well as potential lo-like domains in biological membranes [64]. Together with GPI-anchored proteins, influenza virus HA was one of the first proteins rescued in DRMs [71]. However, since the employment of such detergents is rather aggressive, the aggregation of lipids and proteins in the resulting DRM might be forced, therefore producing artefacts not reflecting the real lateral organization of the membrane [72,73]. Thus, since conventional optical microscopy has failed to visualize such small and dynamic domains, new approaches aimed at proving the existence of membrane microdomains *in vivo* have emerged. Lateral diffusion measurements using single particle tracking (SPT) demonstrated the formation of large lipid rafts upon cross-linking of GPI-anchored proteins [74], or even that lipids can be confined for an average of 11 ms in 230 nm compartments [74]. Fluorescence correlation spectroscopy (FCS) revealed that cholesterol-sensitive microdomains and the cytoskeleton meshwork regulate the dynamic compartmentalization of raft markers [65,75]; finally the combination of homo- and hetero-FRET (Förster Resonance Energy Transfer) microscopy provided the evidence that GPI-anchored proteins exist in extremely small cholesterol-sensitive structures that consist of only few molecules [76,77]. Therefore, FRET measurements, sensitive to distances between molecules in the order of few nanometers, seem to be very suitable for studying the lateral organzation of biological membranes *in vivo*.

1.4 Time resolved fluorescence spectroscopy

Fluorescence spectroscopy, which includes steady-state and time-resolved measurements, is a technique widely used to study dynamic processes *in vivo*. In steady state experiments the emission intensity of the probe is measured upon excitation with a continuous light source. In contrast, for time resolved measurements pulsed light, having a pulse width smaller than the decay time of the probe, is employed to record the intensity decay of the fluorophore. The relationship between the steady state fluorescence intensity (I) and the time decay of a molecule ($I_0e^{-t/\tau}$) is described by the equation [78]:

$$I = \int_0^\infty I_0 e^{-t/\tau} dt$$

It is clear, that the steady state intensity, being the integral over the time of the decay, represents simply an averaged intensity over all fluorophores of the sample at all times, thus neglecting important information which arose from the intensity decay and accessible to time-resolved measurements. Indeed, macromolecules immersed in a heterogeneous environment, e.g. a membrane, generally exist in different conformations. Upon excitation, fluorescent molecules might display intensity decays more complex than single exponentials depending on conformation states or/and on the environment of the molecule itself. Time resolved measurements can reveal the existence of these different decays allowing retrieving information not available from simple steady state measurements. Furthermore, time resolved measurements are independent from the excitation intensity, the local concentration of the fluorophore and from light scattering, but they are highly sensitive to changes in the local environment, changes in pH or temperature and calcium concentration [78,79]. Due to these advantages time-resolved are preferred over steady-state measurements. The lifetime or decay time of a fluorophore is described as the average time a fluorophore remains in the excited state prior to return to the ground state. For a single exponential decay this average time would be the same as the lifetime. However in a sample containing fluorophores the lifetime is not always equal to the decay time of every single molecule. Indeed fluorophores having different conformations or sensing different environments can emit either with shorter or longer lifetimes than the calculated one. Therefore it is important to underline that since the physical meaning of the different exponentials forming a decay is not easy to interpret, the measured lifetime of a sample is simply a statistical average of lifetimes due to different decays.

This mean or average lifetime, is described as

$$<\tau>=\frac{\left(\sum_i \alpha_i \tau_i^2\right)}{\left(\sum_i \alpha_i \tau_i\right)}$$

Where τ_i is the lifetime of the component i and α_i represents the normalized pre-exponential relative to the fraction of molecules showing the decay time i. However in cases in which lifetimes are used to describe phenomena dependent on the steady state intensity (e.g. FRET, see 1.4.1), the so called amplitude weighted lifetime ($\bar{\tau}$), described in the reported equation, should be used [80].

$$\bar{\tau} = \sum_i \alpha_i \tau_i$$

Time resolved fluorescence measurements are carried out in the time domain using the time correlated single photon counting (TCSPC) technique. Briefly, in TCSPC the sample is excited with a pulse of light and the first emitted photon is measured. Only one photon for about 100 laser pulses is detected, hence in order to acquire a number of photons enough for drawing a reliable histogram of the arrival times, the procedure has to be repeated many times [80].

1.4.1 Förster resonance energy transfer (FRET)

FRET, named after Theodor Förster, who first described the phenomena in 1946, is a process involving the radiationless transfer of energy from a fluorophore to another neighbouring fluorophore [78]. In order for FRET, or more precisely hetero-FRET, to occur the emission spectrum of the transferring fluorophore, named donor, must significantly overlap the excitation spectrum of the other fluorophore, referred to as acceptor, which does not need necessarily to be fluorescent. Furthermore, the emission dipole of the donor and the excitation dipole of the acceptor should not be perpendicular to each other since this would result in the mutual avoidance of the donor emission- and the acceptor excitation- oscillating dipoles. The last critical factor is the distance between the two fluorophores, which has to be in the order of less than 10 nm (about 100 Å). Energy transfer (E) depends on to the sixth power of the distance r between the two fluorophores as shown in the equation below (**Figure 10**).

$$E = \frac{R_0^6}{R_0^6 + r^6}$$

where R_0 is the Förster distance defined as the distance at which energy transfer equal 50%, and r is the distance between the two molecules [81]. The efficiency E represents the number of photons absorbed by the donor and transferred to the acceptor.

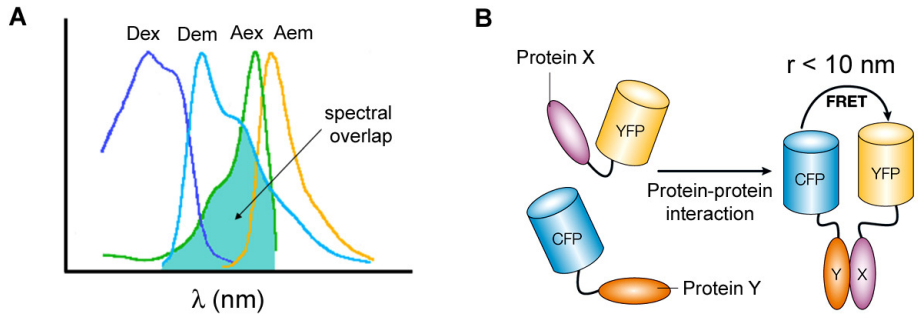

Figure 10: FRET principle. For Förster resonance energy transfer to occur, three parameters have to be fulfilled. A) The emission spectrum (Dem) of the donor should overlap significantly the excitation spectra (Aex) of the acceptor. B) The distance between the two fluorophores has to be in the order of 10 nm. Finally the donor emission and the acceptor excitation dipoles should be in a favourable conformation.

The fact that FRET can reveal distances in the order of a few nanometers, made this technique one of the most powerful tools to investigate unknown interactions between proteins as well as conformational changes of the proteins or of the surrounding environment. Hence, through calculating the distance between proximal molecules it is possible to obtain spatial and structural information otherwise inaccessible. This is why FRET is also defined as "spectroscopic ruler" [78].

Since energy transfer affects different properties of the fluorophores participating in the phenomena, different methods for detecting FRET have been developed. Steady state fluorescence emission methods are used to measure donor intensity quenching, acceptor sensitized emission, increased donor fluorescence emission, anisotropy or depolarization of sensitized acceptor emission. Time resolved methods measure the reduction of donor lifetime in presence of acceptor [82]. One of the biggest problems faced in steady state fluorescence measurements, with respect to FRET, is the spectral bleed through (SBT) of the donor emission spectrum that can contaminate the FRET signal. In particular, since the overlapping of donor emission and acceptor excitation spectra is strictly required for FRET, the acceptor might be directly excited by the donor excitation wavelength, leading to signal contamination. Furthermore, acceptor-photobleaching experiments, in which the complete bleaching of the acceptor is required, might lead to an underestimation or even to neglecting low FRET efficiencies due to partial bleaching of the donor. Measuring FRET by detecting the shortening in the donor lifetime is neither affected by SBT nor by belaching, therefore this technique is widely used for studying protein-protein interactions *in vivo* [83].

Energy transfer occurs also between identical flurorophores, so called homo-FRET or energy migration resonance energy transfer. Anisotropy measurements allow the detection of homoFRET,

which unlike heteroFRET does not affect the lifetime of the fluorophores [84]. The theory of anisotropy is discussed below in details (see 1.4.3 and 1.4.4).

1.4.2 Fluorescence Lifetime Imaging FRET Microscopy (FLIM-FRET)

Fluorescence Lifetime Imaging Microscopy (FLIM) combines the advantages of the time resolved technique with advanced microscopy, providing information in high spatial (nanometers) and temporal (nanosecond) resolution. Typically, in a FLIM-FRET experiment the lifetime of the donor is measured in presence and in absence of the acceptor. Energy transfer from the donor to the acceptor results in a faster decay of the donor, hence in a decrease of its lifetime. The efficiency of energy transfer is calculated as

$$E = 1 - \frac{\tau_{DA}}{\tau_D}$$

where τ_{DA} and τ_D are the lifetimes of the donor measured in presence or in absence of acceptor, respectively [78].

Donor lifetimes obtained from FLIM-FRET measurements are usually a mixture of quenched donors, i.e. FRET donors, and unquenched donors or non-FRET donors. In principle one might be able to distinguish between those two donor populations using a multicomponent analysis, in order to precisely calculate distances between molecules based only on the FRET donors. However when FRET efficiencies are low and differences in lifetimes are not very big, this kind of analysis is rather difficult. Therefore FRET efficiency calculated without distinguishing between quenched and unquenched donors should be referred to as apparent FRET efficiency, since it is due to the contribution of both donor populations [79].

1.4.3 Steady-State Anisotropy

Fluorescence anisotropy is a very sensitive biophysical approach to assess important characteristics of a biological sample such as the size and shape of proteins, the effect of the environment on the mobility and diffusion, the flexibility and wobbling or even the physical properties of the surrounding milieu. This technique is based on the physical principle describing that upon excitation a fluorophore absorbs preferentially those photons showing electric vector parallel to its absorption transition dipole. Therefore when a sample is excited with a polarized source, only a portion of the total fluorophores absorbs the energy, resulting in an oriented or polarized emission. This phenomenon is called photoselection and includes fluorophores either precisely or only partially aligned with the excitation dipole. Usually, samples are excited with vertically polarized light along

the *z*-axis (**Figure 11** A, assuming *z*-axis symmetry) and the anisotropy (r) of a sample is calculated as:

$$r = \frac{I_{VV} - I_{VH}}{I_{VV} + 2I_{VH}}$$

where I_{VV} and I_{VH} are the fluorescence intensities of the parallel and horizontally polarized emission [78].

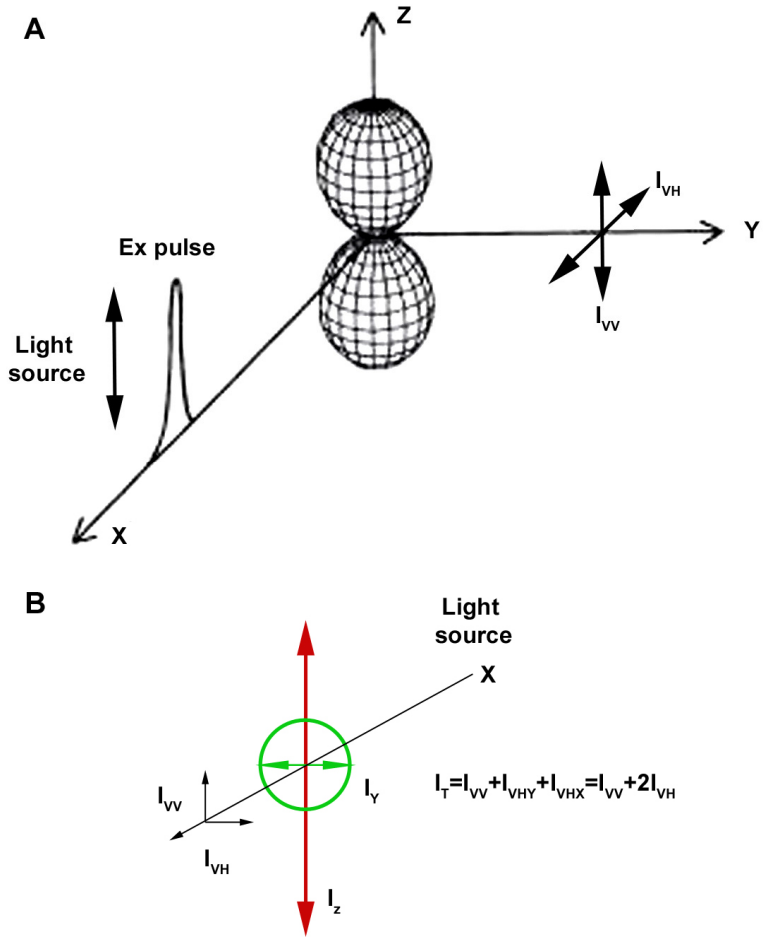

Figure 11: Dipole formation upon excitation along the vertical or z-axis. When a sample is excited with vertically polarized light (along the z-axis), the emission is also polarized. However the polarization of the emission is not exactly the same as the one of the incident source since molecules are not fixed in the environment, but they rotate (A). The polarized emission is measured along the z-axis (IVV) and along the perpendicular axes, x and y (IVHX and IVHY). The polarization is symmetrical along the y- and x- axes therefore they are considered to be equivalent (B). IT = total intensity; IVV = vertically polarized intensity; IVH = horizontally polarized intensity; IVHY = horizontally polarized intensity along the y-axis; IVHX = horizontally polarized intensity along the x-axis.

Parallel and horizontal emissions are measured through a polarizer. The anisotropy is strictly dependent on the total intensity (I_T) of the sample, since the difference I_{VV}-I_{VH} is normalized to this parameter. I_T is calculated as the sum of the vertical emission intensity, along the *z*-axis (I_{VV}) with

the horizontal intensity emissions along the *x*- and *y*-axis (I_{VHX} and I_{VHY}), considered to be equivalent (**Figure 11** B) [78].

$$I_T = I_{VV} + I_{VH_x} + I_{VHy} = I_{VV} + 2I_{VH}$$

When absorption and emission moments are parallel and the system is in absence of depolarization processes (e.g. rotational diffusion or energy transfer, see below), the fundamental anisotropy (r_0) of a molecule is 0,4. On the contrary when the fluorophore is randomly distributed in solution and totally depolarized, the calculated anisotropy is -0,2. However biological samples are not immobile and fluorophores immersed in such an environment are free to move. In other terms, the particular orientation presented by a molecule at the moment of excitation can change during the time in which the molecule remains in the excited state. The extent of orientation rearrangement is determined by the rotational diffusion (ϕ) of the molecule. Therefore, anisotropy (r) describes the rotation of a molecule during the excited state, i.e. it unveils the average angular displacement occurring between the excitation and the emission of a fluorophore. Hence, the rotational diffusion is one of the most critical parameters lowering the maximal theoretical anisotropy value of a molecule. When the rotational diffusion time of a flurophore is much faster than its decay time ($\phi >> \tau$), the molecule can rotate several times while remaining in the excited state, resulting in an almost randomly oriented fluorescence emission and thus in an anisotropy value close to 0. Thus, the anisotropy (r) of a molecule is strictly related to its lifetime as shown by the Perrin equation:

$$r = \frac{r_0}{1 - (\tau / \phi)}$$

where r_0 indicates the fundamental anisotropy of the molecule that would be measured in absence of any rotational diffusion, τ is the lifetime of the molecule and ϕ the rotational correlation time relative to the diffusion process [78]. On the other hand, if the rotational correlation time is much longer than the lifetime of the fluorophore r is equal to r_0.

The rotational correlation time ϕ can be used to determine the steric organization of a protein. Considering a protein in its monomeric conformation it is easy to determine changes in its oligomerization state since this would be reflected in fluctuations of the rotational correlation time. Indeed a protein forming a dimer or complexed with other proteins would displace a higher rotational correlation time, indicating a slower motion. Furthermore modifications of the viscosity of the medium, or the proximity to a membrane can affect the behaviour of a protein and thus its rotational rate.

For a sphere ϕ is described as

$$\phi = \frac{\eta V}{RT}$$

where η is the viscosity, V the molecular volume, R is the gas constant and T the temperature [78]. Another mechanism influencing the anisotropy of a sample is energy transfer. Indeed FRET between proximal like-fluorophores results in the depolarization of the fluorophore emission, i.e. depolarization due to homotransfer (see 1.4.4). Finally, light scattering represents also a critical factor affecting anisotropy. For example in a biological sample containing membranes, the fluorescence intensity should be high enough to overcome the scattered light coming from the lipid content. Indeed light scattering might increase the anisotropy even to values greater than 0,4, thus producing disturbing artefacts. As for steady-state intensity measurements, also in steady-state anisotropy measurements important information are neglected due to the averaging process of the anisotropy decay over the intensity decay. Due to this, time-dependent anisotropy decay measurements are preferable when studying the behaviour of molecules in the space.

1.4.4 Time resolved anisotropy decays

When a sample is continuously excited with vertically polarized light, steady state anisotropy is measured. Anisotropy is also described as the sum of the time dependent decays of the polarized components. The time-resolved decay of anisotropy r(t) for a spherical molecule is calculated as

$$r(t) = r_0 e^{-t/\phi}$$

where r_0 is the anisotropy at time t = 0 and ϕ the rotational correlation time [78]. Since the form of the anisotropy decay is determined by the size, shape and flexibility of the fluorophore as well as by the characteristics of the environment in which it resides, much information can be obtained by analyzing these decays. However, biological samples are not simply spherical entities, free to rotate in water, in contrast they show multiexponential decays, whose components arise not only from the rotation of the molecule along the different axes, but they are also the result of phenomena like homotransfer or due to the proximity of the fluorophore to a membrane. In this regard, the anisotropy of proteins bound to membranes never decays completely to zero since the presence of the bilayer averts a free and fast (in the order of ns) rotation of the molecule. For a multiexponential decay the anisotropy is given by:

$$r(t) = \sum_j r_{0j} e^{-t/\phi j}$$

where r_{0j} are the fractional anisotropies that decay with correlation times ϕ_j [78]. In **Figure 12** B the decay curve relatives to a bi-exponential decay is shown. The decay curve is the result of the two decays, one faster and the second slower. These two components can be then associated to properties of the protein under study, e.g. in the case of a dimeric protein carrying two identical fluorophores in conditions of homotransfer (**Figure 12** A). In this case the fast rotational correlation time (ϕ_1) could be related to the extent of homotransfer between the fluorophores (i.e. the lower the value, the higher the proximity), whereas the slow component (ϕ_2) could be associated to the wobbling of the fluorophores in the medium [85]. In general, rapid segmental motions are associated with an initial rapid decrease in anisotropy decay, followed by the slower anisotropy decay at longer times, due to overall rotational diffusion.

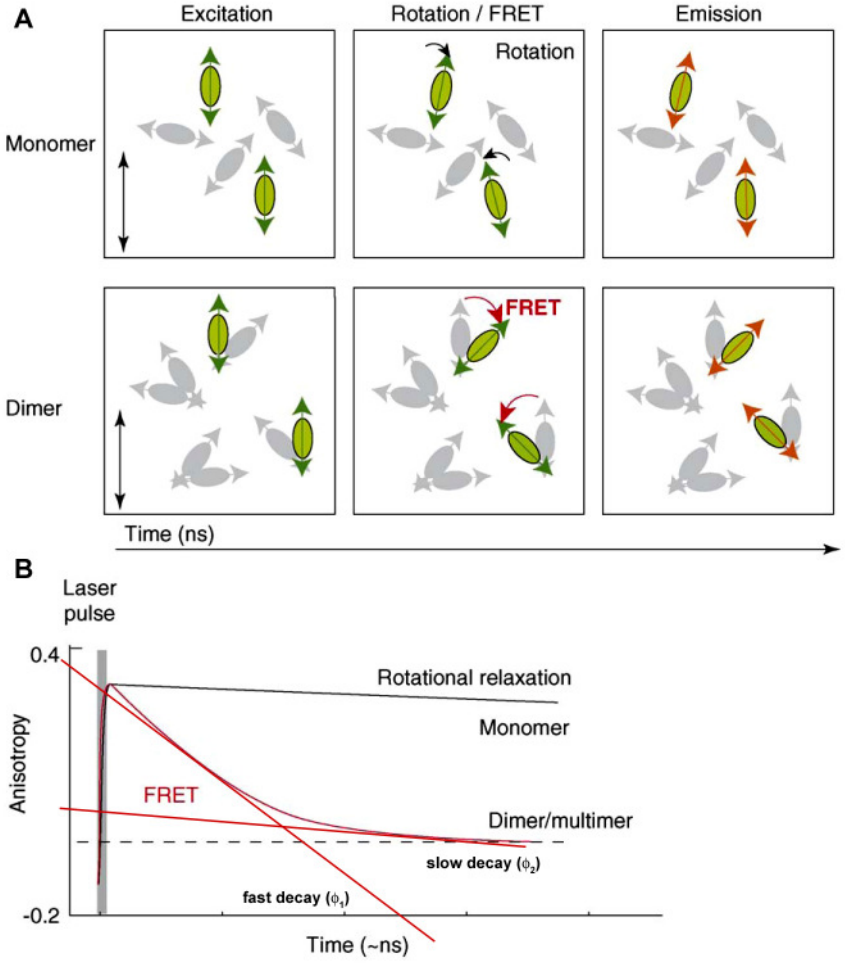

Figure 12: homoFRET detection by time resolved anisotropy. In absence of homoFRET, the excitation and emission polarization of a sample (hypothetically containing only monomers of a protein) excited with vertically polarized light are more or less parallel since the rotational correlation time (ϕ) is longer than the decay time (A, upper panels and B, monomer). In case in which in the samples dimers or oligomers are formed, energy transfer causes a decrease of anisotropy values or loss of polarization (A, lower panels and B, dimer/multimer). The anisotropy decay in case of FRET is the result of two decays, a short decay due to energy transfer and a long decay due to the wobbling of the fluorophores in the medium (B). Adapted from [84].

2 AIM OF THE THESIS

Assembly of enveloped viruses requires the selective recruitment of viral components at distinct sites of the host cell plasma membrane from which viruses bud. This enrichment is due to two non-excluding mechanisms, the association of the viral components with subdomains of the plasma membrane (lipid-rafts) and specific interactions between viral proteins. One of the most intense studied enveloped viruses with respect to assembly is the influenza virus whose budding takes place at the plasma membrane of epithelial cells. Three membrane proteins are embedded into the influenza virus envelope: hemagglutinin (HA), which mediates binding of the virus to the host cell and fusion with cell target membrane [86], neuraminidase (NA) and the proton channel M2. The inner viral membrane leaflet is covered by the matrix protein M1, which is supposed to mediate binding of the eight viral RNA-nucleoprotein complexes harbouring the genetic information of the virus. Several studies support a role of lipid domains as a platform for enrichment of viral components. HA, the most abundant envelope protein of influenza virus, has been found to be enriched in detergent resistant membrane (DRM) fractions [40,87,88]. Typical lipid components of those fractions are saturated phospholipids, glycosphingolipids and cholesterol which are known to form liquid-ordered (lo) domains [89]. This has led to the idea that so-called lipid rafts, which resemble lo domains, could function as assembly sites. Support for this hypothesis was given by the observation that the lipid composition of the influenza virus envelope is more similar to that of a raft than to the overall plasma membrane [38,40]. However, since it has been shown that DRM fractions may not resemble the native state of lipid domains, in particular of rafts [63,72], subsequent efforts have focussed on other techniques to assess the lateral organization of HA. Electron microscopy studies using immunogold labelling [88,90], FRET measurements between fluorescent HA antibodies in fixed cells [90] and investigations on photoactivatable HA in living cells [91] revealed cholesterol sensitive clustering of HA in the plasma membrane of mammalian cells at length scales between 20 and 900 nm. A specific problem encountered in studying the lateral organization of proteins in the plasma membrane is that lipid domains as rafts are typically organized at a submicroscopic level. Indeed, several attempts to image raft domains in biological membranes suggested that rafts are very small and highly dynamic [62,92]. A guiding study in characterization of lipid domains in biological membranes has been performed by Mayor and colleagues on the plasma membrane of CHO-K1 cells [77]. Based on homoFRET measurements they have shown that about 20 to 40% of GFP tagged glycosylphosphatidylinositol (GPI) [93] and other GPI-anchored proteins are organized with about three to four copies in small cholesterol sensitive clusters. Mathematical modelling of those experimental data is consistent with a domain diameter of about 5 nm [77].

In the present study the lateral organization of the HA C-terminus corresponding to the transmembrane domain (TMD) and the cytoplasmic tail (CT) of the protein in the plasma membrane of CHO-K1 cells was investigated. Lateral organization was studied essentially by FLIM based FRET between CFP (donor) and YFP (acceptor) (**Figure 13**). For this purpose, the ectodomain of HA was replaced by YFP and FRET between this construct and GPI-CFP, whose lateral organization in the plasma membrane of CHO cells have been well characterized [77], was studied. As a complementary approach, ensemble measurements in suspensions of plasma membranes purified from cells expressing fluorescent GPI and HA constructs were performed. HomoFRET was measured by time-resolved fluorescence anisotropy providing information on the aggregation/clustering state of the fluorescent constructs which is important to rationalize the FLIM-FRET data.

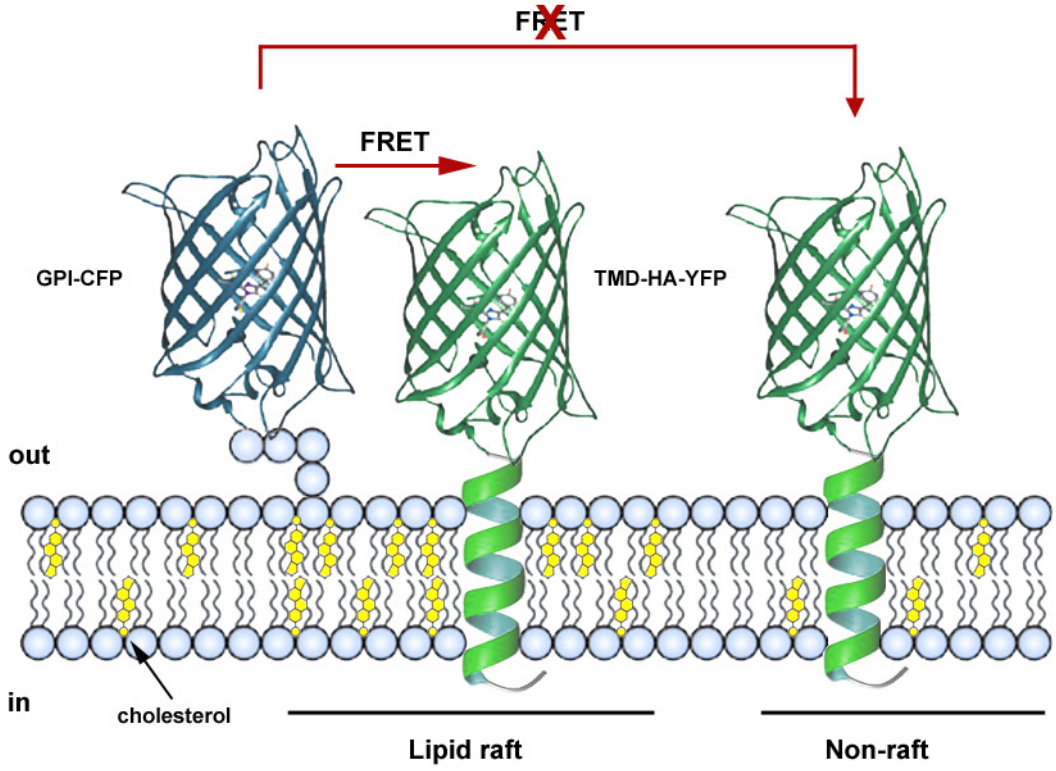

Figure 13: FRET between TMD-HA-YFP and GPI-CFP. Cartoon of the strategy used to study the lateral organization of the HA transmembrane domain and cytoplasmic tail fused to YFP (TMD-HA-YFP) and of the glycosylphohsphatidylinositol-anchored CFP (GPI-CFP) in the plasma membrane of CHO cells.

3 MATERIALS AND METHODS

3.1 Materials

3.1.1 Apparatuses

35-mm-glass-bottom dishes	MaTek Corp., Ashland, MA, USA
Biophotometer plus	Eppendorf, Hamburg, Germany
Centrifuge Avanti J-20XP (Rotor JLA10.500) Ultracentrifuge Optima L-100K (Rotors: 45Ti, 70.1Ti, SW40Ti, SW60)	Backmann Coulter GmbH, Krefeld, Germany
Confocal Microscope Fluo View-1000	Olympus, Hamburg, Germany
Gel-dryer	Uniequip, Martinsried, Germany
Hyperfilm ECL, PVDF-membrane	Amersham Biosciences, Freiburg, Germany
Incubator	Heraeus, Berlin, Germany
Kodak "X-Omat Ar"-Film	Sigma-Aldrich, Taufkirchen, Germany
Luminescence counter "1600 RT"	Packard Perkin Elmer, Jügesheim, Germany
"µ-Slide VI" Ibidi dishes	Ibidi GmbH, Martinsried, Germany
Plate-reader FluoStar Optima	BMG Labtechnologies GmbH
Semi-Dry Transfer cell "TransBlot SD" Thermal Cycler "MyCycler"	BioRad, Munich, Germany
SLM Aminco Spectrophotometer	Aminco Bowman
Time resolved LSM upgrade Kit	PicoQuant, Berlin, Germany

3.1.2 Tissue culture reagents

DMEM DMEM without phenol red DPBS with Ca^{2+} Mg^{2+} DPBS without Ca^{2+} Mg^{2+} Trypsin	PAN, Aidenbach, Germany
L-Glutamine	Biochrom AG, Berlin, Germany
Fetal Bovine Serum, FBS	Invitrogen, Karlsruhe, Germany

Antibiotic

Penicillin/Streptomycin	PAN, Aidenbach, Germany
Kanamycin Neomycin	Sigma-Aldrich, Taufkirchen, Germany

3.1.3 Chemicals

APS Cytochalasin D DMSO EDTA Jodacetamid Methyl-β-cyclodextrine NA-Deoxycholat (DOC) Protease Inhibitor cocktail (PIC) Protein-A-Sepharose Salicilic Acid TEMED Tween-20	Sigma-Aldrich, Taufkirchen, Germany
Acetic acid Acrylamide/Bisacrylamid (Rothiophorese 30) Glycerin Glycin	Roth, Karlsruhe, Germany

fat-free dry milk	
NaCl	
SDS (Na-Dodecylsolfat)	
TBE 50X	
tricloracetic acid (TCA)	
Tris	
PMSF	Applichem, Darmstadt, Germany
Sucrose	
Nycodenz	Axis-Schield PoC, Oslo, Norway
Agarose	Biozym scientific GmbH, Oldendorf, Germany
dNTPs	New England Biolabs, Schwalbach/Taunus, Germany
ECL plus western blotting detection system	Amersham Biosciences, Freiburg, Germany
1kb DNA ladder, “Page Ruler Prestained” protein ladder	Fermentas, St.Leon-Rot, Germany
100bp DNA ladder	Promega, Mannheim, Germany
DAPI nucleic acid stain	
Lipofectamine 2000	Invitrogen, Karlsruhe, Germany
Lipofectin	
R18	
SYBR safe DNAgel stain	
Bacto Agar	BD, Becton, Dickinson and company, Lepont de Claix, France
Bacto Tryptone	
Bacto Yeast	
Rhodamine-Phalloidin	Tebu-bio, Offenbach, Germany
Scintillation Cocktail	Microscint™ 20 Ultima Gold, Perkin Elmers Life ans Analytical Sciences, Boston, USA

Radioactive compounds

[^{3}H]-Cholesterol	GE-Healthcare, Buckinghamshire, UK

[^{35}S]-Methionin (Tran35S-Label)	MP Biomedicals, Heidelberg, Germany
[^{3}H]-Palmitic acid: MT 845 Palmitic acid [9,10-^{3}H]	Hartmann Analytic, Braunschweig, Germany

3.1.4 Enzymes and antibodies

Restriction enzymes

BglII	New England Biolabs, Schwalbach/Taunus, Germany
BsrGI	
DpnI	
NotI	
SacII	

Glycosidase

Endoglycosidase H	New England Biolabs, Schwalbach/Taunus, Germany

Phosphatase

CIP	New England Biolabs, Schwalbach/Taunus, Germany

Ligase

T4-DNA ligase	New England Biolabs, Schwalbach/Taunus, Germany

Polymerase

Phusion High-Fidelity DNA Polymerase	Finnzymes, Oldendorf, Germany
Taq DNA polymerase	Peqlab, Erlangen, Germany

Kinase

T4-polynucleotide Kinase	New England Biolabs, Schwalbach/Taunus, Germany

Antibodies

αIgG (mouse) peroxidase-conjugated	BioRad, Munich, Germany
αIgG (rabbit) peroxidase-conjugated	

anti-β-actin, mouse monoclonal	Sigma-Aldrich, Taufkirchen, Germany
anti-calreticulin, rabbit pAb	Calbiochem, Darmstadt, Germany
anti-caveolin 1, rabbit pAb	BD Biosciences, Heidelberg, Germany
anti-GFP, mouse	Roche Diagnostics, Idianapolis, USA
anti-membrine, mouse monoclonal	Abcam, Cambridge, UK

3.1.5 Kits

QIAprep Spin Miniprep kit QIAquick gel extraction kit QIAgen Plasmid Maxiprep kit	Quiagen, Hilden, Germany
Micro BCA protein assay kit	PIERCE, Rockford, IL,USA

3.1.6 Cells

CHO-K1 cells (chinese hamster ovary cells)	ATCC number: CCL-61
MDCKII (madin darby canin kidney cells)	ATCC number: CCL-34

3.1.7 Bacteria

DH5α (*E. coli*)	F^- endA1 recA1 hsdR17(r_k^- m_k^+) supE44 λ^- thi-1 gyrA(Na1) relA1 Φ80 lacZΔM15Δ(lacZY A-argF)

3.1.8 Plasmids and oligonucleotides

Plasmids pEYFP-N1 (Invitrogen), pECFP-N1 (Invitrogen) and pECerulean-N1 [94] were used for cloning. These plasmids contain a multiple cloning site (MCS) immediately before the N-terminus of the fluorophore (**Figure 14**). Restriction sites within the MCS were used for cloning of the different HA-transmembrane domain and cytoplasmic tail fusion proteins (TMD-HA) and for the

GPI-anchored raft markers. For simplicity, in the text the abbreviation XFP (X fluorescent protein) was used to indicate the fluorophore variants employed for the production of the diverse fusion proteins.

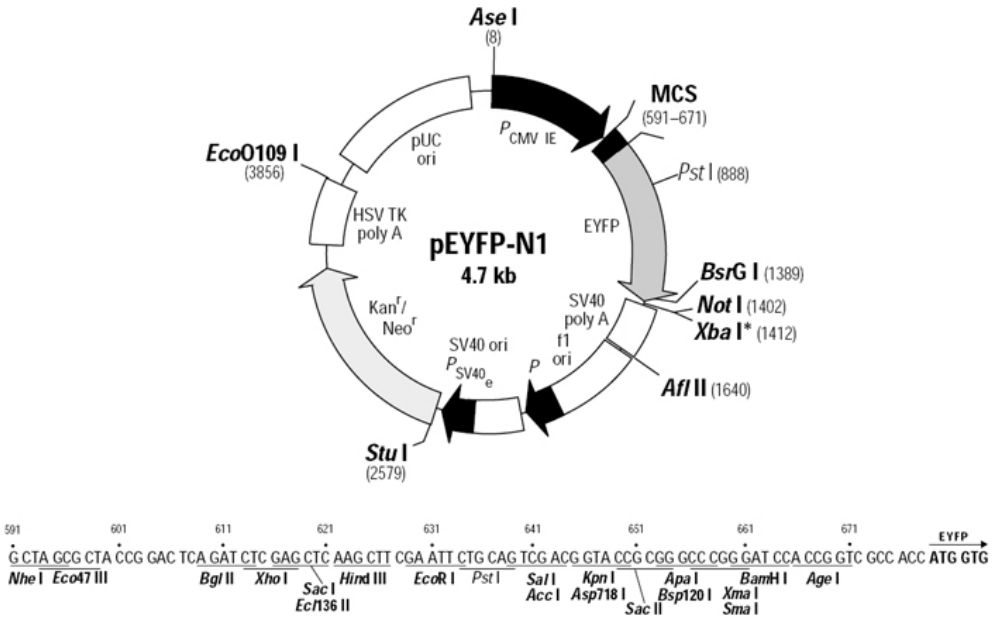

Figure 14: pEYFP-N1 vector. Plasmids pECFP-N1, pEYFP-N1 and pECer-N1 were used for cloning of all the TMD-HA and GPI- anchored fluorescent proteins. The restriction sites BglII and SacII within the multiple cloning site (MCS) were used for insertion of the different singnal peptides. The restriction sites BsrGI and NotI at the C-terminus of the fluorophore were used for fusing the HA transmembrane domain and cytoplasmic tail.

The vector containing the HA sequence corresponding to the HA7 subtype of influenza virus A/FPV/Rostock/34 (H7N1), as well as the vector containing the same HA sequence but carrying the point mutations C551S, C559S and C562S were kindly provided by Stephanie Engel (Free University, Berlin). Four different HA transmembrane domain and cytoplasmic tail fragments (TMD), including also 38 residues of the ectodomain, were obtained as PCR products. The four fragments differ for the presence of linkers at the N-terminus of the sequence (see Table 1). The forward primer (Fw) contains the restriction site *BsrGI*, whereas the reverse (Rw) *NotI* (see plasmid map in Figure 14). TMD-HA-XFPs carrying the mutation C537S in the transmembrane domain were made adapting the "quick change mutagenesis" protocol from Stratagene (see 3.2.1.3). Finally, the VIL3A mutation, corresponding to the mutation of amino acids 527, 528 and 529 to alanines, in the transmembrane domain was inserted using as templates the plasmids HA-mYFP-AAA and HAC3S-mYFP-AAA gently provided by Stephanie Engel (Free University, Berlin). The numbers relative to the point mutations, i.e. C537S, V527A, I528A, L529A, refer to the position that the amino acids occupy in the complete HA sequence.

The HA signal peptide (SpHA) was designed as an oligonucleotide and cloned into the plasmids pECFP-TMD-HA, pEYFP-TMD-HA and pECerulean-TMD-HA using the restriction sites *BglII* and *SacII* (refer to plasmid map in Figure 14). Alternatively, the rabbit lactase phlorizin hydrolase (LPH) signal peptide (SpLPH) derived form the protein GPI-CFP [95] was synthesized as an oligonucleotide and cloned into the different XFP-TMD-HA plasmids. The HA signal peptide carrying the C22S mutation (SpHA-CS), was synthesized as oligonucleotide and ligated into the different TMD-HA-XFP plasmids using the restriction sites *BglII* and *SacII*. All oligonucleotides were purchased from Biotez, Berlin, Germany.

The mutation A206K [96] was inserted into the plasmid pECFP-N1, using "quick change mutagenesis" adapted from the Stratagene protocol (see 3.2.1.3) generating the plasmid pEmCFP-N1. All TMD-HA and GPI- variants were subsequently cloned into the pEmCFP-N1 and pEmYFP-N1 (provided by Stephanie Engel, Free University, Berlin) plasmids. The number relative to the point mutation C22S refers to the position that the amino acid occupies in the complete HA sequence. mCFP and mYFP indicate the non dimerizing counterparts of CFP and YFP, respectively.

The mutations C49S and C71S were introduced in TMD-HA-mCFP and TMD-HA-mYFP using "AB-PCR" (described in 3.2.1.2). Primers and oligonucleotides for the production of the above described fusion proteins are reported below and summarized in Table 1. In brackets the restriction enzymes used for the subsequent cloning are indicated. The numbers relative to the point mutations, i.e. C49S, C71S, refer to the position that the amino acids occupy in the fluorophore sequence.

Fw-mCFPA206K CTG AGC ACC CAG TCC AAA CTG AGC AAA GAC CCC

Rw-mCFPA206K GGG GTC TTT GCT CAG TTT GGA CTG GGT GCT CAG

Fw-TMD GGC TGT ACA AGA GTA GTG GCT ACA AAG ATG TG (*BsrGI*)

Rw-TMD GCG CGG CCG CTT ATA TAC AAA TAG TGC ACC GC (*NotI*)

Fw-TMD(NNT) GGC TGT ACA AGG CTA GTA TAA GGA ACA ATA CT (*BsrGI*)

Fw-TMD(GS) GGC TGT ACA AGG GCT CTG CTA GTA TAA GGA ACA ATA CT (*BsrGI*)

Fw-TMD(LRPEA) GGC TGT ACA AGC TCC GGC CTG AAG CTG CTA GTA TAA GGA ACA (*BsrGI*)

Rw-TMD(C3S) GCG CGG CCG CTT ATA TAG AAA TAG TGG ACC GC (*NotI*)

Fw-TMD-CS AGC TTC GGG GCA TCA TCT TTT TTG CTT CTT GCC

Rw-TMD-CS GGC AAG AAG CAA AAA AGA TGA TGC CCC GAA GCT

FwC49S ACC CTG AAG TTC ATC TCT ACC ACC GGC AAG CTG

RwC49S CAG CTT GCC GGT GGT AGA GAT GAA CTT CAG GGT

Fw-mCFPC71S ACC TGG GGC GTG CAG TCT TTC AGC CGC TAC CCC

Rw-mCFPC71S GGG GTA GCG GCT GAA AGA CTG CAC GCC CCA GGT

Fw-mYFPC71S GGC TAC GGC CTG CAG TCT TTC GCC CGC TAC CCC

Rw-mYFPC71S GGG GTA GCG GGC GAA AGA CTG CAG GCC GTA GCC

Fw-SpHA GAT CTC ATG AAC ACT CAA ATC CTG GTT TTC GCC CTT GTG GCA GTC ATT CCC ACA AAT GCA GAC AAA ATT TGT CTT CCG C (*BglII-SacII*)

Rw-SpHA GGA AGA CAA ATT TTG TCT GCA TTT GTG GGA ATG ACT GCC ACA AGG GCG AAA ACC AGG ATT TGA GTG TTC ATG A (*BglII-SacII*)

Fw-SpLPH GAT CTC ATG GAG CTC TTT TGG AGT ATA GTC TTT ACT GTC CTC CTG AGT TTC TCC TGC CGG GGG TCA GAC TGG GAA TCT CTG CCG C (*BglII-SacII*)

Rw-SpLPH GGC AGA GAT TCC CAG TCT GAC CCC CGG CAG GAG AAA CTC AGG AGG ACA GTA AAG ACT ATA CTC CAA AAG AGC TCC ATG A (*BglII-SacII*)

FwSpHA-CS GAT CTC ATG AAC ACT CAA ATC CTG GTT TTC GCC CTT GTG GCA GTC ATT CCC ACA AAT GCA GAC AAA ATT TCT CTT CCG C (*BglII-SacII*)

RwSpHA-CS GGA AGA GAA ATT TTG TCT GCA TTT GTG GGA ATG ACT GCC ACA AGG GCG AAA ACC AGG ATT TGA GTG TTC ATG A (*BglII-SacII*)

Fw-GPI(DAF) GTA CAA GCC AAA TAA AGG AGG TGG AAC CAC TTC AGG TAC TAC CCG TCT TCT ATC TGG GCA CAC GTG TTT CAC GTT GAC AGG TTT GCT TGG GAC GCT AGT AAC CAT GGG CTT GCT GAC TTA GC (*BsrGI-NotI*)

Rw-GPI(DAF) GGC CGC TAA GTC AGC AAG CCC ATG GTT ACT AGC GTC CCA AGC AAA CCT GTC AAC GTG AAA CAC GTG TGC CCA GAT AGA AGA CGG GTA GTA CCT GAA GTG GTT CCA CTT CCT TTA TTT GGC TT (*BsrGI-NotI*)

Table 1: Fusion proteins. Summary of plasmids, primers and oligonucleotides used for the production of the TMD-HA variants and GPI-anchored fluorophores. Fw = forward, Rw = reverse. Sp= SpHA; SpCS=SpHA-CS.

Protein name	Plasmid template	N- (Fw) and C- (Rw) terminus primers
pEmCFP-N1	pECFP-N1	Fw-mCFPA206K Rw-mCFPA206K
TMD-HA-YFP	PA11sv13-HA pEYFP	Fw-TMD Rw-TMD
TMD(NNT)-HA-YFP	PA11sv13-HA pEYFP	Fw-TMD(NNT) Rw-TMD
TMD(GS)-HA-YFP	PA11sv13-HA pEYFP	Fw-TMD(GS) Rw-TMD
TMD(LRPEA)-HA-YFP	PA11sv13-HA pEYFP	Fw-TMD(LRPEA) Rw-TMD
Sp-TMD(NNT)HA-YFP	TMD(NNT)-HA-YFP Oligonucleotide	Fw-SpHA Rw-SpHA
Sp-TMD(NNT)HA-CFP	Sp-TMD(NNT)HA-YFP pECFP-N1	YFP substituted with CFP (SacII and BsrGI)
Sp-TMD(NNT)HA-mCer	Sp-TMD(NNT)HA-YFP pEmCerulean-N1	YFP substituted with mCerulean (SacII and BsrGI)
SpLPH-TMD(NNT)HA-YFP	TMD(NNT)HA-YFP Oligonucleotide	Fw-SpLPH Rw-SpLPH
Sp-TMD(NNT)C3S-HA-YFP	PA11sv13-HA-M3 Sp-TMD(NNT)HA-YFP	Fw-TMD(NNT) Rw-TMD(C3S)
Sp-TMD(NNT)C3S-HA-CFP	PA11sv13-HA-M3 Sp-TMD(NNT)HA-CFP	Fw-TMD(NNT) Rw-TMD(C3S)
Sp-TMD(NNT)-HA-mYFP	Sp-TMD(NNT)HA-YFP pEmYFP	YFP substituted with mYFP (SacII and BsrGI)
SpCS-TMD(NNT)-HA-YFP	Sp-TMD(NNT)HA-YFP Oligonucleotide	Fw-SpHA-CS Rw-SpHA-CS
SpCS-TMD(NNT)-HA-mYFP	Sp-TMD(NNT)HA-mYFP Oligonucleotide	Fw-SpHA-CS Rw-SpHA-CS
SpCS-TMD(NNT)C3S-HA-YFP	Sp-TMD(NNT)C3S-HA-YFP Oligonucleotide	Fw-SpHA-CS Rw-SpHA-CS
Sp-TMD(NNT)HA-mCFP	Sp-TMD(NNT)HA-CFP pEmCFP-N1	CFP substituted with mCFP (SacII and BsrGI)
GPI-mCFP	GPI-CFP	Fw-mCFPA206K Rw-mCFPA206K
Sp-GPI(DAF)-CFP	Sp-TMD(NNT)HA-CFP Oligonucleotide	Fw-GPI(DAF) Rw-GPI(DAF)

Protein name	Plasmid template	N- (Fw) and C- (Rw) terminus primers
Sp-GPI(DAF)-YFP	Sp-TMD(NNT)HA-YFP Oligonucleotide	Fw-GPI(DAF) Rw-GPI(DAF)
Sp-GPI(DAF)-mCFP	Sp-GPI(DAF)-CFP	Fw-mCFPA206K Rw-mCFPA206K
Sp-TMD(NNT)C3S-HA-mCFP	Sp-TMD(NNT)C3S-HA-CFP	Fw-mCFPA206K Rw-mCFPA206K
Sp-TMD(NNT)-CS-HA-mYFP	Sp-TMD(NTT)HA-mYFP	Fw-TMD-CS Rw-TMD-CS
SpCS-TMD(NNT)C3S-CS-HA-YFP	SpCS-TMD(NNT)C3S-HA-YFP	Fw-TMD-CS Rw-TMD-CS
Sp-TMD(NNT)-HA-mYFP C49S	Sp-TMD(NNT)-HA-mYFP Sp-TMD(NNT)-HA-mYFP	(AB-PCR) Fw-SpHA/ Rw-TMD Fw-C49S/ Rw-C49S
Sp-TMD(NNT)-HA-mYFP C49S-C71S	Sp-TMD(NNT)-HA-mYFP C49S Sp-TMD(NNT)-HA-mYFP	(AB-PCR) Fw-SpHA/ Rw-TMD Fw-mYFPC71S/ Rw-mYFP C71S
Sp-TMD(NNT)-HA-mCFP C49S	Sp-TMD(NNT)-HA-mCFP Sp-TMD(NNT)-HA-mCFP	(AB-PCR) Fw-SpHA/ Rw-TMD Fw-C49S/ Rw-C49S
Sp-TMD(NNT)-HA-mCFP C49S-C71S	Sp-TMD(NNT)-HA-mCFP C49S Sp-TMD(NNT)-HA-mCFP	(AB-PCR) Fw-SpHA/ Rw-TMD Fw-mCFPC71S/ Rw-mCFP C71S
Sp-TMD(NNT)-VIL3A-HA-mYFP	HA-L-YFP-VIL3A Sp-TMD(NNT)-HA-mYFP	Fw-SpHA Rw-TMD
Sp-TMD(NNT)C3S-VIL3A-HA-mYFP	HA-C3S-L-YFP-VIL3A Sp-TMD(NNT)-HA-mYFP	Fw-SpHA Rw-TMD

3.1.8.1 SFV-E2-mCFP

The SFV-E2-mCFP protein was kindly provided by Bastian Thaa (Free University, Berlin). The sequence fused to the N-terminus of the mCFP fluorescent protein is

5'-PVRLWSNLTTEGKPHGWPHQIVQYYYGLYPAATV**SAVVGMSLLALISIFASSYMLVAA**RSKSLT PYALTPGAAVP-3'

The glycosylation site is single underlined, the TMD is in bold letters and the serine residues substituting the palmitoylation sites are double underlined. This fragment was substituted to the TMD-HA fragment in the plasmid containing the TMD-HA-mCFP protein.

3.1.9 Cell culture media and buffers

Culture medium

DMEM, 10% FBS, 5% Penicillin-Streptomycin

DMEM phenol-red free, 10% FBS, 5% Penicillin-Streptomycin, 2 mM L-Glutamine

Freezing medium

20% FBS, 10% DMSO, 70% DMEM

Labelling medium

MEM with EBSS, 4 mM L-Glutamine

Selection medium

DMEM, 10% FBS, 5% Penicillin-Streptomycin, 250-500 µg/ml Neomycin

Bacteria medium and plates

LB-medium	1% Bacto™ Tryptone, 0,5% Bacto™ Yeast Extract, 0,5% NaCl, in ddH_2O, pH 7
Kanamycin-LB-plates	1% Bacto™ Tryptone, 0,5% Bacto™ Yeast Extract, 0,5% NaCl, 1,5% Agar, 50 µg/ml Kanamycin, in ddH_2O, pH 7.

Buffers

105% Nycodenz Solution	10,5 g Nycodenz in gradient buffer to 15,6 g (density=1,56 g/ml)
58% Nycodenz Solution	5,8 g Nycodenz in gradient buffer to 13,1 g (density=1,31 g/ml)
8% Nycodenz Solution	0,8 g Nycodenz in gradient buffer to 10,4 g (density=1,04 g/ml)
10x PAGE-Buffer	30 g Tris-Base, 144 g Glycin, 10 g SDS in 1 l ddH_2O
10x PBS	40 g NaCl, 1 g KCl, 7,1 g Na_2HPO_4 $2H_2O$, 1 g KH_2PO_4 in 500 ml ddH_2O
4x SDS-PAGE-sample Buffer	25% β-mercaptoethanol, 5% SDS, 0,05% Blue Bromophenol, 25% Glycerin, 12,5% 1 M Tris-HCl buffer pH 6,8
4x SDS-PAGE-sample Buffer (non-reducing)	5% SDS, 0,05% Blue Bromophenol, 25% Glycerin, 12,5% 1 M Tris-HCl buffer pH 6,8

Blocking-Buffer	0,1% Tween-20, 5% dry Milk, 1x PBS in ddH_2O
Fixative solution (for polyacrylamide gels)	10% Ethanol, 10% Acetic Acid in ddH_2O
Giant Plasma Membrane Vescicles (GPMV)-Buffer	2 mM $CaCl_2$, 10 mM Hepes, 0,15 M NaCl, 25 mM formaldehyde, 2 mM DTT, pH 7,4
Gradient-Buffer	20 mM Tris-HCl pH 7,5, 100 mM NaCl, 1 mM EDTA in ddH2O
Lysis-Buffer	1 mM Tris-HCl pH 7,4, 0,1 mM MgCl2, 1 mM PMSF, 1% PIC in ddH2O
Resolving gel (12%)	4 ml Acrylamid/Bisacrylamid (30%), 2,5 ml 1,5 M Tris-HCl pH 8,8, 100 µl SDS (10%), 3,3 ml ddH2O, 4 µl TEMED, 100 µl APS (10%)
Resolving gel (15%)	5 ml Acrylamid/Bisacrylamid (30%), 2,5 ml 1,5 M Tris-HCl pH 8,8, 100 µl SDS (10%), 2,3 ml ddH2O, 4 µl TEMED, 100 µl APS (10%)
RIPA-Buffer	1% Triton X-100, 1% Desoxycholat, 0,1% SDS, 0,15 M NaCl, 20 mM Tris, 10 mM EDTA, 10 mM Jodacetamid, 1mM PMSF, in ddH2O, pH 7,4
Stacking gel (5%)	0,5 ml Acrylamid/Bisacrylamid (30%), 0,75 ml 0,5 M Tris-HCl pH 6,8, 30 µl SDS (10%), 1,7 ml ddH_2O, 3 µl TEMED, 30 µl APS (10%)
TNE-Buffer	25 mM Tris-HCl pH 7,4, 150 mM NaCl, 5 mM EDTA, 1% Triton X-100, 0,2 mM PMSF in ddH_2O
Transfer buffer	40 ml PAGE-Buffer, 20 ml Methanol, 0,6 ml SDS (10%), in 100 ml ddH_2O

3.2 Methods

3.2.1 Molecular biology

3.2.1.1 Polymerase Chain Reaction

The polymerase chain reaction (PCR) technique enables the exponential amplification of a specific DNA sequence *in vitro*.

The standard PCR protocol entails the use of the DNA sequence to be amplified, of the nucleotide mixture (dNTPs), of the forward and reverse primers (namely Fw and Rw) and of the enzyme DNA polymerase. The PCR is carried out in a thermocycler machine that allows the fast change of temperature from one PCR step to the next. After the denaturation of the template, occurring in the first step of the reaction, the primers anneal with the DNA open strands and the new DNA copies are formed during the extension cycles. In the table below (**Table 2**) the reagent mixture protocol and the PCR scheme used for the amplification of the different HA transmembrane domain and cytoplasmic tail fragments are reported.

Table 2: Standard PCR. Reagent volumes and the PCR scheme used for the amplification of the HA transmembrane domain and cytoplasmic tail.

PCR reagents		**PCR scheme**		
DNA template	50 ng	CYCLE	T (°C)	Time (min)
dNTPs	0,5 mM	Initial Denaturation	94	5
Taq-polymerase	5 U	*Denaturation	94	1
Fw-primer	1 μM	*Annealing	52	1
Rw-primer	1 μM	*Extension	72	1
PCR Buffer	10x	Final Extension	72	10
ddH_2O	to final volume= 50μl	Cooling	4	10-o.n.

*The denaturation-annealing-extention steps are repeated in this order for 30 times

3.2.1.2 AB-PCR

The mutation C49S and C71S in the XFP proteins have been inserted using an alternative PCR method, called AB-PCR or "overlap-extension PCR" (OE-PCR) [97,98]. To perform this kind of PCR, 4 primers are needed. Primers a1 and b1 are designed complementary to the region in which the desired mutation has to be inserted and contain in the middle the mutated sequence. Primers a2 and b2 are external primers carrying two restriction sites (see Figure 15).

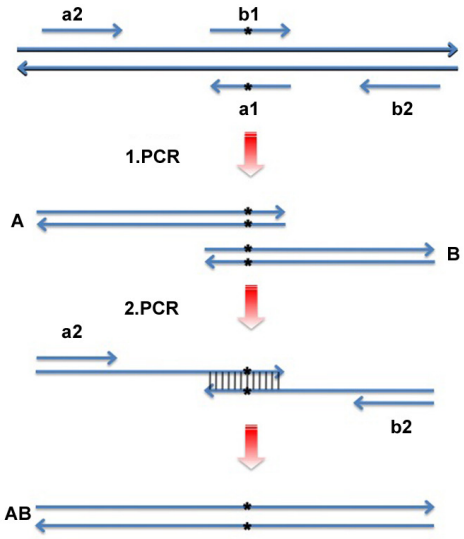

Figure 15: AB-PCR scheme. The AB-PCR procedure allows the insertion of point mutations using two subsequent PCRs. In the first PCR a couple of primers carrying in the middle the mutation (in the picture referred to as a1 and b1, reverse (Rw) and forward (Fw) respectively), is employed. The second couple of primers are complementary to the N- and C- terminus of the fragment of interest and they carry a restriction site used for the subsequent cloning into the vector. In the first step two PCRs are run in parallel, one entailing the use of primers a1 and a2 and the other b1 and b2, thus producing the fragments A and B respectively. These two PCR products together with the primers a2 and b2 are then used in the second PCR for the amplification of the sequence containing the desired mutation.

The complete procedure consists of two sequential PCR. In the first part, two PCR are run in parallel using as Fw and Rw the primers a2 and a1 and b1 and b2, respectively. In the following PCR the "A" and "B" products serve as template for the amplification of the final DNA strain (A+B) containing the desired mutation. Primers a2 and b2 has to be used in order to generate at the N- and C- terminus of the fragment two restriction sites (Figure 15). The protocol and the reagents used are summarized in **Table 3** and **Table 4**.

Table 3: I and II PCR. First (I) and second (II) PCR schemes used in the AB-PCR method described above.

CYCLE	I PCR		II PCR	
	T (°C)	Time (min)	T (°C)	Time (min)
Initial Denaturation	94	3	94	3
*Denaturation	94	30 s	94	30 s
*Annealing	50	30 s	50	30 s
*Extension	68	40 s	68	1
Final Extension	68	10	68	10
Cooling	4	10-o.n.	4	10-o.n.

*The denaturation-annealing-extention steps are repeated in this order for 24 times.

Table 4: AB-PCR reagents summary. The reagents and the related volumes necessary for carrying out the AB-PCR are summarized.

Reagent	A PCR	B PCR	AB PCR
DNA template	50 ng	50 ng	50 ng (A+B fragments)
dNTPs	0,5 mM	0,5 mM	0,5 mM
Taq- polymerase	5 U	5 U	5 U
Fw-primer	1 µM (a2)	1 µM (b1)	1 µM (a2)
Rw-primer	1 µM (a1)	1 µM (b2)	1 µM (b2)
PCR Buffer	10x	10x	10x
ddH_2O	to final V=50µl	to final V=50µl	to final V=50µl

3.2.1.3 Quick change mutagenesis

The Quick change mutagenesis strategy is based on the one developed by Stratagene. The point mutation is inserted into the dsDNA vector in one step and it does not require further purification, restriction and ligation. The primers are designed each complementary to opposite strands of the vector and they carry in the middle the desired mutation. HF-Phusion polymerase is used to extend the annealed primers during temperature cycling. The extension temperature is normally chosen 3 °C above the melting temperature (T_m) of the primers. The final product is a non-methylated nicked plasmid, which is then digested with the endonuclease DpnI (1 hour, 37 °C). This enzyme specifically digests methylated and hemimethylated DNA and it is therefore used to disrupt the parental DNA template. The mutated plasmid is then transformed into DH5α competent cells. In **Table 5** the PCR scheme is reported.

Table 5: Quick change mutagenesis. PCR scheme of the quick change mutagenesis steps for the insertion of point mutations.

PCR scheme		
CYCLE	**T (°C)**	**Time (min)**
Initial Denaturation	98	3
*Denaturation	98	30 s
*Annealing	74	30 s
*Extension	72	3
Final Extension	72	10
Cooling	4	10-o.n.

*The denaturation-annealing-extention steps are repeated in this order for 20 times

3.2.1.4 Oligonucleotides cloning

Alternatively to PCR amplification, short DNA fragments can be designed as oligonucleotides. These peptides contain at the N- and C-terminus the complete restriction site used for further ligation into the plasmid of interest. Oligonucleotides are synthesized as complementary ssDNA, therefore they need to hybridize. Furthermore, in order to allow subsequent ligation, 5'-phosphate should be added. Thus, the two peptides are incubated with the enzyme T4 polynucleotide kinase for 1 hour at 37 °C, in presence of ATP. Finally annealing occurs placing the polypeptides at 97 °C for 10 minutes followed by gradual cooling. This allows the oligos to find the "correct" lowest energy configuration at room temperature.

3.2.1.5 DNA rescue and enzymatic cleavage

In order to control the size, PCR products are run into 1% or 2% (for fragments under 1500bp) agarose gels. For visualization, the DNA is stained with 1x SYBR green before loading into the gel. Extraction of the DNA from the agarose gel is done using the QIAquick gel extraction kit. This passage is necessary to eliminate the PCR reagents that might interfere with the subsequent cloning steps. PCR fragments, oligonucleotides, as well as the vector in which the fragments should be inserted, are subjected to enzymatic cleavage with restriction enzymes. These enzymes cut the DNA within specific sequences, whose digestion leads to the formation of overlapping or "sticky" ends. Restriction occurs mixing the DNA with the suitable buffer and 1-2 µl of the enzymes in a final volume of about 10 to 30 µl. The reaction is incubated for 1 hour or even over night at 37 °C, depending on the percentage of activity of the enzymes in the selected buffer. In order to avoid self-ligation, after digestion the vector has to be dephosphorylated using CIP (calf intestinal alkaline phosphatase), that catalyzes the removal of reactive 5'-phosphate. Before proceeding with ligation it is necessary to purify PCR fragments, oligonucleotides and vector from the restriction and the dephosphorylation reagents. Therefore, DNA is again run and extracted from agarose gel.

3.2.1.6 Ligation of the DNA fragment and transformation

Ligation occurs with the aid of the T4-DNA-ligase. This enzyme catalyzes the formation of a phosphodiester bond between juxtaposed 5' phosphate and 3' hydroxyl termini in duplex DNA or RNA. Thus, it joins blunt or cohesive ends, leading to the production of DNA molecules with the desired insert. The ratio fragment:vector should be 5:1 and the reaction occurs for 10 min at room temperature and then for 3 hours (to over night) at 16 °C.

Ligated plasmids are then transformed into DH5α chemically competent bacteria. The ligation reaction is dilued to a final volume of 100 µl and incubated on ice for 30 min with 250 µl of bacteria. The transformation proceeds with 45 seconds "heat-shock", followed by fast transfer on ice

for 2 min. About 600 µl of LB-medium are then added and bacteria are shaken at 37 °C for 1 hour. Transformed cells are finally plated on Kanamycin-agar plates (Kanamycin final concentration 50 µg /ml).

3.2.1.7 Plasmid purification from bacteria

For the purification of the plasmid from 3 ml of overnight culture in 50 µg /ml Kanamycin containing LB-medium, the QIAprep Spin Miniprep kit is used. The DNA is concentrated in 30-50 µl of dd H_2O.

Extensive plasmid purification is carried out using the QIAgen Plasmid Maxiprep kit. The overnight bacteria culture is increased to about 200 to 400 ml of Kanamycin-LB medium (final concentation 50 µg/ml). The DNA is concentrated in 800 µl of ddH_2O.

The DNA concentration is measured with a Biophotometer plus spectrophotometer.

Plasmids were sent to Invitek (Invitek, Berlin, Germany) for sequencing and the following sequencing-primers were used:

CMV for CGC AAA TGG GCG GTA GGC GTG

TMD-HA for ACA TCG AGG ACG GCA GCG TGC AGC TCG CCG

TMD-HA-VIL3A for TGC TGC CCG ACA ACC ACT ACC TGA

3.2.2 Cell culture

CHO-K1 and MDCKII cell suspensions (1 ml) are thawed in 13 ml DMEM supplied with 10% FBS and 5%PS (complete medium). After 5 min of centrifugation at 1000 rpm at room temperature, the cell pellet is resuspended in 12 ml of complete medium and transferred to a T75 flask. Cells are incubated at 37 °C and 5% CO_2 till the density reaches 70% confluency. Confluent cells are first washed with 5 ml DPBS without Ca^{2+} and Mg^{2+} and detached from the flask with 2 ml Trypsin/EDTA (1 min at 37 °C and 5% CO2). Trypsin reaction is blocked with 10 ml DMEM complete and 1 ml of cells are transferred to a new flask supplied with 11 ml of fresh medium (dilution 1:12).

CHO-K1 and MDCKII stable transfected cell lines are cultured in DMEM complete supplied with 250 µg/ml Neomycin.

CHO-K1 cells used for microscopy and spectroscopy experiments are grown in DMEM without phenol red and supplied with 2mM L-Glutamine, 10% FBS and 5% PS (and 250 µg/ml Neomycin for stable transfected cell lines).

CHO-K1 and MDKII cell lines stably expressing TMD-HA-YFP, TMD-HA-mYFP, GPI-CFP and GPI-mCFP are detached either using a cell scraper or diluting Trypsin/EDTA 1:2.

For freezing, cells are detached from the flask, as previously described, transferred to a falcon tube and centrifuged for 5 min and 1000 rpm at room temperature. Cell pellet is then resuspended in 1,5 ml of freezing medium composed of DMEM complete and cryo medium (3:1) and transferred to cryo-vials. The cryo medium is made of FBS and DMSO (2:1). The cryo-vials are stored in a polystyrene box at -80 °C, overnight and then moved to liquid nitrogen.

3.2.2.1 Transient and stable transfection

Transient transfection is done using Lipofectamine 2000. About 10 µl of reagent is necessary for transfecting one 35 mm dish with 90% confluent cells. Lipofectamine is diluted to a final volume of 250 µl with DMEM pure (without FBS and PS) and incubated at room temperature for 5 min. For each transfection 4 µg of DNA plasmid is diluted in 250 µl of DMEM pure. Lipofectamine 2000 and DNA solutions are then combined and incubated for 20 min at room temperature. In the meanwhile cells are washed 2 times with DMEM pure, afterwards the Lipofectamine-DNA complexes are added. The plates are swirled carefully in order to homogeneously distribute the complexes before incubation at 37 °C and 5% CO_2. After 4 hours the medium is changed with DMEM without FBS and PS. Imaging of cells is done 20-22 hours post-transfection.

The stable transfection of CHO-K1 and MDCKII with the TMD-HA-YFP, TMD-HA-mYFP, GPI-CFP and GPI-mCFP plasmids entails the aid of Lipofectin. Cells are seeded in 6 cm cell culture dishes and grown to 30-50% confluency. For transfection, 10 µl of Lipofectin and 2 µg DNA are diluted in 100 µl DMEM pure and incubated at room temperature for 45 min. Then the two solutions are mixed and incubated at room temperature for further 15 min. Before transferring the complexes to the cells, they are washed 2 times with DMEM pure and 1,8 ml of DMEM is added to the Lipofectin-DNA mixture. Finally, the plates are swirled carefully in order to homogeneously distribute the complexes before incubation at 37 °C and 5% CO_2 for 24 hours. The day after transfection medium is substituted with DMEM complete. When transfected cells are 90% confluent, they are diluted 1:50, 1:20 and 1:10 in new 9,4 cm dishes and cultivated with selective medium (DMEM complete with 500 µg/ml Neomycin) at 37 °C, 5% CO_2. Medium is changed every 2-3 days and resistant clones are picked and transferred to 24 well plates with a cover slip. Cells are maintained in complete medium with 250 µg/ml Neomycin at 37 °C, 5% CO_2 until they reach 70%

confluency. Then, the cells on the cover slip are fixed with paraformaldheyde and imaged for detection of fluorescent protein expression. Positive clones are transferred to T25 and subsequently to T75 flasks prior to freezing. For further cultivation of stable transfected cell lines DMEM complete with 250 µg/ml is used.

3.2.2.2 Cell treatments

Transfected cells are subjected to treatment with different substances. Dithiothreitol (DTT) is used to reduce TMD-HA-disulfide linked dimers localized in the plasma membrane. Cytochalasin D is a cell permeable fungal toxin whose binding to actin filaments causes their disruption and therefore it inhibits also their polarization [99]. This substance is employed to disrupt the cell cytoskeleton. Methyl-β-cyclodextrins are cyclic oligosaccharides composed of 7 α-D-glucopyranoside units. The highly hydrophobic cholesterol molecule is easily lodged inside the ring; therefore cyclodextrins are used as raft-perturbing agents for extracting cholesterol from the cell plasma membrane [100]. The different treatments are summarized in **Table 6**.

Table 6: Cell treatments.

Substance	Concentration	Incubation conditions
DTT	10 mM (DPBS)	5 min, RT
Cyochalasin D	1 µM (DMSO)	20 h, 37 °C
Methyl-β-cyclodextrin (MβCD)	5-10 mM (DPBS)	1 min, 4 °C 30 min, 37 °C

3.2.2.2.1 Cytochalasin D treatment

CHO-K1 transfectants were incubated with a 1 µM solution of Cytochalasin D at 37 ºC for 20 hours. Cells were then washed with DPBS and supplied with DMEM without phenol red before measurement.

3.2.2.2.2 DTT treatment

CHO-K1 transfectants were incubated with a 10 mM solution of DTT for 5 min at room temperature. Cells were then washed with DPBS and supplied with DMEM without phenol red before measurement.

3.2.2.2.3 Cholesterol depletion

CHO-K1 cells were incubated at 4 ºC for 1 min with a 5 mM solution of methyl-β-cyclodextrin (MβCD) in DPBS. Alternatively cells were incubated for 30 min at 37 ºC with 5 or 10 mM MβCD.

3.2.2.3 Cellular polarization

MDCK II are epithelial cells and therefore can be polarized. The plasma membrane of epithelial cells is divided into two domains: an apical domain. In order to allow MDCKII polarization, cells are grown in Transwells, permeable supports with microporous PET (Polyester)-membranes that permit cells to uptake and secrete molecules on both their basal and apical surfaces. The selection medium (250 µg/ml Neomycin) is changed every day for the next 10-18 days. Correct polarization of the cells is checked by confocal imging of the apical or basolateral membrane protein distribution (Figure 38).

3.2.2.4 Giant Plasma Membrane Vescicles (GPMV) formation

Cells are forced to produce giant plasma membrane vescicles (GPMVs) or "blebs" upon treatment with buffer containing DTT and formaldheyde as previously described [101,102]. Briefly, almost confluent cells seeded in T25 flasks are washed twice with GPMV buffer, then 1,5 ml of GPMV buffer containing 2 mM DTT and 25 mM formaldheyde are added and flasks are finally incubated at 37 °C for 1 hour, under gently shaking (60-80 cycles per minute). GPMVs detached from cells are then collected from the bottom of the flask and decanted into a conical glass tube where they are allowed to sediment for about 30 min at 4 °C. For imaging of liquid disordered (ld) domains, about 30 µl of vesicles are labeled with a 20 µM R18 solution and they are imaged in a ibidi-dish. Images of the equatorial plane of the blebs were taken at 10 °C and the temperature was controlled with a water circulating bath.

3.2.2.5 Cell fixation and DAPI/Rho-Palloidin labelling

DAPI and rhodamine-phalloidin labelling are used to stain the DNA and the cell actin cytoskeleton, respectively. Cells are grown in 35 mm dishes with glass cover slip. They are then washed twice with DPBS at 37 °C to remove the culture medium and residues of phenol red which might interfere with fluorescence imaging. Cells are fixed with 1 ml of 4% formaldehyde solution in DPBS, for 10 min at room temperature. After fixation, cells are rinsed once with DPBS for 30 s and permealized with a 0,5% Triton X-100 solution for 5 min at room temperature. After a second wash step with DPBS for 30 seconds at room temperature, cells are stained with 200 µl of a 100 nM rhodamine-phalloidin solution. Incubation is carried out in a humid chamber for 30 min at room temperature in the dark. Cells are then washed three times with DPBS prior to DNA counterstaining with 200 µl of 100 nM DAPI (4´6-diamidino-2-phenylindole). Cells are finally rinsed once with DPBS and imaged.

3.2.3 Biochemistry

Proteins are separated according to their size by SDS-polyacrylamide gel electrophoresis. Prior to application into the gel, samples are mixed with SDS-sample buffer (reducing or non-reducing) and heated at 95 °C for 5 min. The electrophoresis is run at a constant voltage of 180 V until complete resolution. Gels are then transferred to PVDF membranes (Western Blot) or they are fixed and dried for autoradiography.

3.2.3.1 Gel Autoradiography

Radioactive-labeled proteins subjected to electrophoresis can be revealed by autoradiography. After running, the gel is incubated over night in fixative solution, washed two times in ddH_2O, incubated for 30 min with a 1 M salicylic acid solution and dried in a gel dryer. The decay emission pattern of the radioactive proteins (autoradiograph) is then obtained upon incubation of the gel with an X-ray film in a film-cassette at -80 °C for few days up to weeks, depending on the strength of the signal.

3.2.3.2 Western Blot

In Western Blotting (or immunoblotting), proteins are immobilized on a PVDF (Polyvinylidene fluoride) membrane prior to detection with monoclonal or polyclonal antibodies. The blotting of the proteins on the membrane occurs in a semi-dry transfer cell for 30 min at 15 V. The membrane is subsequently blocked for 1 hour with blocking buffer, to prevent any nonspecific binding of antibodies to the surface of the membrane. The membrane with the transferred proteins is incubated with the primary antibody for 1 hour up to over night, at room temperature under gently shaking. The membrane is washed 3 times with ddH_2O or 1x PBS and incubated with the secondary antibody for 1 hour at room temperature under gently shaking. The secondary antibody is linked to an enzyme used for detection with the "ECL plus Western Blot Detection System". The membrane is moved to a cassette and incubated with a film for different times before developing and fixation.

3.2.3.3 Isolation of membrane microdomains

Treatment of cells with anionic cold detergent, such as Triton X-100, leads to the isolation of the so called “detergent resistant membranes” (DRMs) or lipid rafts. Proteins and lipids resistant to the extraction with Triton X-100 float in the lighter fractions in sucrose density gradient, while the other proteins distribute along the different gradient density solutions. Briefly, CHO-K1 transfectants expressing constructs are lysed on ice for 20 min in 1 ml of ice cold 1% Triton X-100 in TNE buffer and homogenized with a loose-fitting dounce homogenizer. The homogenates are mixed with 1,25 ml of 80% sucrose prepared in TNE buffer and placed at the bottom of a centrifuge tube. The samples are then overlaid with 6 ml of 35% sucrose and 3 ml of 5% sucrose in TNE buffer and

centrifuged at 23000 rpm in a Beckman SW35 rotor, for 16 hours. Fractions (1 ml) are collected from the top of the gradient and subjected to trichloracetic acid (20% TCA) precipitation. For detection, analysis by Western blot with GFP-antibody was performed. As control, β-actin, caveolin, membrane and calreticulin antibodies were used.

3.2.3.4 Plasma membrane purification

Plasma membrane purification is necessary to carry out time resolved anisotropy measurments in cuvette. Stably transfected CHO-K1 cells expressing either GPI-mCFP or TMD-HA-mYFP were grown to about 90% confluence in T75 flasks. Cells were first washed with 2 ml DPBS, then collected from the flask using a cell scraper and centrifuged at 4 ºC for 5 min, at 1500x *g*. The pellet was resuspended in 2 ml DPBS and centrifuged again at 4 ºC for 5 min, at 1500x *g*. Cells were then resuspended in 800µl of lysis buffer and incubated on ice for 1 hour. Cells were homogenized using a loose-fitting dounce homogenizer and centrifuged at 4 ºC for 5 min, at 1500x *g*. The supernatant was mixed with about 2,1 ml 105% Nycodenz solution prepared in TNE buffer and placed at the bottom of an ultracentrifuge tube. The samples were overlaid with 7 ml of 58% Nycodenz solution and 2,7 ml of 8% Nycodenz solution in TNE buffer and centrifuged at 100000x *g* in a Beckmann SW 40Ti rotor for 18 hours at 4 ºC. One milliliter fractions were collected from the top of the gradient. Two hundred microliter of every fraction was subjected to TCA precipitation and subsequent Western Blot analysis with GFP-antibodies (monoclonal anti-GFP). In order to collect the purified plasma membrane 800 µl of the plasma membrane-containing fractions was diluted 10 times with TNE buffer and centrifuged 2 h at 100000 *g* in a SW 70.1 Ti Beckmann rotor. The pellet was resuspended in 600 µl DPBS. Enrichment of cytoskeleton, endoplasmic reticulum and Golgi was checked by β-actin, calreticulin and α-membrine antibodies, respectively.

3.2.3.5 Metabolic labelling experiments

For the biological characterization of TMD-HA fusion proteins metabolic labelling with ^{3}H-palmitic acid and ^{35}S-methionine was carried out. Labelling experiments were started at approximately 24 h after transfection. Labelling with [9,10(n)^{3}H]-palmitic acid (0.5mCi/ml of DMEM) and L-[^{35}S]-methionine (1000 Ci/mmol, 50 µCi/ml of DMEM without methionine) was done for 4 hours. For investigation of intracellular processing of TMD-HA, transfected cells were pulse-labeled with L-[^{35}S]-methionine for 2 hours (t_0 = corresponds to the time after the 2 hours of labelling and before starting chasing) and chased by adding unlabeled methionine for 1 (t_1), 2 (t_2) or 4 (t_4) hours. Subsequently cells were lysed with 800 µl ice-cold RIPA buffer and unlysed material was pelleted for 20 min at 14000 rpm. Anti-GFP antibody was added to the samples and incubated overnight at 4 ºC. To bind antigen-antibody complexes, 40 µl of Protein A-sepharose was added to each sample and incubated for 2,5 hours at 4 ºC. The samples were then washed with RIPA buffer and boiled for 2

min in 50 mM phosphate buffer with 0,1% SDS and with or without 0,5% mercaptoethanol (reducing and non-reducing conditions) and analyzed by SDS-polyacrylamide gel electrophoresis on a 12% polyacrylamide gel. For endoglycosidase H (EndoH) digestion, immunoprecipitated samples were boiled for 10 min in 1% Glycoprotein Buffer (0,5% SDS), divided into three aliquots and digested with EndoH or mock digested for 1 h at 37 ºC prior to electrophoresis and fluorography.

3.2.3.6 ^{3}H-cholesterol efflux

To estimate the amount of extracted cholesterol, (see par. 3.2.2.2.3), CHO-K1 cells stably expressing GPI-mCFP or TMD-HA-mYFP were labeled with [1α, 2α(n)-^{3}H]-cholesterol (1mCi/ml) for 4 hours. Cells were then washed with DPBS and incubated with MβCD as described above. Subsequently, the supernatant was incubated with scintillation cocktail. Cells were lysed with a 0,1M NaOH solution for 20 min at 25 ºC and incubated with scintillation cocktail. Radioactivity (in counts per minute, CPM) was measured with a luminescence counter and the percentage of cholesterol extracted was calculated as CPMs/(CPMs + CPMc) where CPMs are the CPM in the supernatant and CPMc are the CPM in the cell lysate. The experiment was carried out in 35 mm glass dishes in order to minimize the absorption of cholesterol to the plastic dishes. To carry out background subtraction, empty dishes were also labelled and subjected to the same treatment as the samples. However, high radioactivity was measured in the supernatant of the control dishes, indicating that high amount of cholesterol was still absorbing to the glass. Therefore it was very difficult to estimate the real amount of cholesterol extracted from the cells and carry out a precise background subtraction. Thus, the reported values supply the indication that cholesterol efflux occurs but they represent only semi-quantitative values.

3.2.4 Protein determination

Total protein content in purified plasma membrane was determined using the micro-BCA protein assay kit. This assay allows the detection of protein concentrations in the range of 2-40 µg/ml taking advantage of the very well known bicinchoninc acid (BCA) formulation. Briefly, samples are incubated with the BCA reagent according to the manufacturer's protocol for 2 hours at 37 ºC. The absorbance is read at 562 nm on a plate reader. Protein concentration of the unknown samples is determined using a standard curve.

3.2.5 Confocal microscopy

Intensity measurements as well as FRET measurements were carried out using an inverted FluoView 1000 microscope and a 60x (1,35 N.A) oil-immersion objective at 25 ºC. Images with a frame size of 512 x 512 pixels were acquired. CFP was excited at 440 nm using a Laser Diode and detected in the range 460 – 490 nm. YFP was excited at 515 nm using an Argon Laser and detected in the range

535 – 575 nm. Selection of cells coexpressing both proteins was based on the fluorescence emission in the CFP and YFP channels after sequential excitation.

3.2.5.1 Measuring protein expression in the plasma membrane

TMD-HA- as well as GPI- protein expression levels were monitored by measuring the fluorescence intensity of proteins at the plasma membrane. Confocal images were collected after sequential excitation of CFP and YFP keeping all measurement conditions constant. The plasma membrane fluorescence intensity was analyzed by the Image J analysis program enabling selection and analysis of the same area for pictures taken sequentially. The mean intensity of the acceptor was taken as a measure of the amount of acceptor expressed, after subtraction of the background. In order to determine the amount of unquenched donor in the plasma membrane of cells expressing both acceptor and donor, the measured donor intensity (I_D) had to be corrected for the fluorescence decrease of the donor due to FRET. To estimate the efficiency of energy transfer (E) for every single cell, the average lifetime of a cell coexpressing donor and acceptor and the mean average lifetime of 10 cells expressing the donor alone were used (see 3.2.5.2). The unquenched donor amount (D) is then calculated as $D = I_D/(1-E)$.

3.2.5.2 FLIM-FRET imaging

Fluorescence lifetime imaging microscopy (FLIM) was used to study energy transfer (FRET) between the GPI-CFP raft marker (donor) and the different TMD-HA-YFP variants (acceptor). FLIM images have been acquired using the time-resolved LSM upgrade Kit (PicoQuant, Berlin, Germany) based on the time-correlated single photon counting (TCSPC) technique. This method is based on the repetitive measurement of the time difference between the excitation (e.g. laser pulse) and the subsequent emission of a fluorescent photon. Only a single photon every 100 laser pulses is registered, therefore the measurement is repeated very often and the measured time differences are sorted into a histogram. This histogram of photon arrival times, which represents the fluorescence decay, can then be analyzed to extract the fluorescence lifetime. FLIM images of donor and donor in presence of acceptor were acquired upon excitation of the donor at 440 nm using a pulsed laser diode. The CFP lifetime of cells expressing only GPI-CFP was first measured. The fluorescence was detected by a single photon avalanche photodiode (SPAD) and a 470 ± 15 nm bandpass filter. Electrical signals were processed by the TimeHarp 200 PC card. The analysis of the FLIM images was performed using the SymPhoTime software (PicoQuant,) taking into account the instrument response function (IRF). FLIM pictures were accumulated for 90 seconds (60 frames with an average photon count rate of ~2-4 x 10^4 counts/s) and the plasma membrane was selectively analyzed. The measured photons-per-pixels corresponding to the plasma membrane were combined into a decay curve which was further analyzed by fitting it using a non-linear least squares iterative

procedure, as the sum of two exponential terms. This kind of fitting is required since fluorescent proteins variants are known to show a multiple exponential decay [78]. For every single cell the average lifetime, or more precisely the **amplitude weighted lifetime**, of CFP was calculated using the equation

$$\bar{\tau} = \sum_i \alpha_i \tau_i \text{ [78]}$$

For simplicity in the text this lifetime is referred to as τ_{AV}. Quality of fitting was judged by the distribution of the residuals and the χ^2 value.

In a typical FLIM-FRET experiment at least two probes are necessary: one sample transfected with the donor and the second with donor and acceptor. The donor lifetime is measured in both of the samples as described above and used for calculating the FRET efficiency (see 3.2.5.3).

3.2.5.3 FRET efficiency calculation and data analysis

The efficiency of FRET (E) was calculated using equation

$$E(\%) = 1 - \frac{\tau_{DA}}{\tau_D}$$

where τ_{DA} is the average lifetime of donor in presence of acceptor and τ_D is the average lifetime of the donor expressed alone [78].

In order to assess whether FRET efficiency is independent from the acceptor concentration, the FRET efficiency E(%) of every cell co-expressing donor and acceptor was plotted against the fluorescence intensity of the acceptor F_{YFP} in this cell, measured as described above. The data points were fitted according to the equation:

$$E(\%) = \frac{E_{\max}(\%) \times F_{YFP}}{F_{YFP} + K_D}$$

assuming that E is a hyperbolic function of the amount of acceptor. E_{max} (in %) is the maximal FRET efficiency calculated from the fitting [96,103]. The equation gives the dissociation constant K_D as a parameter to assess the associative properties of donor and acceptor since it represents the concentration of acceptors that cluster with the 50% of the donors. Indeed, when $F_{YFP} << K_D$, FRET efficiency is proportional to the acceptor surface density. When $F_{YFP} >> K_D$, FRET efficiency is independent from the acceptor density. In the former case donors and acceptors are mutually randomly distributed, whereas in the latter each donor is already clustered with at least one acceptor.

3.2.5.4 Steady-state and Time-resolved fluorescence spectroscopy

The steady-state and time-resolved fluorescence instrumentation is the same as described in [104]. For steady-state fluorescence anisotropy measurements on purified plasma membrane suspensions at 25 °C, excitation and emission wavelengths were 435 and 477 nm for CFP, and 515 and 535 nm for YFP, respectively. Fluorescence intensity and anisotropy decays were obtained by the single-photon timing technique. The excitation and emission wavelengths were 415 nm and 460-490 nm respectively (CFP channel) or 490 nm and 520-560 nm (YFP channel). For fluorescence anisotropy decay collection and analysis see de Almeida et al. 2006. Both fluorescence intensity and anisotropy decays were analysed with the TRFA software (Scientific Software Technologies Center, Minsk, Belarus). Based on rates of fluorescence anisotropy decay due to homoFRET the distance R between fluorophores was calculated according to [85,105] as described in [106]:

$$\tau_{\phi_1} = \frac{1}{2\omega}$$

with

$$\omega = \frac{3}{2}\kappa^2\left(\frac{R_0}{R}\right)\tau_{AV}{}^{-1}$$

τ_{ϕ_1} = short rotational correlation time (see Results), $\kappa^2 = 2/3$, and R_0 = Förster radius obtained from [107].

4 RESULTS

4.1 Construction of the raft markers

The construction of a fluorescent raft marker was necessary in order to study *in vivo* colocalization of different proteins in membrane microdomains. The easiest way to produce such a marker is to fuse a signal peptide, necessary for the delivery of the protein to the plasma membrane (see Methods), directly to the N-terminus and a GPI-anchor signal directly to the C-terminus of the fluorophore. Hence, the fluorescent protein is recruited to sphingolipid and cholesterol enriched domains in the cell plasma membrane [108,109], as shown in **Figure 16**.

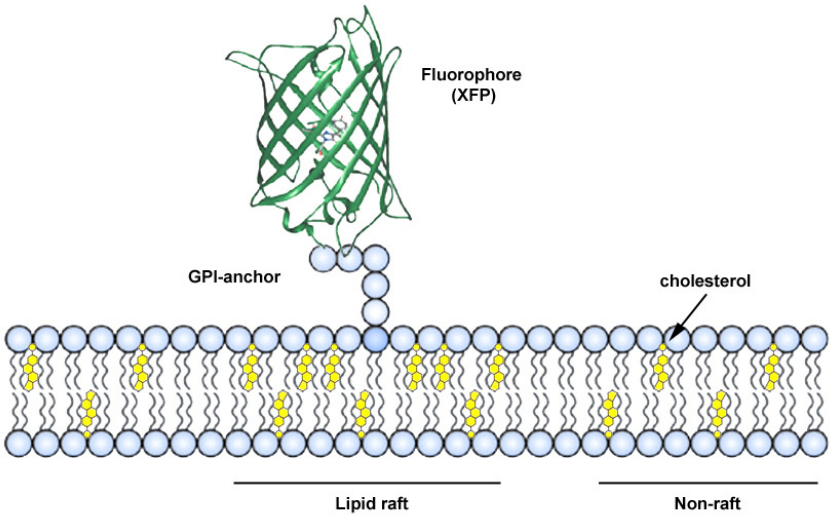

Figure 16: The raft marker GPI-XFP. The GPI-anchor attaches the fluorophore (XFP indicates all the fluorophore variants used to produce the different raft markers, see Figure 17) to the external leaflet of the cell plasma membrane. GPI-anchored proteins partition preferentially into lipid microdomains enriched in sphingolipids and cholesterol (in yellow in the cartoon), the so called “lipid rafts”.

The GPI-anchor signal of the decay accelerating factor (DAF) was designed as an oligonucleotide, based on the plasmid sequence GFP-GPI(DAF) kindly provided by Daniel Legler [109], and fused to the C-terminus of YFP and CFP. The signal peptide derived from the influenza virus strain A/FPV/Rostock/34 was fused to the N-terminus of YFP and CFP in order to produce the proteins GPI(DAF)-CFP and GPI(DAF)-YFP. The cDNAs of GPI-CFP and GPI-YFP were gently provided by Patrick Keller [95].

Since it was reported that fluorescent protein variants (XFP) have a natural propensity to form dimers, the GPI-linked CFP was substituted with its monomeric form. As shown previously any potential of YFP and CFP for dimerization can be suppressed by the mutation A206K in the fluorescent proteins [96]. Therefore, the mutation A206K was inserted into the pECFP-N1 plasmid by the "quick change mutagenesis" adapted protocol (see 3.2.1.3). The monomeric form of CFP,

namely mCFP, was released from the vector as a *SacII-BsrGI* fragment and ligated into the GPI-CFP plasmid, yielding the GPI-mCFP plasmid. As shown in **Figure 17** upon transfection in CHO-K1 cells all raft markers are transported to the plasma membrane. Additionally, CHO-K1 cell lines stably transfected with GPI-CFP, GPI-mCFP and GPI-YFP were generated.

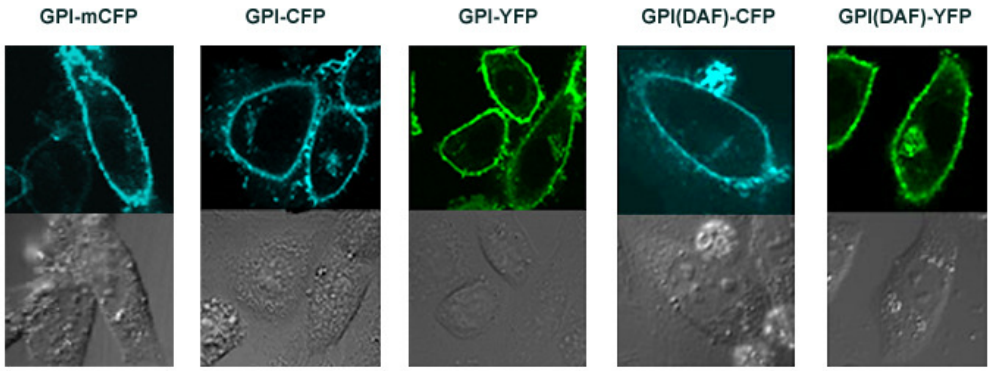

Figure 17: GPI-XFP proteins localization. The different GPI-XFPs are transported to the plasma membrane upon transfection in CHO-K1 cells.

4.2 Construction of TMD-HA fusion proteins

In order to study *in vivo* the properties of the HA transmembrane domain (TMD) and cytoplasmic tail (CT) and its behaviour in the plasma membrane of mammalian cells, an artificial HA consisting of a fluorophore (XFP) replacing the HA ectodomain fused to the transmembrane domain and cytoplasmic tail fragment (TMD-CT) of the glycoprotein was made. **Figure 18** depicts the scheme of the TMD-HA-XFP fusion protein.

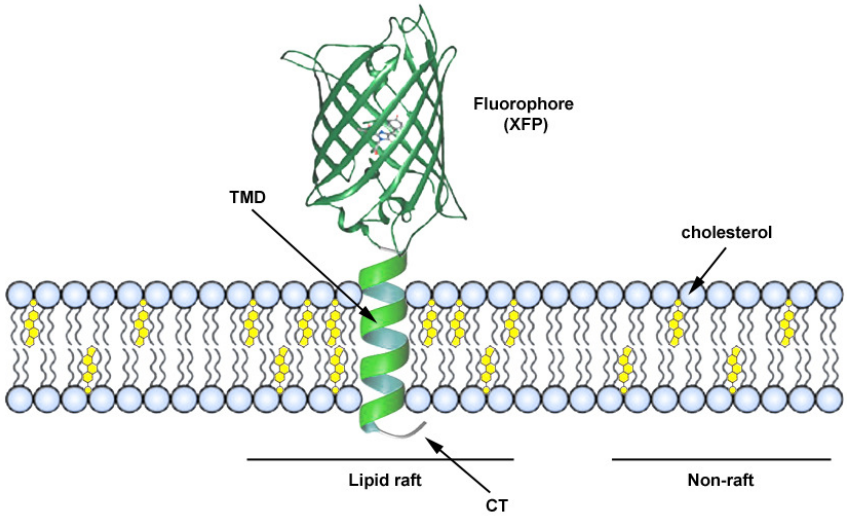

Figure 18: TMD-HA-XFP scheme. The HA transmembrane domain (TMD) and cytoplasmic tail (CT) were fused to the C-terminus of different fluorophores (XFP) to investigate the role of this fragment in the HA lateral organization in the plasma membrane of mammalian cells.

For enhancing the transport to the plasma membrane, the TMD and CT sequence including a glycosylation site (NNT in red in the **b**, **c** and **d** sequences reported in **Figure 19**), 38 amino acids ahead from the C-terminus of the TMD, was also used. Furthermore, two other constructs including, beside the NNT site, also a linker made of two residues (GS, in blue in sequence **c** reported in **Figure 19**) or 5 residues (LRPEA, in blue in sequence **d** reported in **Figure 19**), were made. In this way the protein should acquire more flexibility, factor important for the delivery to the plasma membrane. The protein scheme is summarized in **Figure 19**.

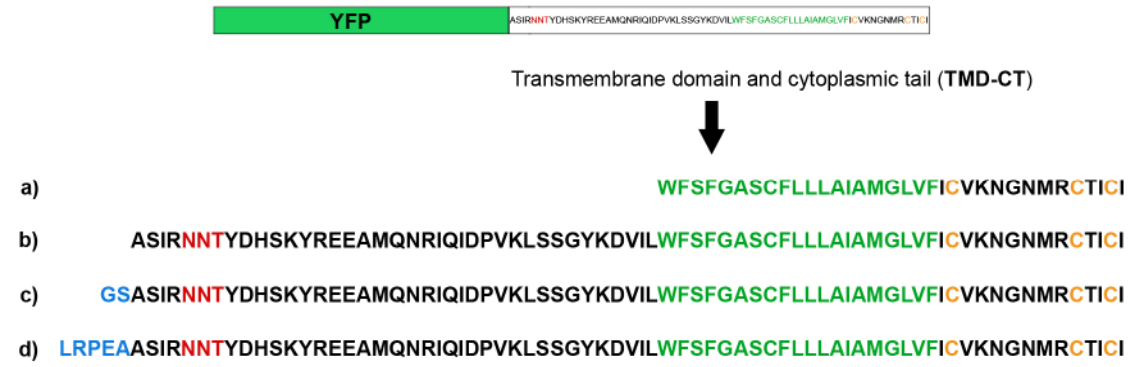

Figure 19: TMD-HA-YFP variants. The different TMD-HA fusion proteins were produced fusing the HA transmembrane domain (TMD) and cytoplasmic tail (CT) fragment (TMD-CT) to the C-terminus of the fluorophore (YFP). The four fragments, are named TMD-HA (**a**), TMD-HA(NNT), including a glycosylation site (red residues in the sequence) (**b**), TMD-HA(GS), including beside the glycosylation site (in red) also a 2 amino acid linker (blue residues in the sequence) (**c**), and TMD-HA(LRPEA), including beside the glycosylation site (in red) also a 5 amino acid linker (blue residues in the sequence) (**d**). In **a**, **b**, **c**, **d**, the TMD sequence is in green, the CT sequence (downstream of the TMD) is in balck and the palmitoylation sites are in orange. In b, c and d the sequence upstream of the TMD corresponds to 38 residues of the ectodomain.

Although all the four TMD-HA constructs, TMD-HA-YFP, TMD-HA(NNT)-YFP, TMD-HA(GS)-YFP and TMD-HA(LRPEA)-YFP were fluorescent and exported from the nucleus upon transfection in CHO-K1 cells, none of them was transported to the surface, instead they accumulated in the cytoplasm (**Figure 20**).

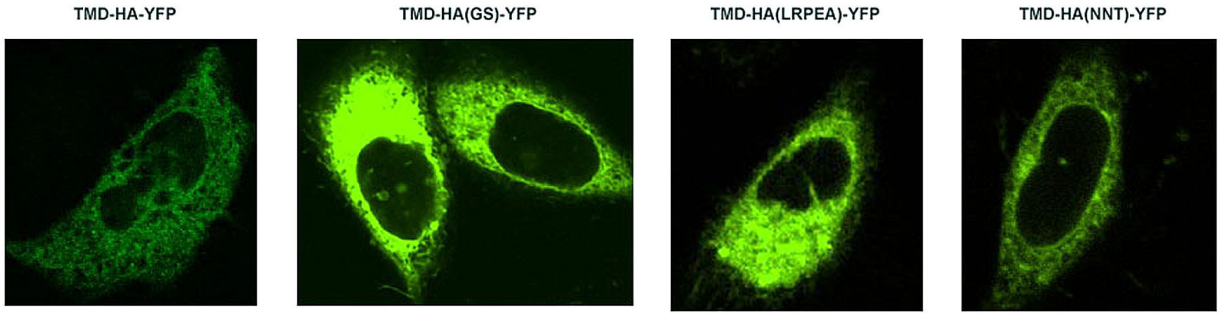

Figure 20: Expression of TMD-HA-YFP variants in CHO cells. The four different TMD-HA fusion proteins are retained into the cytosol.

The fact that these proteins were not delivered to the plasma membrane was also confirmed by EndoH digestion upon labelling with ^{35}S-Met. Glycosylated proteins allocated to the plasma membrane acquire resistance to this enzyme during their passage through the Golgi apparatus [110]. As shown in **Figure 21**, TMD-HA-YFP, TMD-HA(NNT)-YFP, taken as examples, were digested with EndoH (H) or not digested (-). The band pattern (pointed by the black arrow in **Figure 21**) presented by the proteins does not change upon incubation with EndoH (lines "H", **Figure 21**), confirming that proteins never acquire this resistance. Finally, as expected, the control sample (last two lines from the right) shows the total absence of the TMD-HA proteins band.

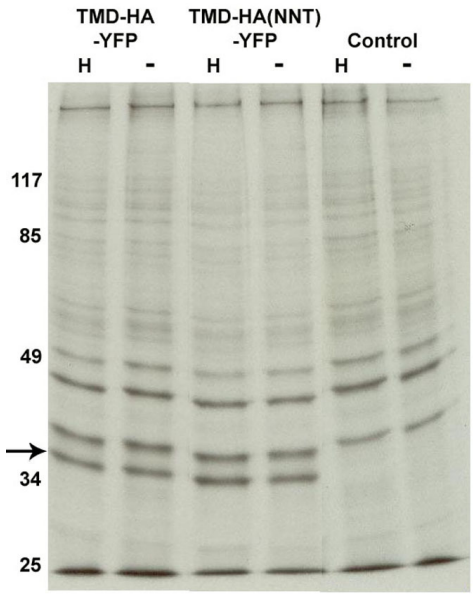

Figure 21: EndoH resistance assay. TMD-HA-YFP and TMD-HA(NNT)-YFP (pointed in the gel by the black arrow) do not acquire EndoH resistance, in agreement with the cytosolic localization of these proteins in CHO-K1 transfected cells. H = EndoH treated; "-" = non-EndoH treated.

It has been reported that the HA signal peptide is critical for the delivery and the transfer of the polypeptide across the membrane [17]. Therefore, this sequence was fused to the N-terminus of the TMD-HA fusion protein. Alternatively to the HA signal peptide, the signal sequence of the protein LPH (lactase phlorizin hydrolase), was used (**Figure 22**). The sequence **a** reported in **Figure 22** A, as well as either SpHA or SpLPH (also indicated in **Figure 22** A) were merged for the production of SpHA-TMD-HA(NNT)-YFP and SpLPH-TMD-HA(NNT)-YFP, which were efficiently transported to the plasma membrane (**Figure 22** B) as confirmed also by EndoH resistance assay (**Figure 22** C, band between 48 and 36 kDa. TMD-HA fusion proteins have a molecular weight of about 39 kDa).

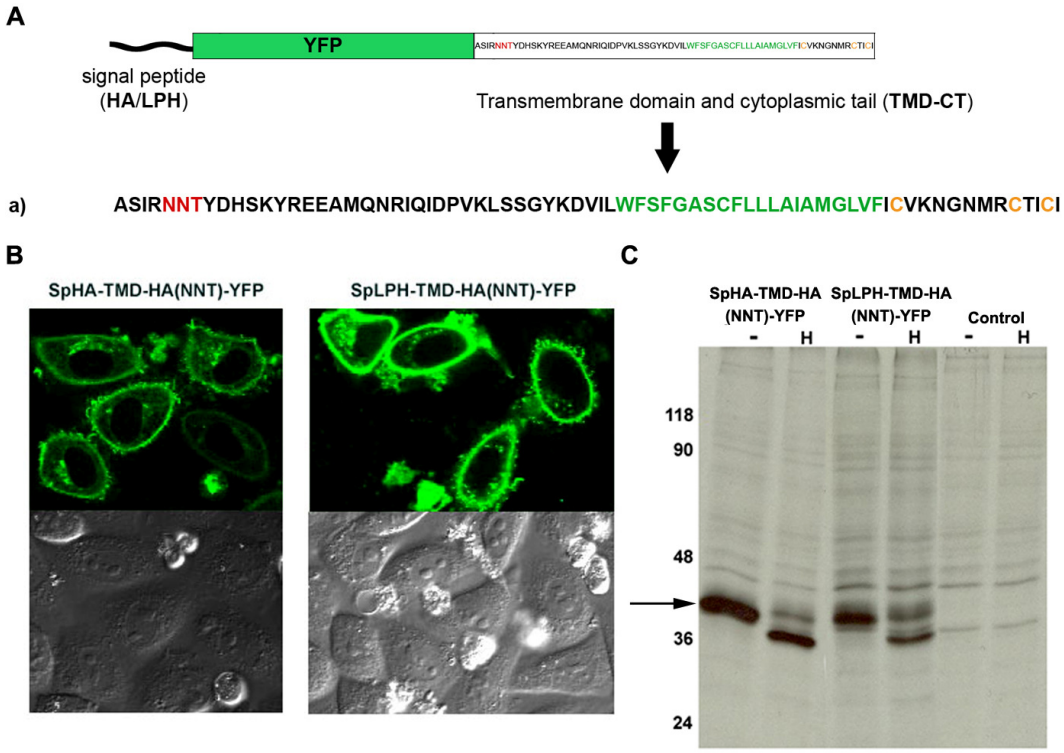

Figure 22: Sp-TMD-HA(NNT)-YFP and SpLPH-TMD-HA(NNT)-YFP transport. A) The different TMD-HA fusion proteins were produced fusing either the HA or the LPH signal peptide to the N-terminus of the fluorophore (YFP) and the HA transmembrane domain and cytoplasmic tail (TMD-CT) to the C-terminus. In **a** the TMD-CT sequence is reported (from the left: in black the 38 aa sequence of the ectodmain with in red the glycosylation site, in green the TMD sequence, in black the CT sequence and in orange the palmitoylation sites). **B**) SpHA-TMD-HA(NNT)-YFP and SpLPH-TMD-HA(NNT)-YFP localize in the plasma membrane of CHO-K1 cells; **C**) EndoH resistance assay shows that the two proteins acquire resistance to this enzyme. Two bands, indicated by the balck arrow, can be distinguished in lane two (from the left of the gel): the upper band, running as the non-treated proteins (thick black band in the first line) represents the proteins resistant to EndoH. The same is seen in line 3 and 4 for the protein SpLPH-TMD-HA-YFP. H = EndoH treated; "-" = non-EndoH treated.

Thus, for cloning of different TMD-HA variants the protein SpHA-TMD-HA(NNT)-YFP was always used and simply named TMD-HA-YFP. Constructs TMD-HA-CFP, TMD-HA-mCer, TMD-HA-mYFP, TMD-HA-mCFP were made replacing YFP with CFP, mCer, mYFP and mCFP respectively. Localization of the proteins in the plasma membrane was verified by confocal microscopy (**Figure 23**).

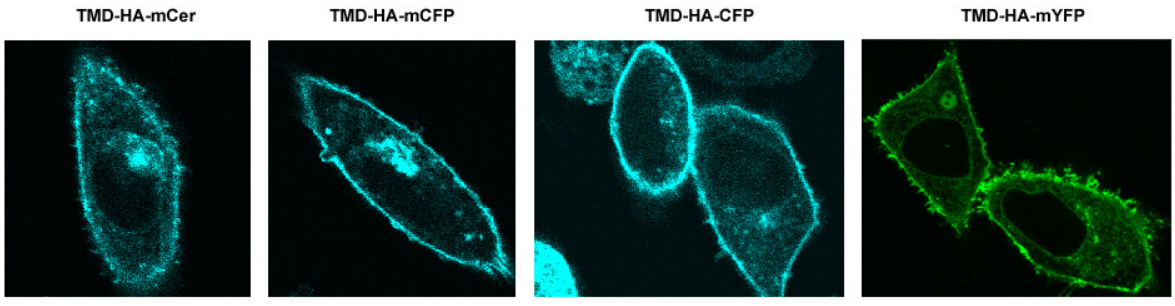

Figure 23: TMD-HA-XFP variants. All the different TMD-HA fusion proteins are transported to the plasma membrane in CHO-K1 cells.

4.2.1 Construction of TMD-HA mutants lacking raft localization signals

Palmitoylation is one of the most common post-translational modifications among proteins enriched into lipid domains. HA presents three conserved palmitoylated cysteines, two localized in the cytoplasmic tail and the third at the border between cytoplasmic tail and transmembrane domain. Therefore, to study the relevance of palmitoylation for lipid domain organization of TMD-HA, the corresponding mutant lacking the palmitoylation sites was made (see scheme in **Figure 24**, sequence in **b**).

a) ASIRNNTYDHSKYREEAMQNRIQIDPVKLSSGYKDVILWFSFGASCFLLLAIAMGLVFICVKNGNMRCTICI

b) ASIRNNTYDHSKYREEAMQNRIQIDPVKLSSGYKDVILWFSFGASCFLLLAIAMGLVFISVKNGNMRSTISI

c) ASIRNNTYDHSKYREEAMQNRIQIDPVKLSSGYKDAAAWFSFGASCFLLLAIAMGLVFICVKNGNMRCTICI

d) ASIRNNTYDHSKYREEAMQNRIQIDPVKLSSGYKDAAAWFSFGASCFLLLAIAMGLVFISVKNGNMRSTISI

Figure 24: Scheme of TMD-HA fusion proteins lacking the raft signals. The TMD-HA sequences used for producing the mutants lacking the raft signals are shown. **a** is the sequence of the TMD-CT fragment wild type where residues in orange are the palmitoylation sites (cysteines) while in **b** these are substituted with serines (C3S mutation, see text), in pink. The sequence in **c** includes the mutation VIL3A (see text) underlined in violet and in the sequence in **d** both the C3S and VIL3A mutations are inserted (amino acids in pink and violet, respectively).

As template, the cDNA encoding for the HA gene from influenza virus strain A/FPV/Rostock/34 (H7N1) mutated at acylation positions 551, 559, 562 (C→S) [23] was used. The TMD-CT(C3S) PCR fragment was ligated into the TMD-HA-YFP plasmid generating the protein TMD-HAC3S-YFP. The construct TMD-HAC3S-mCFP was made replacing YFP with mCFP. Other potential "raft localization signals" have been described by Takeda et al.[88]. They reported a study on different HA subtypes in which groups of three residues in the HA transmembrane domain were substituted with alanine residues. Several of these mutants presented a loss in DRM localization upon extraction with Triton X-100, pointing out the importance of specific amino acid sequences for the lateral organization of HA in lipid microdomains. Therefore, according to the above mentioned publication, the sequence VIL (amino acids 527-529 of the HA transmembrane domain) was substituted with AAA into the TMD-HA-YFP and TMD-HAC3S-YFP proteins in order to investigate the effect of this mutation on the lateral organization of the HA transmembrane domain (**Figure 24**, sequence in **c** and **d**). Proteins TMD-HA-AAA-mYFP and TMD-HAC3S-AAA-mYFP were produced as described

in Methods and used in FLIM-FRET experiments (see 4.4.3). In **Figure 25** confocal pictures show the plasma membrane localization of the molecules.

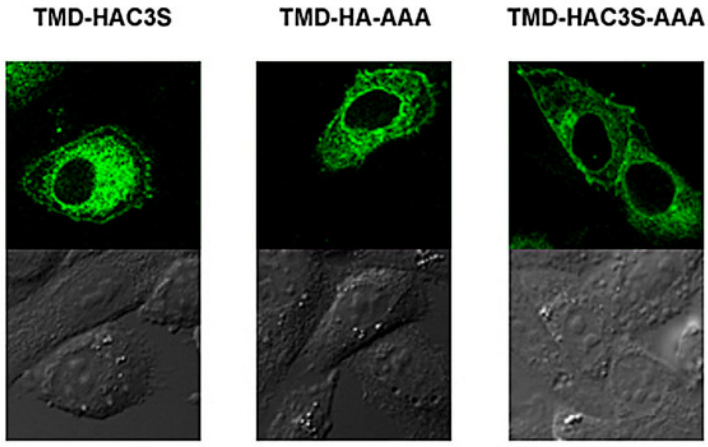

Figure 25: TMD-HA proteins lacking the raft signals. Confocal pictures showing that the TMD-HA variants lacking the raft signals are transported to the plasma membrane.

4.2.2 Post-translational modification of TMD-HA-YFP and TMD-HAC3S-YFP

To ensure that the absence of the ectodomain was not interfering with the TMD properties and that the mutation C3S indeed abolished palmitoylation, the TMD-HA-YFP and TMD-HAC3S-YFP fusion proteins were labelled with [^{3}H]-palmitic acid. As control, proteins were in parallel labelled with [^{35}S]-Met. Autoradiography (**Figure 26**) of the gel shows clearly that palmitoylation occurs in TMD-HA-YFP proteins while it is totally absent in the C3S mutant. Two bands are clearly distinguishable in lane 1 (from the left of the gel, black arrows), representing palmitoylation of wild type TMD-HA monomers and dimers (discussed below). [^{35}S]-Met labelling ensures that both the proteins are expressed at the same level (see gel in **Figure 26**, last two lines from the left). Thus, TMD-HA fusion proteins preserve palmitoylation, a characteristic of the full length HA.

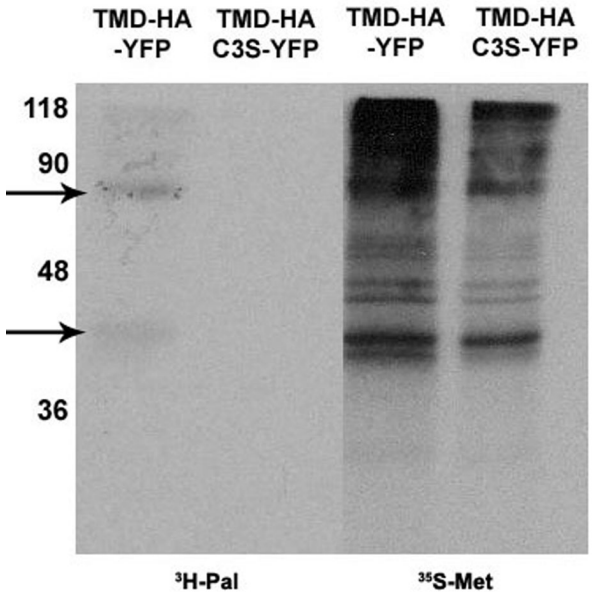

Figure 26: Palmitoylation of TMD-HA fusion proteins. TMD-HA and TMD-HAC3S proteins were labelled with [^{3}H]-palmitic acid to ensure that palmitoylation of the construct containing the HA TMD wild type was still occurring (line 1). The arrows on the gel point to the monomeric and to the dimeric form of the protein (see text). As it is clearly visible, the C3S mutant does not present any band (line 2). As a control for expression, proteins were in parallel labelled with [^{35}S]-Methionin (bands 3 and 4).

4.2.3 TMD-HA variants localize in detergent resistant membranes (DRM)

Hemagglutinin was one of the first proteins recovered in detergent resistant membranes (DRM). These sphingolipid-cholesterol domains or "rafts" can be biochemically isolated because of their insolubility in non-ionic detergents, such as Triton X-100, at low temperature [55]. Since HA is anchored to the lipid bilayer through its transmembrane domain, it was important to verify that TMD-HA constructs as well as the raft marker were still rescued in the raft fractions upon extraction with Triton X-100. TMD-HA-mYFP, TMD-HAC3S-YFP, GPI-mCFP, MyrPal-mYFP and HA-mCer were subjected to Triton X-100 extraction and sucrose gradient purification (see Methods). MyrPal anchors the fluorophore to the inner leaflet of the plasma membrane through myristoyl- and palmitoyl- residues. HA-mCer was made by fusing the fluorescent protein Cerulean to the cytoplasmic tail of the full length HA. Both these proteins were kindly provided by Stephanie Engel (Free University, Berlin). Proteins present in the different fractions were collected from the top of the gradient, precipitated with TCA and analyzed by Western Blot (see Methods). For detection of XFP linked proteins, GFP-antibody was employed. As control, β-actin (cytoskeleton marker), caveolin (protein forming lipid rafts), membrin (Golgi apparatus marker) and calreticulin (ER marker) antibodies were used. In **Figure 27** the Western Blot results are depicted.

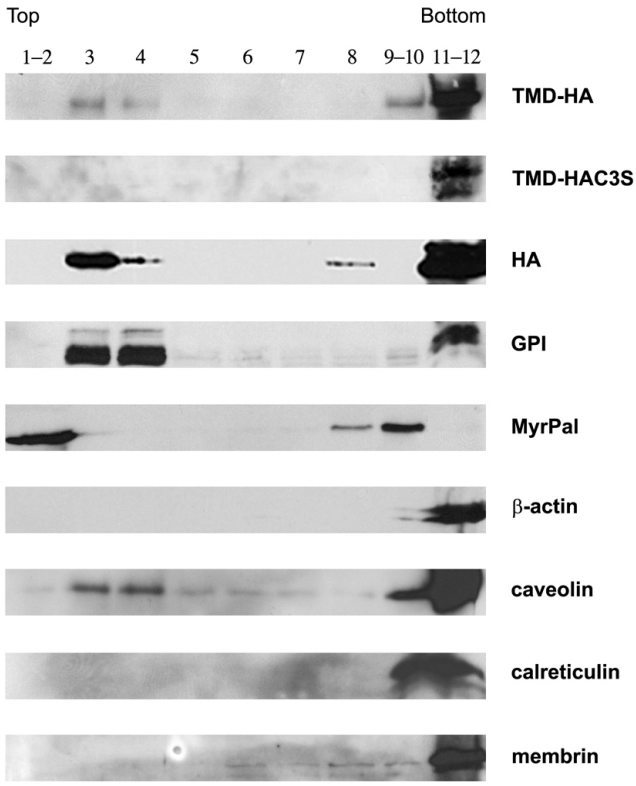

Figure 27: Triton X-100 extraction. Proteins subjected to Triton X-100 extraction were precipitated with TCA and analyzed by Western Blot. Proteins enriched in DRMs should localize in the top fractions (see text). The TMD-HA protein is partially rescued at the top of the gradient (in fractions 3 and 4) as well as the wild type full length HA. As control also GPI- and MyrPal- anchored proteins were subjected to the extraction and sucrose gradient. These proteins as well as the protein caveolin and the TMD-HA and HA proteins are partially localized at the top of the gradient (fractions 1-4). In contrast the TMD-HAC3S mutant is only found at the bottom of the gradient (in fractions 11-12), where also the proteins calreticulin, membrin and β-actin are localized. Numbers indicate the different fractions.

Since DRMs are lighter than the rest of the membrane, they float at the top of the gradient. Hence proteins enriched in DRMs should be rescued in the top fractions. HA-mCer, TMD-HA-mYFP, GPI-mCFP and the raft marker caveolin are localized both in fractions 9-12 (bottom of the gradient) and partially in fractions 3 and 4 (top of the gradient). This is in agreement with previous results reported for full length HA [88,111]. The inner leaflet raft marker MyrPal-YFP is also found at the top of the gradient in fractions 1 and 2 and at the bottom of the gradient in fractions 9-12 as the external leaflet raft marker GPI-mCFP. Finally, the TMD-HAC3S-YFP protein is rescued exclusively at the bottom of the gradient in fractions 11 and 12 as well as the controls β-actin, membrin and calreticulin. This result confirms that palmitoylation is an important determinant for DRM partitioning and that TMD-HA fusion protein behaves like the full length HA.

4.2.4 TMD-HA fusion proteins form disulfide linked dimers and trimers

Trimerization is a critical step for hemagglutinin. It has been reported that HA oligomerization is necessary for the delivery to the Golgi apparatus and that it strongly depends on the pool of available monomers. Only few monomers are found in the Golgi apparatus and HA localizes in the cell plasma membrane exclusively as a trimer [112]. Therefore it was studied whether TMD-HA has the ability to oligomerize. CHO-K1 cells were transfected with TMD-HA-YFP, and TMD-HAC3S-YFP and labeled with [^{35}S]-Methionin. After immunoprecipitation, proteins were mixed with non-reducing loading buffer and applied to a 12% polyacrylamide gel. As shown in **Figure 28**, gel autoradiography revealed the clear presence of dimers and potential trimers, together with monomers, for both the proteins.

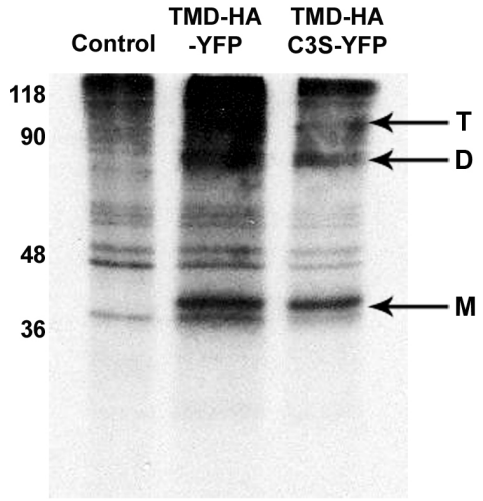

Figure 28: TMD-HA-XFP forms oligomers. The arrows in the picture indicate the TMD-HA monomer (M, 39 kDa), dimer (D, 78 kDa) and trimer (T, 117 kDa), respectively.

However it has to be stressed that the monomer was the most abundant species and that dimers and trimers represent a minor population of TMD-HA proteins. In order to investigate the nature of this oligomerization, the experiment was repeated adding as a control the protein TMD-HA-mYFP. This was necessary to exclude that these oligomers were due to dimerization of the "non-monomeric" form of YFP (i.e. without A206K mutation, see Methods). Furthermore, samples were divided into two parts, which were mixed either with non-reducing or with reducing loading buffer to investigate whether oligomerization was driven by disulfide bond formation. The gel (**Figure 29**) showed the presence of dimers for all three proteins, which disappear under reducing conditions.

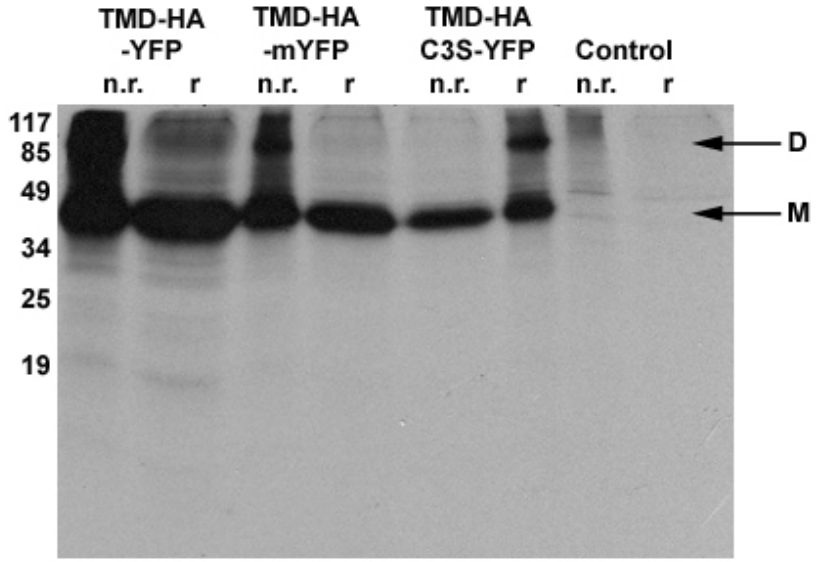

Figure 29: TMD-HA-XFP dimers. The mutation A206K was introduced in the fluorescent protein (producing the protein TMD-HA-mYFP) in order to avert the possible formation of dimers driven by the fluorophore. TMD-HA-YFP, TMD-HAC3S-YFP and TMD-HA-mYFP are compared. The gel clearly shows the presence of dimers (D, black arrow) even for the mutated protein (line 3 from the left, non-reducing conditions). The lower black arrow points to the monomer (M). n.r. = non-reducing conditions; r. = reducing conditions.

It has to be noted that in this experiment a 15% acrylamide gel was used. Therefore trimers might be masked by dimers since 10 and 12% gels clearly revealed the presence of this species (see below and gel in **Figure 28**). This result confirms that the formation of TMD-HA oligomers is not due to the intrinsic propensity to dimerizing of XFPs and that they are disulfide linked. Even though the oligomers were due to disulfide linkages, this experiment enforced the hypothesis that HA oligomerization might be critical not only for the export from the ER but also for the transport to the cell surface. The rate of dimer and trimer formation was then investigated. CHO-K1 cells transfected with TMD-HA-mYFP were labeled with [^{35}S]-Methionin for 2 hours (t_0) and then pulse-chased for 1 (t_1), 2 (t_2) or 4 (t_4) hours (see 3.2.3.5). Autoradiography revealed that the formation of oligomers follows the same kinetics of monomer synthesis (**Figure 30**) and that the amount of protein per species remains more or less unaltered during the chasing time. However this experiment points out that the degradation of the protein starts approximately 30 hours post transfection (compare the bands thickness in line t_4 with the other bands; t_4 = corresponds to more or less 30 hours, since protein are [^{35}S]-Met labeled 24 hours post transfection, for 2 hours and chased for 4 hours).

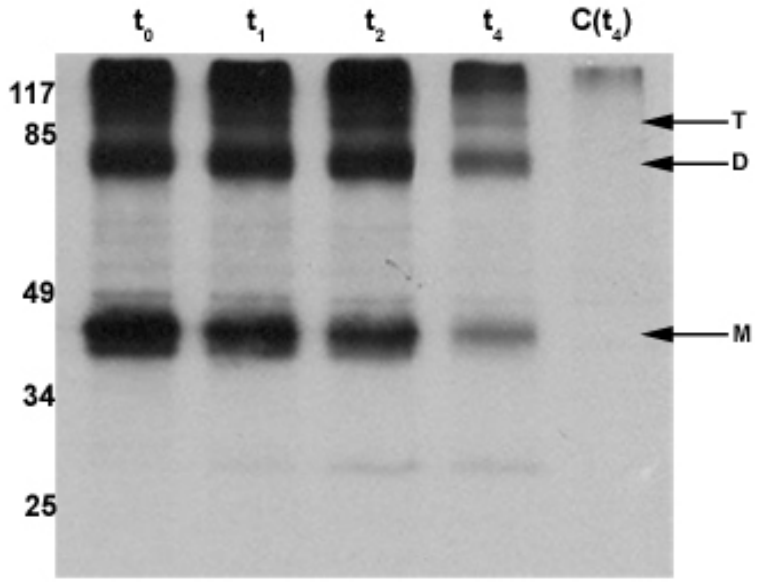

Figure 30: Pulse chase experiment. TMD-HA monomers (M), dimers (D) and trimers (T), indicated by the black arrows, are synthesized equally in the cell. The bands in line t_4 are less pronounced than the bands in the other lines pointing to a reduction of the protein amount probably due to degradation. t_0, t_1, t_2 and t_4 indicate the chasing times, i.e. t_0 corresponds to starting point of the chasing, t_1, t_2 and t_4 correspond to 1, 2 or 4 hours chasing (for details see text). The gel was run under non-reducing conditions.

4.2.4.1 TMD-HA-XFP CS mutants

The TMD-HA-XFP fusion protein contains 7 cysteine residues in its sequence. As already outlined, three of these are palmitoylated and they are localized within the transmembrane domain and the cytoplasmic tail (**Figure 31**, orange C residues in sequences **a** and **b** and mutated to S, pink colored in sequences **c** and **d**). Two other cysteines are found at position 537 of the TMD (**Figure 31**, C mutated to S, blue colored in sequences **b** and **d**) and in the signal peptide of the protein (indicated in **Figure 31** as C22S and blue colored). The remaining two cysteines are allocated in the fluorophore, precisely at position 49 and 71 (indicated in **Figure 31** as C49S and C71S and coloured in blue). In order to elucidate the dimerization mechanism and the cysteines involved in disulfide bond formation, several CS (mutation of cysteine to serine) mutants were made (see molecule scheme in **Figure 31**).

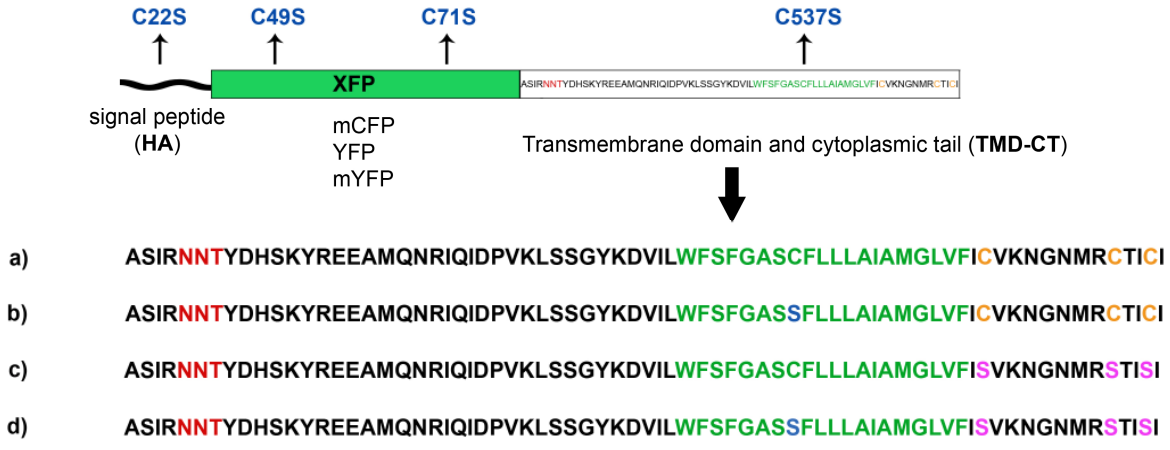

Figure 31: Summary of CS mutants. The different mutations inserted into TMD-HA protein in order to abolish dimerization are reported. In the signal peptide cysteine 22 was mutated to serine (C22S in blue) and fused to TMD-HA-XFP (XFP stands for mCFP, YFP and mYFP, see abbreviations). Mutations C49S and C71S were also inserted into mYFP and mCFP (indicated as C49S and C71S in blue). Finally, **a** is the TMD-HA wild type sequence; **b** is the same sequence with the mutation C537S (S in blue in the sequence) in the transmembrane domain; **c** is the sequence of the TMD-HAC3S (serines in pink correspond to the cysteine in orange mutated from sequences **a** and **b**) and d the TMD-HAC3S sequence with the CS (S in blue in the sequence) mutation in the transmembrane domain.

The cysteine 22 in the signal peptide was first mutated to a serine (namely SpCS mutation) generating the proteins SpCS-TMD-HA-YFP, SpCS-TMD-HA-mYFP and SpCS-TMD-HAC3S-YFP (In **Figure 31** indicated as C22S). Upon transfection, [^{35}S]-Methionine labelling and immunoprecipitation, gel autoradiography (**Figure 32**) revealed that the C22S mutation in the signal peptide did not have any effect on the oligomerization of TMD-HA variants. Indeed a thick band between 85 and 49 kDa could still be seen under non reducing conditions and it disappeared under reducing conditions. Again, trimers were not distinguishable since a 15% gel was used (**Figure 32**). This experiment demonstrates that disulfide linked oligomers, in particular dimers, are formed even in absence of C22 in the signal peptide.

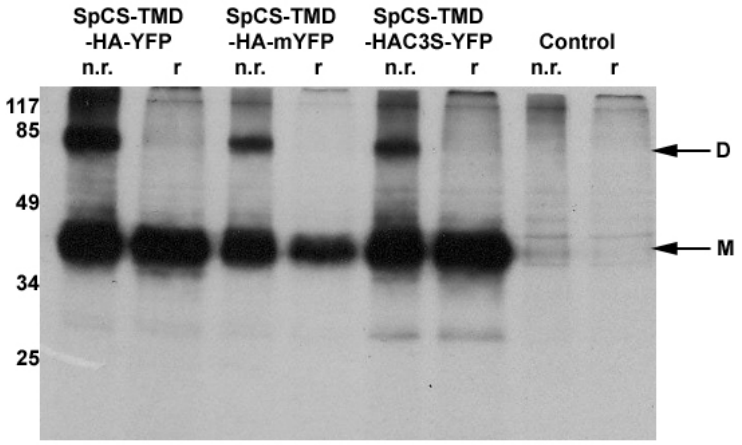

Figure 32: SpCS mutants form disulfide linked dimers. The mutation C22S did not have any effect since still disulfide linked oligomers are present under non-reducing conditions (n.r. bands between 85 and 49 kDa in lines l, 3, 5). Nore that under reducing conditions (r.) the dimer bands disapper (lines 2, 4 and 6). The black arrows point to the dimer (D) and monomer (M) bands.

For further investigation, cysteine 537 in the transmembrane domain was mutated to a serine (indicated in blue in the TMD-CT sequence shown in **Figure 31**, sequence **b**). The protein TMD-CS-HA-mYFP was generated in order to investigate the direct effect of the mutation. Furthermore, the protein SpCS-TMD-CS-HAC3S-YFP was also made to observe the effect of the mutation in a protein in which the only two cysteine residues left are localized within the fluorophore β-barrel (note, this protein contains the C22S mutation in the signal peptide and the C537S mutation in the transmembrane domain; furthermore the palmitoylation sites were also mutated to serines). Autoradiography (**Figure 33**) revealed that these two mutants still form dimers under non reducing conditions, since a faint band between 85 and 49 kDa was visible (compare lines 2, 4 and 6, **Figure 33**). However, in contrast to other experiments, the dimer signal was not that strong, even for the control protein TMD-HA-mYFP (e.g. compare the dimer band (D) in **Figure 33** with the one in **Figure 30**, line t_0). Due to this, also the presence of trimers could not be confirmed since a band at about 117 kDa was not clearly visible.

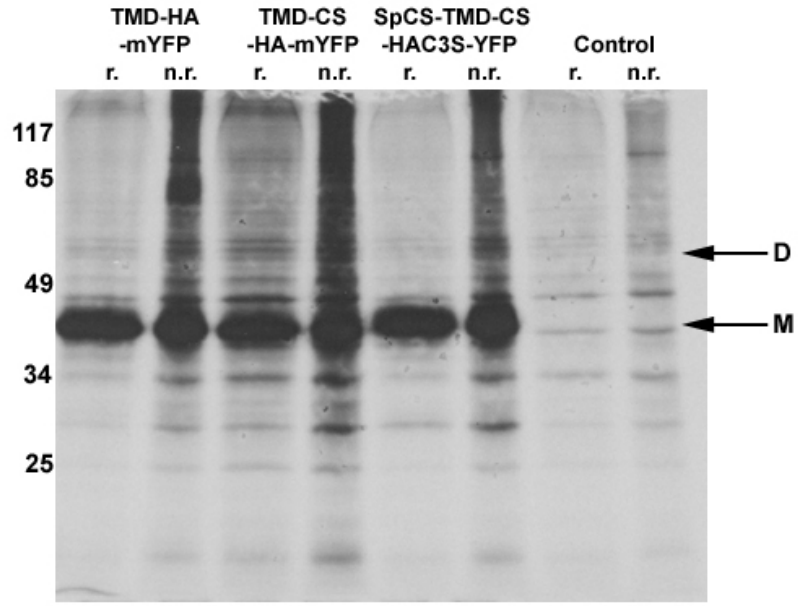

Figure 33: TMD-CS mutants form disulfide linked dimers. The CS mutation in the transmembrane domain did not abolish the formation of disulfide linked dimers (band between 49 and 85 kDa, pointed by the black arrow) as can be seen from the gel. The black arrows indicate the dimer (D) and monomer (M) bands. n.r. = non-reducing conditions; r. = reducing conditions.

The protein TMD-HA-mYFP and TMD-CS-HA-mYFP were also subjected to EndoH digestion in order to elucidate whether the mutation might affect the transport to the plasma membrane. The experiment was carried out under non-reducing conditions in order to distinguish between monomers, dimers and trimers (**Figure 34**). Only TMD-HA monomers, of both of the variants, were not resistant to EndoH digestion as can be seen from the bands between 34 and 49 kDa, in lines 1 and 3 (namely H). In fact, proteins not sensitive to EndoH should move in the gel as the non digested proteins (bands between 34 and 49 kDa in lanes 2 and 4, indicated with "–"). Therefore the monomeric form of TMD-HA variants is not delivered the cell surface. This result is in agreement with previous data showing that no full length-HA monomers are embedded in the cell plasma membrane [112]. Thus this experiment confirms that the artificial HA forms disulfide linked oligomers, irrespectively from the presence of the cysteine residue in the transmembrane domain and it also emphasizes that oligomer formation is a fundamental prerequisite for the transport of the TMD-HA proteins to the plasma membrane.

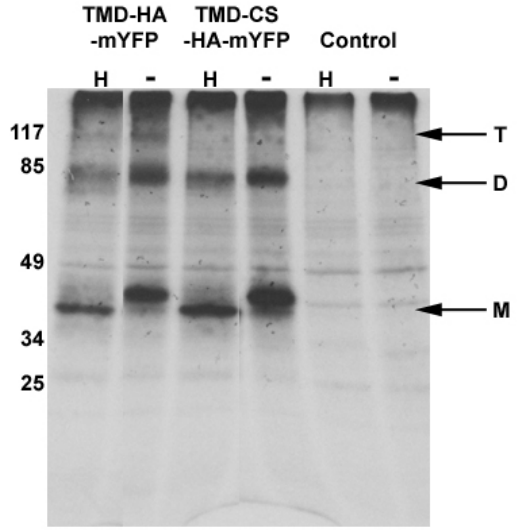

Figure 34: TMD-CS mutant. The TMD-HA mutant carrying the C537S mutation in the transmembrane domain as well as the TMD-HA wild type forms disulfide linked oligomers. Only oligomers (T and D indicated by the black arrows) of both of the variants are resistant to EndoH digestion (line 1 and 3), while the monomeric form (M, lower black arrow) are sensitive to this treatment. H = EndoH treated; "-" = non-EndoH treated.

According to the above results, it was hypothesized that TMD-HA oligomerization might be driven by disulfide bond formation between C49 and C71 in the XFP protein (as previously shown by Jain et al.[113]). Therefore, the double mutation C49S-C71S was introduced in the TMD-HA-mYFP sequence. CHO-K1 cells were transfected with TMD-HA-mYFP-C49S-C71S and labeled with [^{35}S]-Methionine. Samples were also subjected to EndoH resistance assay carried out under non reducing conditions. Surprisingly, oligomers (see gel in **Figure 35** A, line 4 (n.r.)) of TMD-HA-mYFP-C49S-C71S were still visible, but none of the species was EndoH resistant (**Figure 35** B, compare M, D and T bands in lines 2 and 4). These proteins retain the ability to oligomerize but they are not transported to the plasma membrane. Indeed, in this case, not only monomers were not EndoH resistant, but also dimers and trimers, (see gel **Figure 35** B, compare bands in lines 3 and 4), reported to be always EndoH resistant for all other TMD-HA variants discussed. Furthermore, confocal imaging of cells transfected with this construct revealed the total absence of fluorescence suggesting the uncorrect folding of YFP. Previous results also showed that C49 and C71 mutations in CFP and YFP led to the misfolding of the fluorophores [113]. Therefore due to defected folding, the protein undergoes uncorrect processing reflected in the lack of EndoH resistance. It has to be stressed that even in absence of both of the cysteines tought to be responsible for the oligomer formation, TMD-HA fusion proteins were still forming dimers and trimers (see protein C49SC71S in the gel in **Figure 35**, lines 3 and 4).

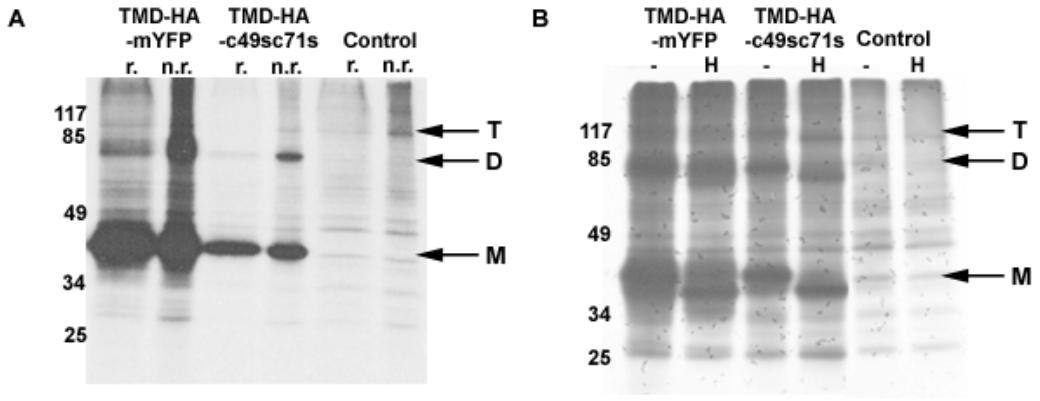

Figure 35: TMD-HA fusion proteins with mutations in the fluorophore form disulfide linked dimers. Mutations of residues C49 and C71 in the fluorophore, considered responsible for oligomerization did not abolish the formation of dimers and trimers (black arrows, T= trimer, D=dimer, M= monomer). In **A** the gel autoradiography of TMD-HA-mYFP and TMD-HA-C49SC71S under reducing (r.) and non reducing (n.r.) conditions, is shown. Oligomers (T and D pointed by the balck arrows) of the C49S-C71S mutant are still clearly visible under non reducing conditions (compare line 3 and 4 and also with line 1 and 2 of the wild type protein). In **B** the two proteins were subjected to EndoH digestion. Again in both cases, three different bands, representing the monomers (M), dimers (D) and trimers (T) are clearly distinguishable. TMD-HA-mYFP monomers (line 2 from left, lower band) only and in contrast, all the three TMD-HA-C49SC71S species (line 4 from left) were sensitive to EndoH digestion. H = EndoH treated; "-" = non-EndoH treated.

Single C49S or C71S mutations were also inserted and CHO-K1 cells were transfected with the constructs. Again confocal imaging showed the total absence of fluorescence probably due to the misfolding of the fluorophores. Hence, for this reason and since even the absence of both these residues was not enough for abolishing oligomerization, these proteins were not further studied.

4.2.4.2 Quantification of TMD-HA oligomers

Previous results showed that TMD-HA monomers form oligomers, mainly dimers and trimers. The amount of monomers, dimers and trimers produced, varies among the different TMD-HA mutants. To investigate this further, CHO-K1 cells were transfected with TMD-HA variants and labeled with [^{35}S]-Methionine. Immunoprecipitated proteins were then subjected to EndoH digestion and gel electrophoresis under non-reducing conditions. The result is reported in **Figure 36** and summarized in **Table 7**.

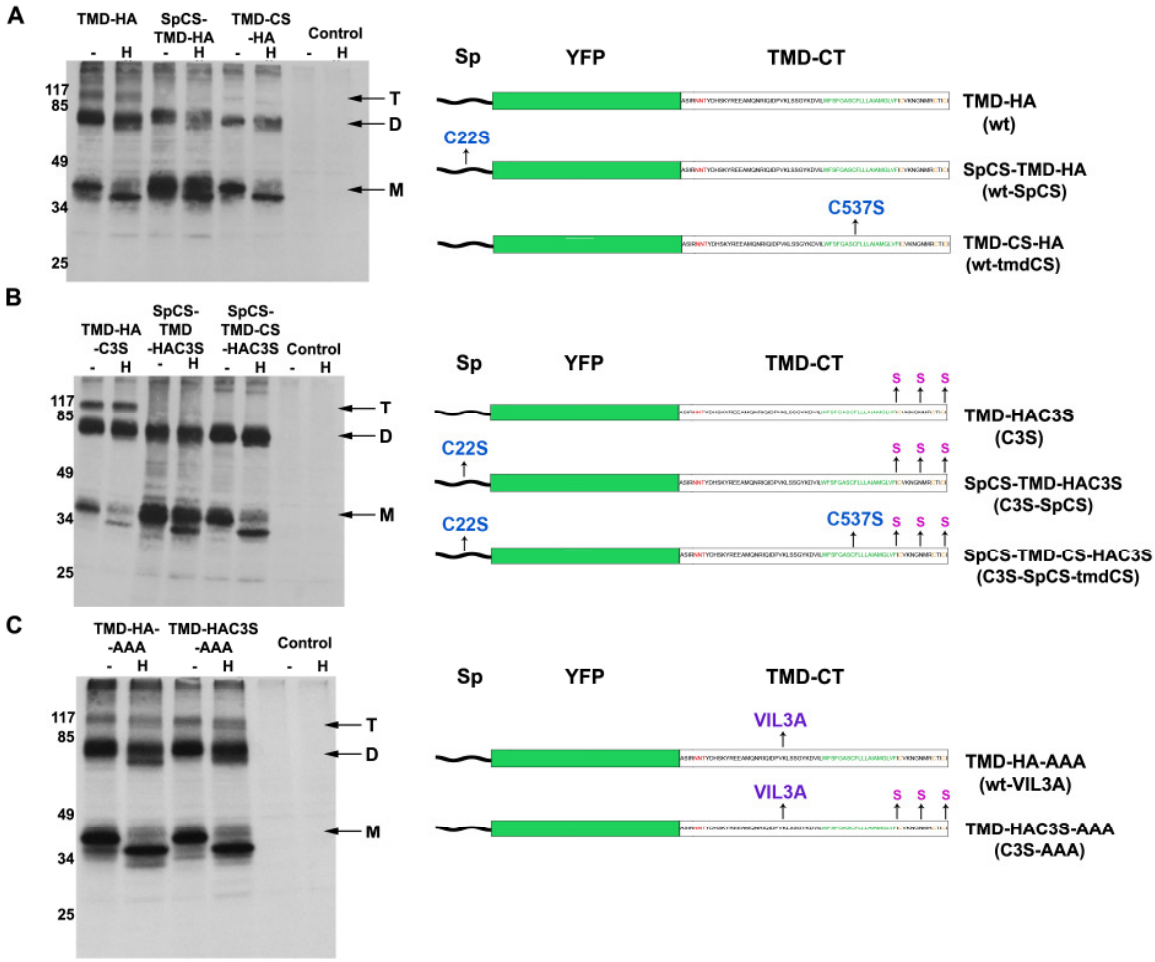

Figure 36: TMD-HA fusion proteins form different amounts of oligomers. The cartoons on the right side show the TMD-HA variants carrying different mutations, either in the transmembrane domain (TMD-CT, C537S in blue) or in the signal peptide (Sp, C22S in blue). In pink the S residues substituting the palmitoylation sites and in violet the mutation VIL3A are shown. The scheme of the TMD-HA wild type (wt) fusion protein is also depicted. The mutants as well as TMD-HA wild type, were subjected to EndoH digestion under non-reducing conditions, in order to elucidate which of the synthesized species, monomers (M), dimers (D), and trimers (T), indicated by the black arrows in the gels, and the relative amount effectively reaching the plasma membrane. In **A**, the SpCS with the C22S mutation in the signal peptide and the TMD-CS with the C537S mutation in the transmembrane domain are compared to the TMD-HA wild type. It is evident that the amount of trimers (T) formed by the two mutants is significantly decreased with respect to the trimers formed by the wild type protein. In **B**, the mutations C22S and C537S were inserted in the C3S protein (lacking palmitoylation sites). The gel shows the result of this experiment. Again it is visible that the C22S mutation in the signal peptide leads to the reduction or even absence of trimers. In **C** proteins with the VIL3A mutation in the transmembrane domain are shown. This mutation did not affect the oligomerization process, however it beared on the transport of the different species to the plasma membrane. H = EndoH treated; "-" = non-EndoH treated.

Table 7: Percentage of TMD-HA monomers, dimers and trimers. Monomer (M), dimer (D) and trimer (T) percentage of TMD-HA variants. The (H) indicates the EndoH sensitive subgroup of the species. Numbers represent the percentage of the species calculated on the total amount of protein (Ptot = T+D+M). Densiometric analysis of the bands was carried out using the Image J analysis program (see 3.2.5.1).

Oligomer	wt* (%)	wt-SpCS* (%)	wt-tmdCS* (%)	C3S* (%)	C3S-SpCS* (%)	C3S-SpCS-tmdCS* (%)	wt-VIL3A* (%)	C3S-VIL3A* (%)
M	-	41	-	12	42	23	-	-
M(H)	31	29	41	16	21	26	35	34
D	49	30	51	50	37	51	32	31
D(H)	-	-	-	-	-	-	19	17
T	20	-	8	22	-	-	14	17
T(H)	-	-	-	-	-	-	-	-

***wt** = TMD-HA; **wt-SpCS** = SpCS-TMD-HA; **wt-tmdCS** = TMD-CS-HA; **C3S** = TMD-HAC3S; **C3S-SpCS** = SpCS-TMD-HAC3S; **C3S-SpCS-tmdCS** = SpCS-TMD-CS-HAC3S; **wt-VIL3A** = TMD-HA-AAA; **C3S-VIL3A** = TMD-HAC3S-AAA

For simplicity, the full name of the different proteins is abbreviated in the text and in **Table 7**, but it is reported in **Figure 36** with the corresponding abbreviation on the right of the molecule scheme.

In general, apart from monomers, all the TMD-HA variants formed oligomers. Of these, usually dimers are more abundant than trimers, when present. Furthermore, in most cases, monomers do not show EndoH resistance, indicating that they are not transported to the plasma membrane. In contrast, oligomers always reach the cell surface.

wt TMD-HA forms 31% monomers, 49% dimers and 20% trimers (**Table 7**) whereas the C3S mutant presents 28% monomers (12% EndoH resistant, 16% (H) non EndoH resistant), 50% dimers and 22% trimers (**Table 7**). Interestingly, the protein C3S (lacking palmitoylation sites) formed monomers, which were partially transported to the plasma membrane (12%) in comparison to the total amount of wt monomers (31%), EndoH sensitive. However, the fraction of monomers, dimers and trimers was very similar for both TMD-HA variants (**Table 7**). Therefore, this result assured that FLIM-FRET (see 4.4.3.1) data could be directly compared. Surprisingly, monomers carrying the SpCS point mutation (C22S mutation in the signal peptide, see above), wt-SpCS, C3S-SpCS and C3S-SpCS-tmdCS, were partially delivered to the cell surface (**Table 7**, line M(H)). Moreover, these mutants do not form trimers. This indicates that probably trimerization occurs exclusively when the C in the signal peptide is present. Indeed, in the protein wt-tmdCS, carrying the C537 mutation in the transmembrane domain but not the C22S mutation in the singal peptide, trimerization was partially restored (8% of trimers were formed). The abolished trimerization of SpCS mutants was reflected in an increase of monomers with respect to the non mutated variants. In particular, the monomeric form (M) of wt represents the 31% of the whole protein, while the 70% (divided in 29%

M(H) and 41% M, **Table 7**) of the corresponding SpCS mutant (wt-SpCS) is monomeric. Likewise, the C3S-SpCS protein formed 63% of monomers (divided in 21% M(H) and 42% M, **Table 7**) whereas C3S only the 38% (16% M(H) and 12% M, **Table 7**). Thus, the reduced oligomerization, reflected in the total absence of trimers, is strongly related to the lack of the cysteine in the signal peptide. Mutation C537S in the transmembrane domain (TMD-CS) led to a slight decrease of trimer production. In particular, wt formed 20% of trimers, while the corresponding mutant carrying the TMD-CS mutation (wt-tmdCS) showed only 8% of trimers (**Table 7**). This result suggests that also the cysteine in the transmembrane domain might be involved in trimerization, but that its presence or absence is not as critical as the presence of the cysteine in the signal peptide. Finally, the VIL→AAA mutation (527-529 residues in the transmembrane domain, named VIL3A) did not affect the fraction of monomers, dimers and trimers compared to those observed for the wt and C3S proteins. Nevertheless, the amount of dimers transported to the plasma membrane was decreased. Indeed the wt-VIL3A dimers were only partially delivered to the plasma membrane (32% D and 19% D(H), see **Table 7**). Also the amount of C3S-VIL3A dimers reaching the plasma membrane was reduced to only 2/3 of the dimer fraction (31% D and 17% D(H), see **Table 7**).

4.2.4.3 Mutations in the HA-TMD do not affect protein stability

In order to investigate whether the C3S and VIL3A mutations could affect the stability and the transport of the proteins to the cell surface, TMD-HA-mYFP, TMD-HAC3S-YFP, TMD-HA-AAA-mYFP and TMD-HAC3S-AAA-mYFP were labeled with [^{35}S]-Methionine and pulse-chased for 1, 2 and 4 hours. The different samples were then subjected to EndoH resistance assay. This experiment, shown in **Figure 37**, revealed no significant differences in the synthesis of the four TMD-HA variants, thus confirming that the insertion of the mutations either alone (TMD-HAC3S or TMD-HA-AAA), or together (TMD-HAC3S-AAA) do not interfere with the correct folding of the proteins. As can be seen in **Figure 37** the oligomerization process of all four proteins follows the same kinetics. Furthermore, also the amount of monomers, dimers and trimers produced is comparable among the different TMD-HA species (**Figure 37**). As already pointed out, the monomeric form of some of the TMD-HA variants never acquires EndoH resistance. The formation of dimers occurs probably during the synthesis of the proteins (line **0** or $\mathbf{t_0}$, corresponding to about 26 hours after transfection. In all gels, the dimer band is indicated by a black arrow, between 80 and 58 kDa) and they acquire EndoH resistance after one hour of chasing (**1** or $\mathbf{t_1}$). In contrast, the trimeric form of all proteins is totally absent at t_0 and trimers (band between 80 and 175 kDa) appear only at t_1 showing EndoH resistance. It has to be outlined that while both monomers and dimers present an EndoH sensitive form, this is not the case for trimers. Hence, this result might indicate that while the formation of dimers occurs during the folding of the proteins (shown by EndoH sensitivity of the dimers at time **0**), trimerization might start when proteins have already passed

through the ER, either during the transport to the plasma membrane or directly into the plasma membrane.

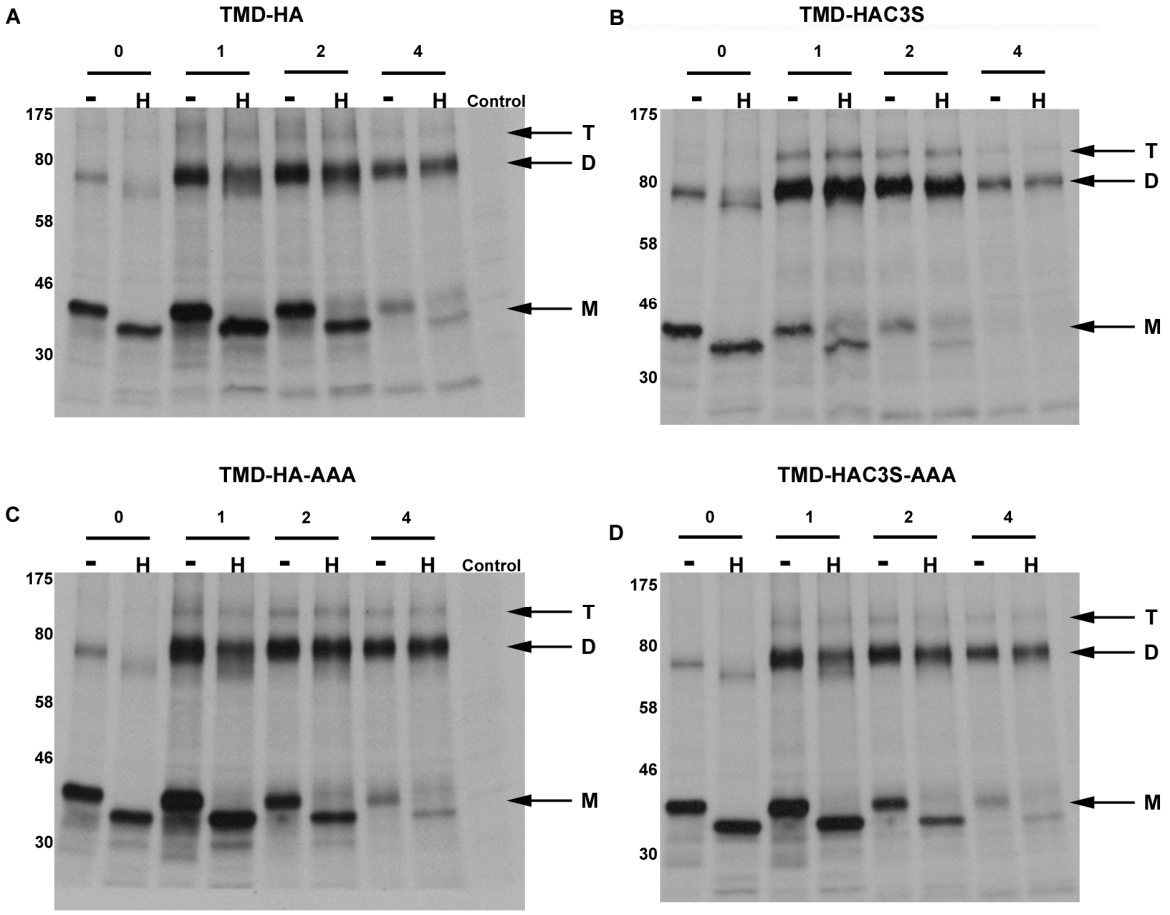

Figure 37: Absence of raft signals does not affect the synthesis and the intracellular transport of TMD-HA fusion proteins. Gel **A** and **C** show the EndoH pulse-chase experiment of the protein TMD-HA and its variant lacking the raft localization sequence VIL. Gel **B** and **D** report the result of the same experiment carried out with the TMD-HAC3S protein and its variant TMD-HAC3S-AAA. All four proteins present the same kinetics. The monomeric form is found to be sensitive to EndoH at all chasing times (0, 1, 2, 4), meaning that monomers are not transported to the plasma membrane. Although dimers are present at t_0, they acquire EndoH resistance only at t_1 (compare bands between 80 and 58 kDa, lines 0 H and 1 H). Finally trimers seem to be produced only secondly, since they apper only at t_1. 0 = t_0; 1 = t_1; 2 = t_2; 4 = t_4 (for more details see 3.2.3.5). Monomers (M), dimers (D) and trimers (T) are indicated by the black arrows.

4.3 Cell polarization and apical localization of GPI and TMD-HA proteins

MDCKII cells were transfected with TMD-HA-mYFP, TMD-HAC3S-YFP, GPI-YFP and MyrPal-mYFP and polarized in transwell plates. MyrPal-mYFP (kindly provided by Stephanie Engel) was used as control for apical transport. As shown in Figure 38 the four proteins were all transported to the apical membrane. As known, GPI-YFP and MyrPal-mYFP localize exclusively at the plasma

membrane, while TMD-HA variants are also abundant in the ER (compare Figure 17 with Figures 22, 23 and 25).

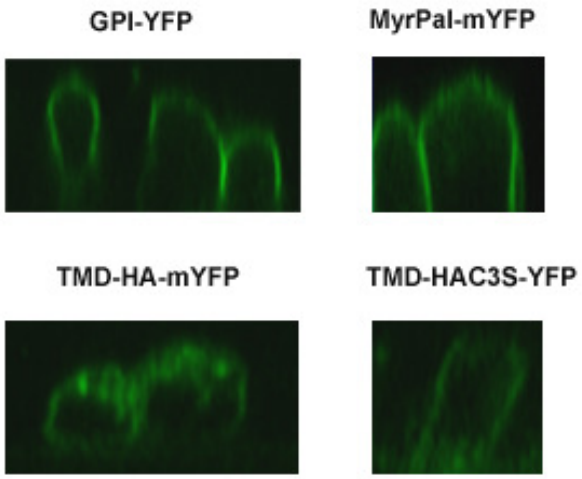

Figure 38: Cellular distribution of fluorescent constructs in polarized cells. CHO-K1 cells transfected with different constructs were polarized in order to investigate whether TMD-HA-YFP and TMD-HAC3S-YFP were apically transported.

4.4 Fluorescence lifetime imaging microscopy (FLIM)

In a living system it is impossible to know the local concentration of a fluorophore and also controlling its expression level. Furthermore, when samples are excited with a continuous laser beam, photobleaching leads to fluorescence intensity decrease. Therefore, quantitative studies based on intensity measurements become not reliable and very difficult to interpret. In contrast, fluorescence lifetime imaging microscopy (FLIM) measures the lifetime of a fluorophore, property typically independent of the probe concentration (see 1.4). FLIM is a very useful tool for measuring FRET since close proximity between donor and acceptor is reflected in a variation of the donor lifetime. Thus, FLIM-FRET was used to investigate *in vivo* the lateral organization of GPI-XFP proteins and TMD-HA-XFP variants. In Figure 39, typical FLIM images are shown for a cell expressing donor only (Figure 39 A, C), and a cell expressing both donor and acceptor (Figure 39 B, D) (A, B – whole cells, C, D – region of interest (ROI) corresponding to the plasma membrane). As evident from pseudocoloring the average lifetime of the donor in the plasma membrane was significantly reduced in the presence of the acceptor. This could be attributed to FRET from the donor to the acceptor.

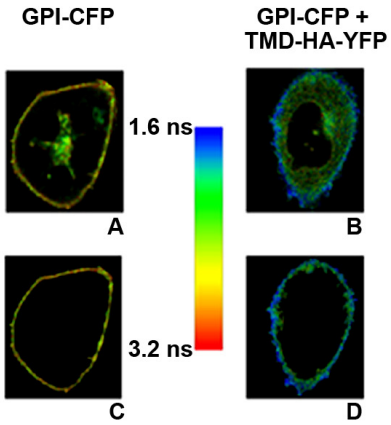

Figure 39: FLIM images. Typical examples of FLIM images are shown. A cell expressing only the donor (CFP) presents a significantly different coloring (**A** and **C**) compared to a cell coexpressing donor and acceptor (GPI-CFP and TMD-HA-YFP) as can be seen in **B** and **D**. The selection of the plasma membrane (**C** and **D**) allows calculating the lifetimes of the donor at different conditions. Experiments were carried out at 25 °C.

4.4.1 Monitoring donor and acceptor expression levels

Even if lifetime measurements are independent of protein levels, FRET efficiencies depend strongly on the acceptor concentration. Thus, in order to compare the results obtained from different cells, it had to be verified that the protein amount on the cell membrane was stable and comparable among the different experiments. Therefore, the expression level of different TMD-HA variants was monitored by measuring the fluorescence intensity of the proteins at the plasma membrane (see Methods). Figure 40 shows the mean intensity ratio between donor and acceptor (D/A ratio) for different donor and acceptor pairs. The standard error of estimate is low indicating that the scattering between individual cells is relatively small. Data set were obtained averaging the fluorescence intensity of donors and acceptors of about 30 to 50 cells. Only the D/A ratios of the most relevant D/A pairs are reported.

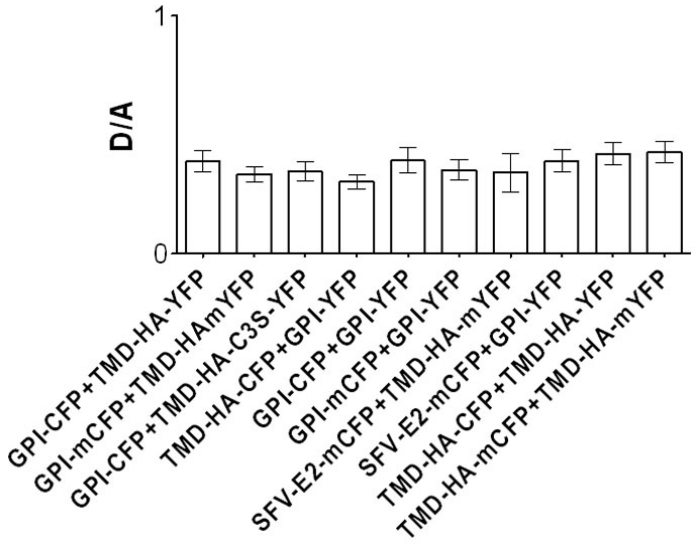

Figure 40: D/A ratio. The picture compares the donor to acceptor ratios of diverse pairs. As can be seen there is no significant difference within the probes, therefore FLIM-FRET experiments can be directly compared. Columns represent mean ± SEM.

4.4.2 Clustering of GPI-anchored proteins detected by FLIM-FRET

GPI-anchored fluorophores were used as raft markers to study *in vivo* the TMD-HA variants lateral organization. Therefore, it had first to be verified that GPI-anchored fluorescent proteins are raft associated. Transfection of CHO-K1 cells was carried out always under the same conditions and protein expression levels monitored as described above. Cells were transfected either with GPI-CFP or cotransfected with GPI-CFP and GPI-YFP (both proteins provided by Patrick Keller, [95]). In **Figure 41** the results of typical experiments for various donor-acceptor pairs are shown. Each point refers to a single cell. As can be observed, the average lifetime (τ_{AV}) of cells expressing only the donor varies in a range, which does not significantly overlap with the τ_{AV} of donor-acceptor coexpressing cells. The lifetime of GPI-CFP was shorter when the protein was coexpressed with the acceptor GPI-YFP indicating FRET (Figure 41). Furthermore, to ensure that energy transfer was due to clustering into lipid microdomains and not to dimerization of the fluorophores, CHO-K1 cells were transfected either with GPI-mCFP or with GPI-mCFP and GPI-YFP and the donor lifetime was measured (Figure 41). No significant variation in energy transfer was detected between the different donor-acceptor pairs, confirming that the clustering of the molecules was not caused by possible CFP dimerization.

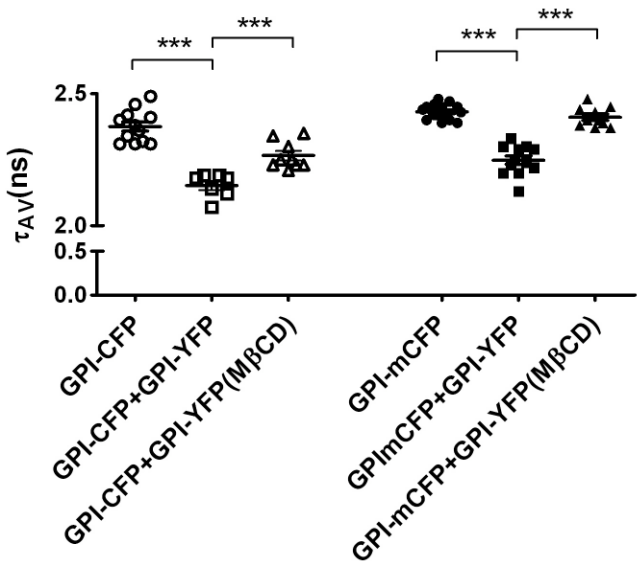

Figure 41: τ_{AV} measured in cells expressing GPI-CFP or GPI-mCFP and coexpressing GPI-YFP either with GPI-CFP or with GPI-mCFP. The result of a typical FLIM-FRET experiment is shown. FRET was measured pre and post incubation for 1 min at 4 °C, with a 5 mM solution of methyl-β-cyclodextrine (MβCD). Experiments were carried out at 25 °C. The t-test confirmed that the difference between the GPI-CFP lifetimes measured without or with acceptor are statistically significant (***p<0,0001). Each point refers to a single cell.

The mean average lifetime of about 10 cells was taken and the FRET efficiency E was calculated (see Material and Methods). FRET efficiency values vary between 10 and 12%, which are in agreement with previous data [106]. In order to disrupt rafts, plasma membranes were depleted of cholesterol by preincubation of cells with MβCD as described in Materials and Methods. Under those conditions 12 ± 1% (n = 4) of cholesterol was extracted from cells. Cholesterol depletion by MβCD of GPI-CFP/GPI-YFP coexpressing cells led to an increase of GPI-CFP lifetime (**Figure 41**) and to a reduction of the FRET efficiency (**Figure 42**), which dropped to 2-4%. The same set of experiments was repeated with the donor-acceptor pair GPI-mCFP/GPI-YFP and comparable results were obtained (see **Figure 41** and **Figure 42**).

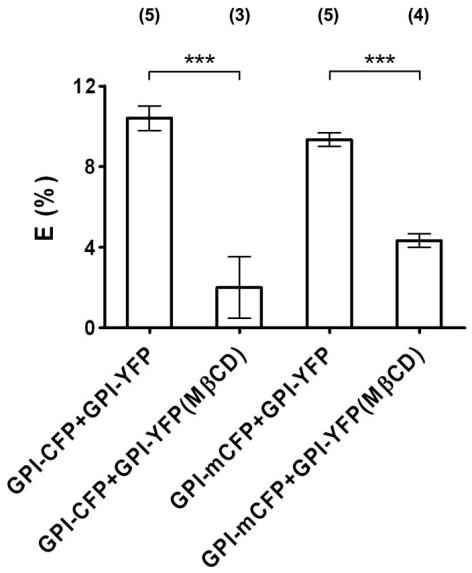

Figure 42: FRET efficiencies measured for GPI-XFP donor acceptor pairs in different conditions. FRET efficiency is drastically lowered upon extraction of cholesterol with MβCD, confirming raft localization of the proteins. Numbers in brackets indicate the number of experiments carried out. ***p<0,0009 between GPI-CFP+GPI-YFP and GPI-CFP+GPI-YFP(MβCD); ***p<0,0004 between GPI-mCFP+GPI-YFP and GPI-mCFP+GPI-YFP(MβCD). Columns represent mean ± SEM. The measurements were carried out at 25 °C.

Thus, these experiments not only confirmed that GPI-CFP localizes into rafts [93,106,114], but also ensured that FLIM-FRET is sensitive for measuring protein proximity in such a system.

4.4.3 Clustering of GPI- and TMD-HA proteins detected by FLIM-FRET

FLIM was used to study FRET between the GPI-CFP raft marker (donor) and the different TMD-HA-YFP variants (acceptor). To exclude that FRET was due to dimerization of the fluorophores, constructs with mutated residue 206 of CFP and YFP to lysine were also measured. Again, we could not detect any difference between constructs with wild type (CFP, YFP) and mutated fluorescent proteins (mCFP, mYFP) (compare sets of data in Figure 43 and **Figure 44**). The coexpression of TMD-HA-YFP or TMD-HA-mYFP with GPI-CFP or GPI-mCFP led to a significant shortening of donor lifetime (**Figure 43**). When cells coexpressing donor and acceptor were treated with MβCD, CFP lifetime increased very likely due to lipid raft disruption and increased distance between the fluorophores.

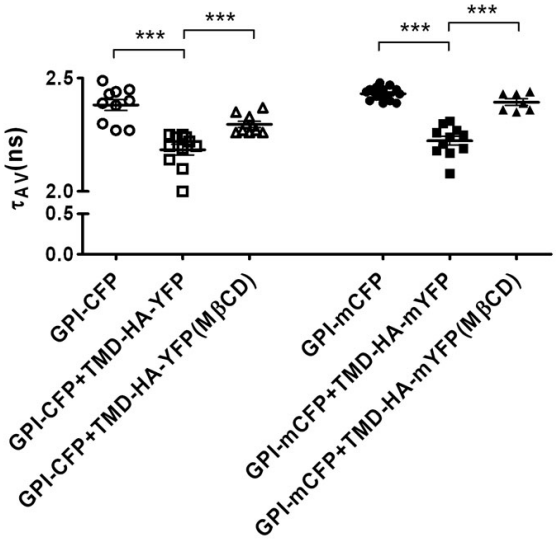

Figure 43: τ_{AV} distribution of GPI- and TMD-HA proteins. FLIM-FRET experiments were carried out in cells expressing GPI-CFP and GPI-mCFP, either alone or coexpressed with TMD-HA-YFP or TMD-HA-mYFP, respectively. Measurements were done at 25 °C. ***p<0,0001. Each point refers to a single cell.

As for the donor-acceptor pair GPI-CFP/GPI-YFP, the mean average lifetime of about 10 cells was taken and the FRET efficiency E was calculated. In **Figure 44** the average E is shown. Upon cholesterol depletion, a decrease of E between GPI- donors and TMD-HA-acceptors was observed (**Figure 44**, see also **Figure 42**).

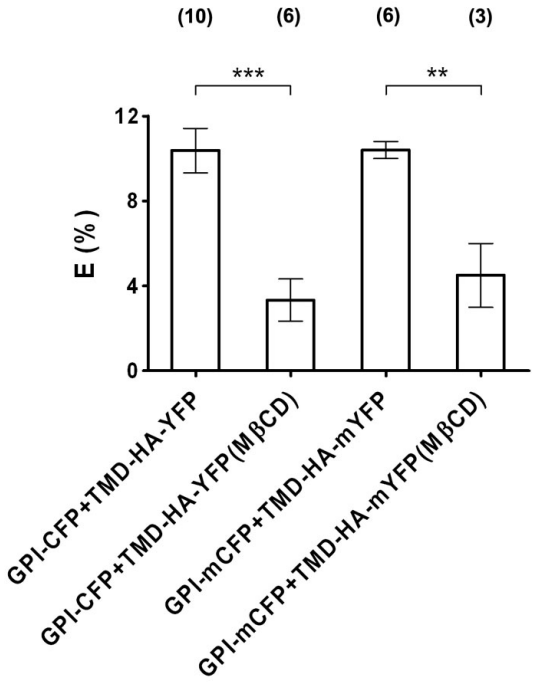

Figure 44: FRET efficiencies measured in cells coexpressing GPI-XFP and TMD-HA-XFP. Numbers within parenthesis indicate the number of experiments carried out. Measurements were done at 25 °C. ***p=0,0005 and **p=0,0024. Columns represent mean ± SEM.

Although FRET efficiencies would not be affected by diminishing the donor concentration, it was probed whether MβCD was extracting GPI-CFP. Cells were incubated with 5 mM MβCD for 1 min at 4 °C and the CFP fluorescence in the supernatant was measured. The fluorescence intensity was in the range of a few percent (3%) of the total CFP intensity, showing that the donor was stably anchored to the membrane. Moreover, CFP lifetime in cells expressing only the donor was not affected by MβCD treatment (τ_{AV} 2,37 ± 0,07 ns, in non treated cells and 2,33 ± 0,07 ns after MβCD treatment; values represent mean ± SD). Pretreatment of cells with the cytoskeleton disrupting agent cytochalasin D (as described in Methods) did not affect the lifetimes and thus the FRET efficiency between GPI-mCFP and TMD-HA-mYFP (as reported in **Figure 45** A and B).

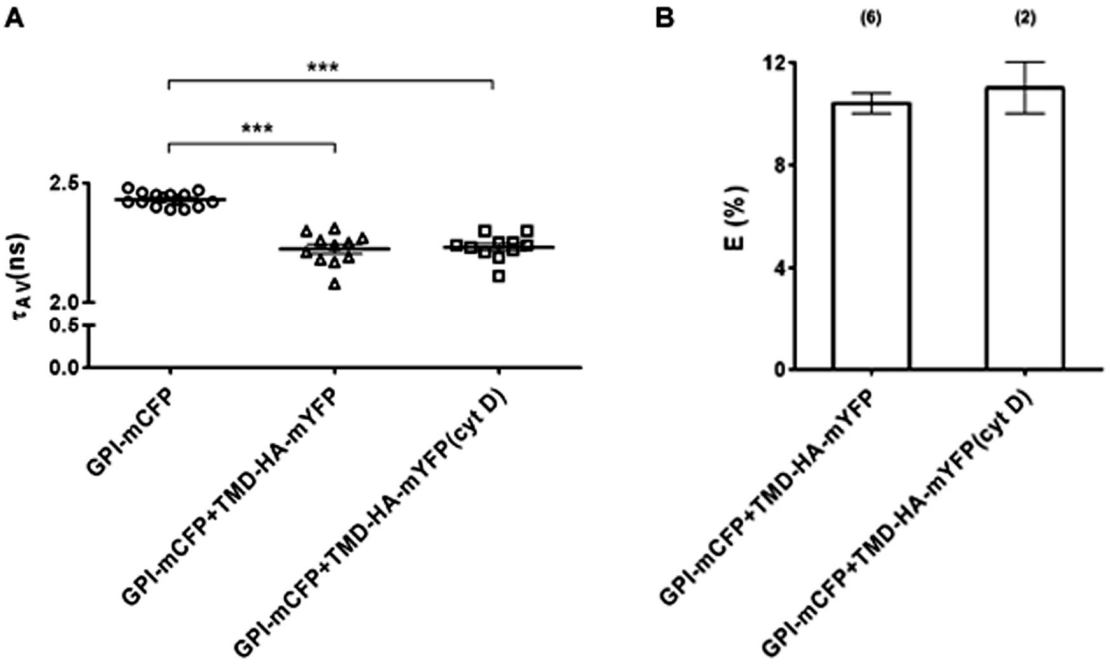

Figure 45: τ_{AV} and FRET efficiencies measured in cells treated with the cytoskeleton disrupting agent cytochalasin D (cyt D). The lifetime distribution (**A**) as well as the FRET efficiency (**B**) is not affected by the disruption of the cell cytoskeleton, which therefore might not be involved in the protein lateral organization. ***p<0,0001. In **A** each point refers to a single cell. In **B** numbers above bars refer to the number of independent experiments; columns represent mean ± SEM. Measurements were carried out at 25 °C.

Hence, it could be hypothesized that the cellular cytoskeleton might not play a critical role in the partitioning of TMD-HA fusion proteins into lipid enriched microdomains. Finally, DAPI (in blue in **Figure 46**) and Rhodamine-Phalloidin (in red in **Figure 46**) staining confirmed that the cytoskeleton was disrupted after cytochalasin D incubation without inducing cell death or affecting at the same time TMD-HA-mYFP distribution at the cell surface (see **Figure 46** D, in green). However, it has to be noted that cells adopt a more elongated form upon treatment.

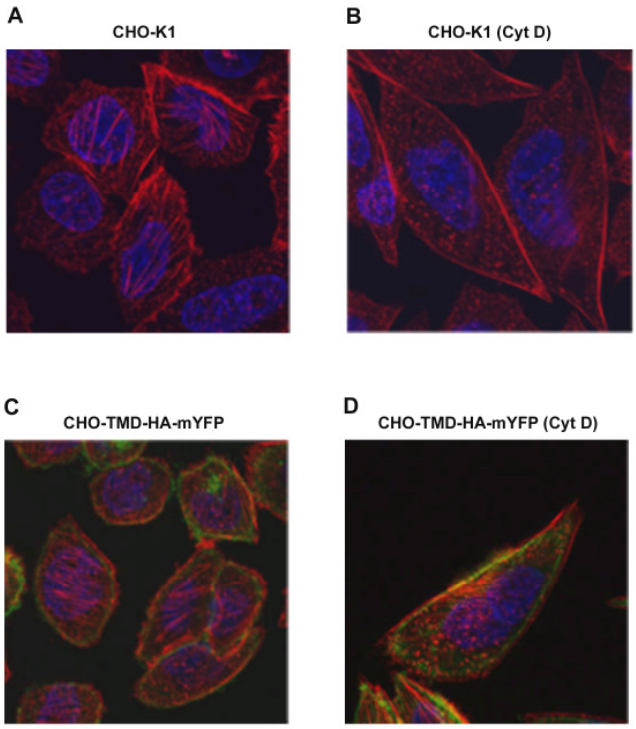

Figure 46: CHO cells treated with cytochalasin D. CHO-K1 cells and CHO-K1 cells stably expressing the TMD-HA-mYFP protein were stained with Rho-Pahlloidin (red) and DAPI (blue) pre (**A** and **C**) and post (**B** and **D**) cytochalasin D incubation. As can be seen in figure **B** and **D** the cytoskeleton depolarized under the effect of cytochalasin D, as indicated by the increased numbers of dotted structures and the absence of a real filamentous network (as in pictures **A** and **C**).

Coexpression of GPI-CFP with a fluorescent raft marker in the inner leaflet of the plasma membrane (MyrPal, provided by Stephanie Engel, Free University, Berlin) did not lead to any change in GPI-mCFP lifetime 2,43 ± 0,03 ns and 2,40 ± 0,06 ns in presence and absence of MyrPal-mYFP, respectively. Therefore the shortening of CFP lifetime in the presence of TMD-HA-YFP is not simply due to coexpression of a raft marker.

In principle, since energy transfer occurs between GPI-(m)CFP and TMD-HA-(m)YFP, FRET should have been observed also for the donor-acceptor pair TMD-HA-CFP and GPI-YFP. Surprisingly, in this case the difference between the lifetimes of the donor without and with the acceptor (**Figure 47** A), as well as the FRET efficiency (**Figure 47** B) was less pronounced in comparison to the pair GPI-CFP and TMD-HA-YFP (compare **Figure 44** and **Figure 47** B). Again the coexpression of TMD-HA-mCFP with GPI-YFP provided essentially the same results; therefore this pair was not studied further.

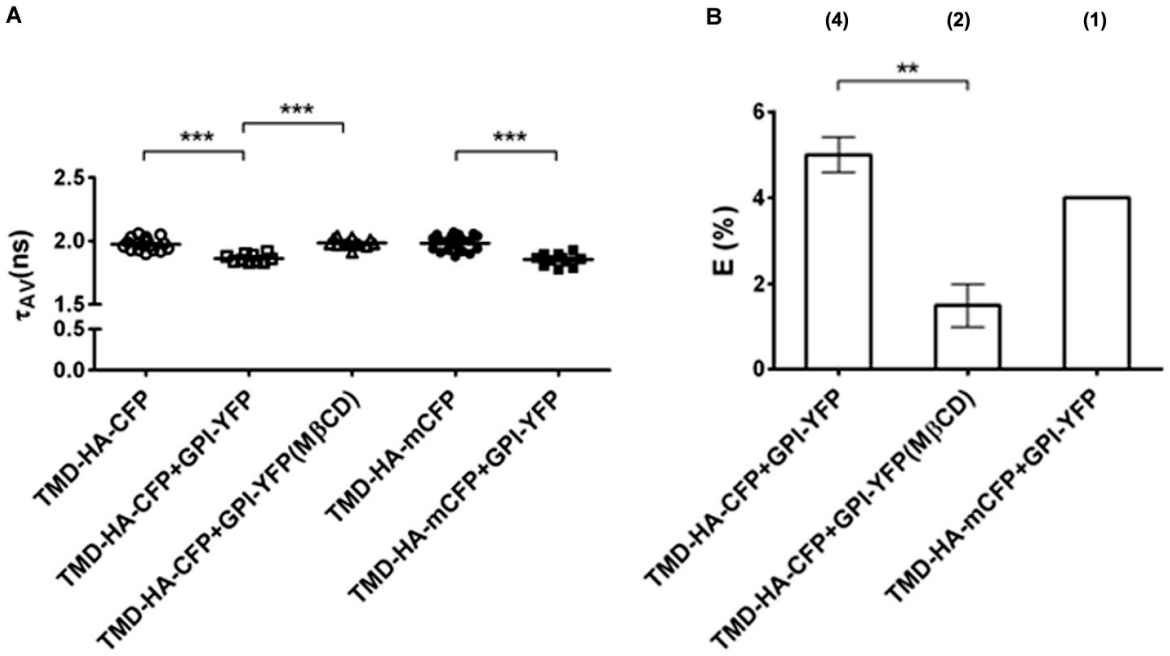

Figure 47: FRET between TMD-HA-CFP and GPI-YFP. In (**A**) the τAV distribution of TMD-HA-CFP expressed alone or coexpressed with GPI-CFP is reported. It can be noted that TMD-HA-CFP presents a shorter lifetime than GPI-CFP (see Figure 44). This is due to dimerization of the donor (described in the text). Nevertheless, FRET was measured (**B**). Although efficiencies were lower than normally calculated (see Figure 44), they were reproducible and they were decreased upon extraction of cholesterol (MβCD). ***p<0,0001 and **p<0,0069. In **A** each point refers to a single cell. In **B** columns represent mean ± SEM and numbers above bars refer to the number of independent experiments. Measurements were carried out at 25 °C.

Notably, TMD-HA-CFP lifetime was much shorter than that of GPI-CFP when expressed in the absence of the respective YFP acceptor (compare **Figure 43** and **Figure 47** A). As discussed above, TMD-HA fusion proteins are organized as dimers in the plasma membrane. Thus, CFP molecules of TMD-HA-CFP are in very close proximity and may undergo self-quenching (also named pseudo-homoFRET, see 5.1.1) [115] or larger aggregates may even change the local refractive index, which may strongly affect CFP average lifetime [116].

4.4.3.1 Clustering of GPI- and TMD-HA mutants detected by FLIM-FRET

To investigate the role of palmitoylation in lateral organization, the non-palmitoylated mutant, TMD-HA-C3S-YFP, was coexpressed with GPI-CFP. In that case the lifetimes were longer than those measured for GPI-CFP in TMD-HA-YFP coexpressing cells (compare Figure 43 and **Figure 48** A).

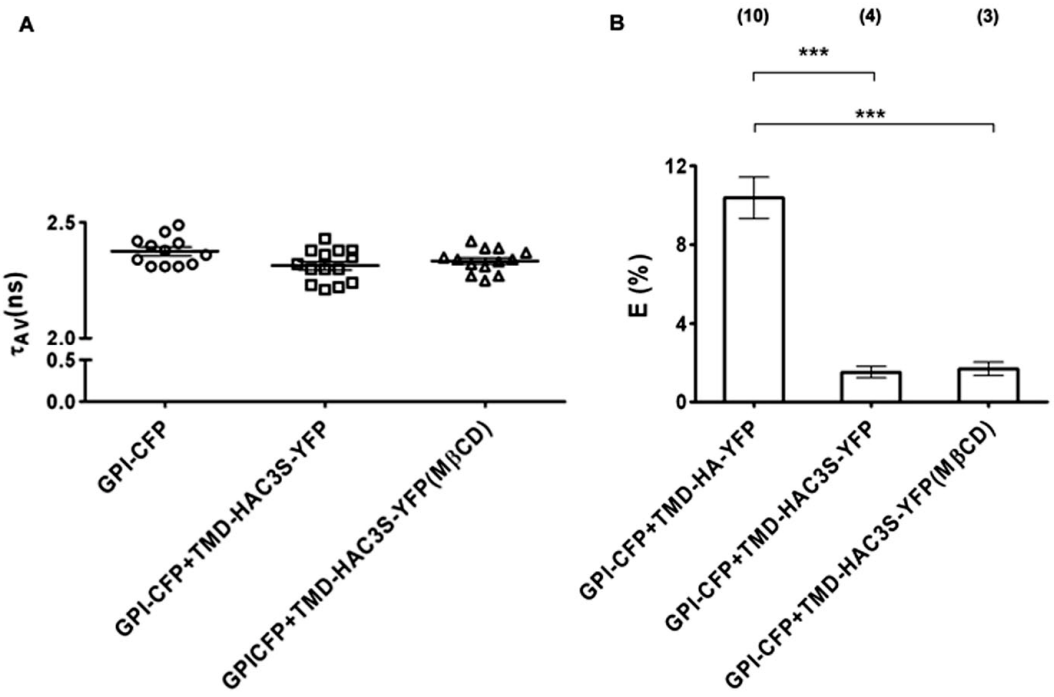

Figure 48: FRET efficiency and τ_{AV} of samples coexpressing GPI-CFP and TMD-HAC3S-YFP. GPI-CFP lifetime does not change when coexpressed with TMD-HAC3S-YFP (**A**), leading to a very low FRET efficiency (**B**) which did not change upon preincubation with MβCD. ***p<0,0002 between GPI-CFP+TMD-HA-YFP and GPI-CFP+TMD-HAC3S-YFP; ***p<0,0009 between GPI-CFP+TMD-HA-YFP and GPI-CFP+TMD-HAC3S-YFP(MβCD). In **A** each point refers to a single cell. In **B** columns represent mean ± SEM and numbers above bars refer to the number of independent experiments. Measurements were carried out at 25 °C.

The FRET efficiency was only about 2% (**Figure 48** B). Depletion of cholesterol by treatment of cells with MβCD-extraction did not show any effect on lifetimes (**Figure 48** A), and thus on the FRET efficiency (**Figure 48** B) in contrast to the sample expressing TMD-HA-YFP (**Figure 44**). Therefore this result confirms the importance of palmitoylation for lipid raft localization of TMD-HA fusion proteins.

In order to study the effect of raft signal abolishment (see above) on the TMD-HA sequence, GPI-mCFP was also coexpressed with TMD-HA-AAA and TMD-HAC3S-AAA mutants. As expected, mCFP lifetime did not vary when coexpressed with the acceptor (**Figure 49** A) and no significant energy transfer was measured in both cases, underlining the critical role played by this sequence as raft-localization signal (see **Figure 49** B).

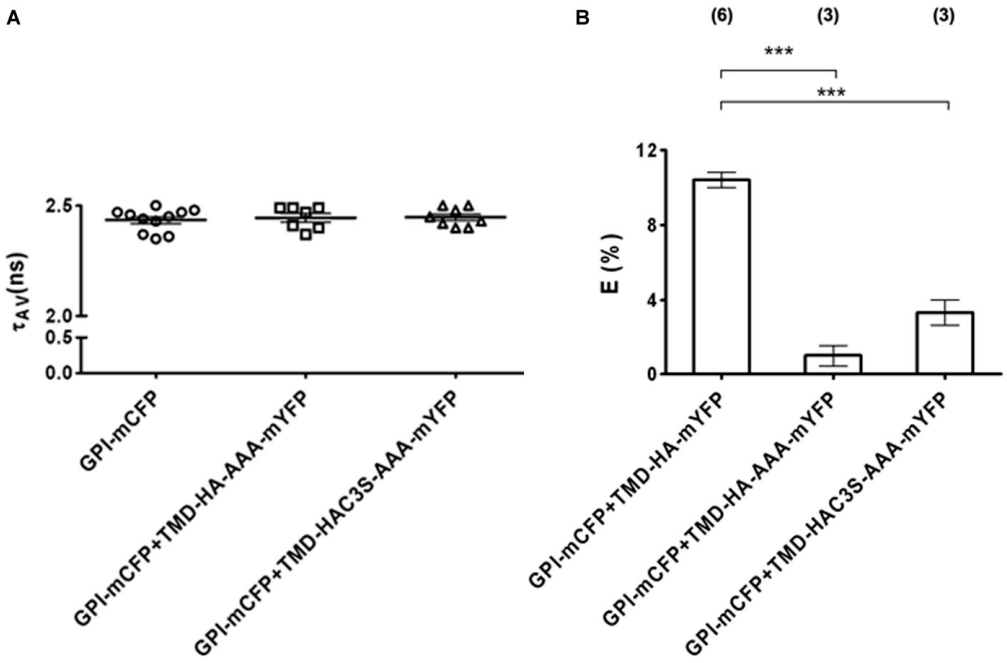

Figure 49: FRET between GPI-mCFP and TMD-HA mutants. GPI-mCFP lifetime did not change upon coexpression with the TMD-HA mutants, TMD-HA-AAA-mYFP and TMD-HAC3S-AAA-mYFP (**A**). Therefore no significant energy transfer was measured (**B**). ***p<0,0001. In **A** each point refers to a single cell. In **B** columns represent mean ± SEM, and numbers above bars refer to the number of independent experiments. Experiments were carried out at 25 °C.

4.4.3.2 FRET efficiency as a function of the acceptor intensity

In order to verify that energy transfer was indeed due to clustering, FRET efficiencies were plotted against the acceptor intensity and fitted with a one-site hyperbola function (as described in Methods). In **Figure 50** A and C the result for the donor-acceptor pairs GPI-CFP/TMD-HA-YFP and GPI-mCFP/TMD-HA-mYFP and GPI-CFP/GPI-YFP and GPI-mCFP/GPI-YFP is reported. As can be observed, increased acceptor levels did not lead to an increase in FRET efficiencies, thus assuring that the FRET efficiency fluctuations are not directly proportional to the acceptor amounts. This result is also reflected in the K_D value (Table 8), significantly smaller than the averaged acceptor intensity. Therefore, the influence of the acceptor expression level on the calculation of the FRET efficiencies could be neglected and the cells cotransfected with different combinations of donor-acceptor pairs directly compared. In **Figure 50** B and D the fitting was done for the same donor-acceptor pairs after extraction of cholesterol. The curve acquires a more linear shape, pointing to a higher dependence of FRET from the acceptor concentrations. Furthermore, the K_D value was about 4 times higher (Table 8), indicating less clustering of the molecules due to lipid rafts disruption.

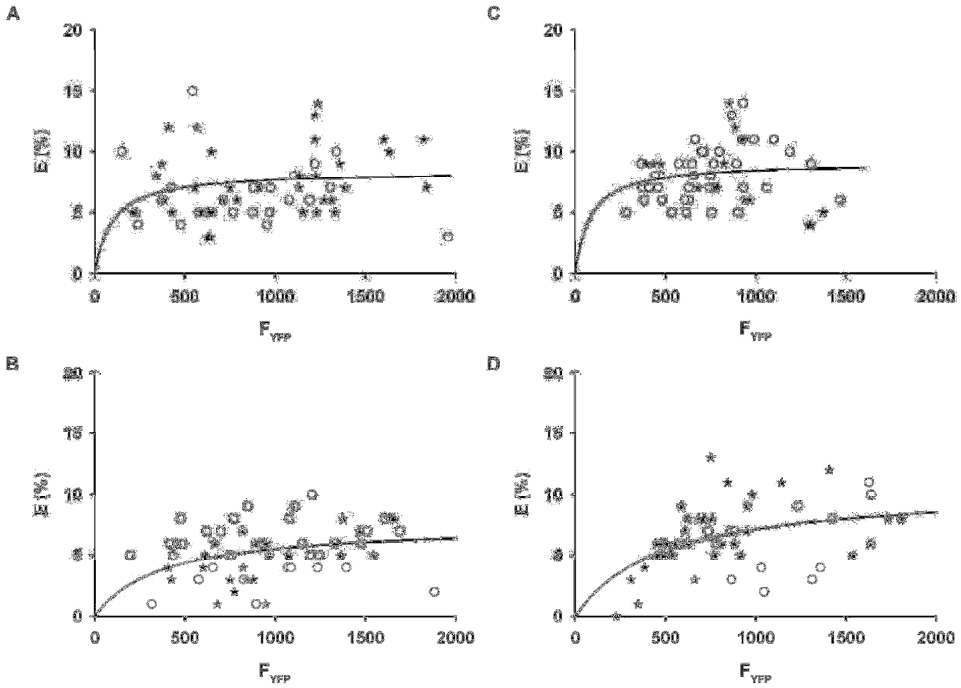

Figure 50: One site hyperbola fitting of FRET efficiencies vs acceptor concentration. In pictures **A** and **C** the fitting was done for the donor-acceptor pairs GPI-CFP/TMD-HA-YFP (o) and GPI-mCFP/TMD-HA-mYFP (*), GPI-CFP/GPI-YFP (o) and GPI-mCFP/GPI-YFP (*). Curves reach a plateau and clearly, increasing the acceptor concentration does not lead to an increase in FRET efficiency. In contrast, upon extraction of cholesterol (**B** and **D**) the residual FRET depends from the acceptor concentration as demonstrated by higher K_D values (see text). E(%) = FRET efficiency in %; F_{YFP} = acceptor concentration.

Table 8: K_D values. FRET efficiencies and acceptor intensities of the donor-acceptro pairs GPI-CFP/TMD-HA-YFP and GPI-mCFP/TMD-HA-mYFP, GPI-CFP/GPI-YFP and GPI-mCFP/GPI-YFP were fitted with a one-site hyperbola function (see Methods). The K_D values calculated from the fitting indicate the reduced clustering between the proteins upon exctraction of cholesterol (MβCD). For more details see text and Methods. n= number of cells analized.

D-A couple	K_D	K_D (MβCD)
GPI-CFP/GPI-YFP **GPI-mCFP/GPI-YFP**	81 (n = 52)	475 (n = 48)
GPI-CFP/TMD-HA-YFP **GPI-mCFP/TMD-HA-mYFP**	94 (n = 59)	366 (n = 56)

This kind of fitting was not carried out when both donor and acceptor were TMD-HA variants. Since they form disulfide linked oligomers, the curve as well as the K_D values would reflect the oligomerization state and therefore would not give further information about the clustering of the proteins in lipid microdomains.

4.4.4 Clustering of TMD-HA and TMD-SFV detected by FLIM-FRET

Unlike influenza virus, semliki forest virus (SFV) does not appear to utilize lipid rafts as recruitment site of its components [117,118]. No enrichment of virus spike proteins in detergent resistant fractions was found [40]. In order to generate a protein acting as a non raft marker, a transmembrane domain based on the SFV glycoprotein E2 was fused to mCFP. Potential palmitoylation sites were replaced to abolish any residual interaction with raft-like lipid domains. FLIM-FRET experiments were carried out in cells coexpressing SFV-E2-mCFP and either TMD-HA-mYFP or GPI-YFP. As shown in **Figure 51** B, in both cases no significant energy transfer was detected as well as no significant variation of mCFP lifetime was measured (**Figure 51** A). Thus, these results indicate that the spike proteins of SFV do not associate preferentially with cholesterol enriched domains and enforce the hypothesis of a preferential localization of TMD-HA fusion proteins into lipid rafts domains. The comparison between the donor-acceptor pairs TMD-HA-CFP+GPI-YFP and SFV-E2-mCFP+GPI-YFP shows that indeed the energy transfer measured for the former pair is due to clustering into lipid domains and not to random interaction. We can also exclude that the higher FRET is due to higher expression levels of the proteins since the D/A ratio presented by the two different couples is similar (see **Figure 40**).

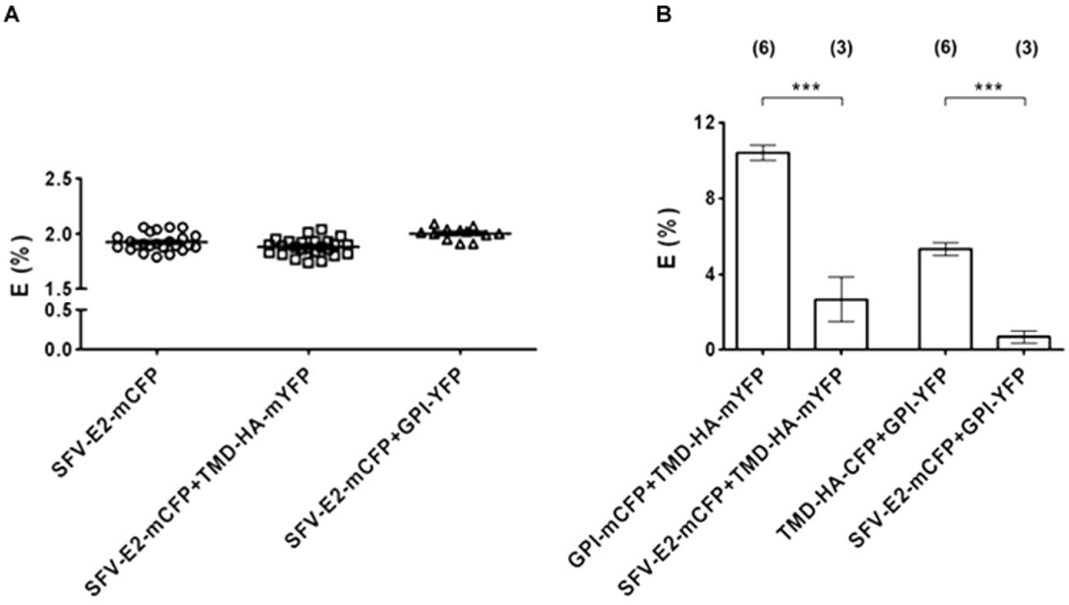

Figure 51: Energy transfer does not occur between the non raft protein SFV-E2-mCFP and TMD-HA-mYFP. SFV-E2-mCFP coexpressed either with TMD-HA-mYFP or with the raft marker GPI-YFP, did not show significant FRET (B) or a shortening of SFV-E2-mCFP lifetimes (A). Indeed there is a clear difference between FRET efficiencies measured when TMD-HA-mYFP is coexpressed with GPI-mCFP or SFV-E2-mCFP (***p<0,0003), as well as when GPI-YFP is coexpressed with TMD-HA-CFP or SFV-E2-mCFP (***p<0,0006). In A each point refers to a single cell. In B columns represent mean ± SEM, and numbers above bars refer to the number of independent experiments. Experiments were carried out at 25 °C.

4.4.5 TMD-HA protein clustering

FLIM-FRET was also used to investigate clustering of TMD-HA molecules with each other. To this aim, several combinations of different TMD-HA donor-acceptor pairs were coexpressed and energy

transfer was measured. Surprisingly, FRET was observed in all cases (summarized in **Table 9**, numbers are FRET efficiencies given in %), even upon MβCD treatment. **Figure 52** reports the lifetimes and FRET efficiency of selected TMD-HA pairs. FRET efficiencies oscillate between 10 and 18% and it was measured even between TMD-HA variants previously demonstrated to localize in different regions of the cell plasma membrane (e.g. between TMD-HAC3S-YFP and TMD-HA-CFP, see **Figure 52**). It has also to be stressed that upon extraction of cholesterol FRET efficiency increases. This result is totally in contrast with the above results showing a decrease of energy transfer in cells treated with MβCD.

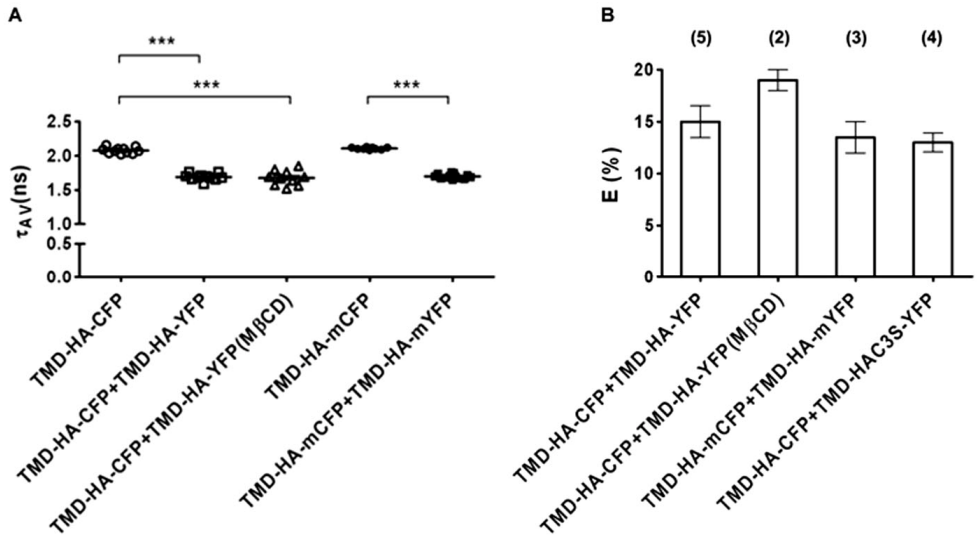

Figure 52: TMD-HA fusion proteins form oligomers. Upon coexpression of TMD-HA-XFP proteins high energy transfer was measured. Explanation for this behaviour is given by the fact that the proteins form disulfide linked dimers and trimers. In **A** the lifetimes for the most significant experiments (***p<0,0001) are reported and in **B** the corresponding FRET efficiencies are shown. In **A** each point refers to a single cell. In **B** columns represent mean ± SEM, and numbers above bars refer to the number of independent experiments. Experiments were carried out at 25 °C.

Table 9: FRET efficiencies between TMD-HA constructs expressed in CHO cells. The table reports the experiment carried out with different TMD-HA donor-acceptor pairs. In red samples subjected to MβCD extraction. The numbers within parentheses refers to the number of experiments. n.m. = not measured.

Acceptor / Donor	TMD-HA-YFP	TMD-HA-mYFP	TMD-HAC3S-YFP
TMD-HA-CFP	12 ± 2 (5) / 18 ± 1 (2)	17	13 ± 1 (4)
TMD-HA-mCFP	n.m.	10 ± 2 (4)	12 ± 1 (2)
TMD-HAC3S-YFP	9	n.m.	8 / 8

Different observations led to the hypothesis that TMD-HA fusion proteins are forming stable oligomers. The first observation concerned CFP lifetimes, which varied significantly when the fluorophore was fused either to GPI or to TMD-HA. In **Table 10** the lifetimes (in ns) for the different donor proteins are reported.

Table 10: Fluorescence lifetime of different CFP constructs. The numbers within parentheses refer to the number of experiments. In every experiment about 10 to 12 cells were measured. Numbers represent mean ± SD. Measurements were carried out at 25 °C.

GPI-CFP	TMD-HA-CFP	GPI-mCFP	TMD-HA-mCFP
2,37 ± 0,03 (8)*	1,97 ± 0,03 (10)*	2,49 ± 0,04 (8)*	1,99 ± 0,06 (4)*

The lifetime of both GPI-CFP and GPI-mCFP is longer than the one of TMD-HA-CFP and TMD-HA-mCFP. The shortening in lifetime for TMD-HA fused donors is probably due to pseudo-homoFRET or self-quenching (see Discussion), which can occur only when fluorophores are in very close proximity (e.g. due to oligomer formation). The second observation was based on experiments in which cotransfected cells were depleted of cholesterol. As shown above, extraction of cholesterol from cells expressing GPI-/GPI- and GPI-/TMD-HA- CFP/YFP pairs leads to a decrease of FRET efficiencies. In contrast, this was not observed when the treatment was applied to cells coexpressing TMD-HA fusion proteins (**Table 9**). In particular, significant energy transfer was measured when TMD-HAC3S-CFP was coexpressed either with TMD-HA-YFP or with TMD-HAC3S-YFP (**Table 9**). Notably, no clustering between GPI-CFP and TMD-HAC3S-YFP (4.4.3.1) was observed. Finally it has also to be stressed that the FRET efficiency between coexpressed donor-acceptor pair TMD-HA-CFP and TMD-HA-YFP was higher than for the pair TMD-HA-YFP and GPI-CFP. Finally, in order to investigate FLIM-FRET between TMD-HA monomers, cells transfected with TMD-HA-mCFP and TMD-HA-mYFP were incubated with DTT (10 mM). As shown in **Figure 53**, the treatment did not have any effect on the TMD-HA-mCFP lifetimes. However, it has to be stressed that the DTT solution used was only 10 mM, 40 times less concentrated than the one normally used in protein electrophoresis to disrupt disulfide bonds. Therefore, it cannot be proved that DTT really disrupted the disulfide linkages between the proteins. A 400 mM DTT solution led to cell death and thus could not be used.

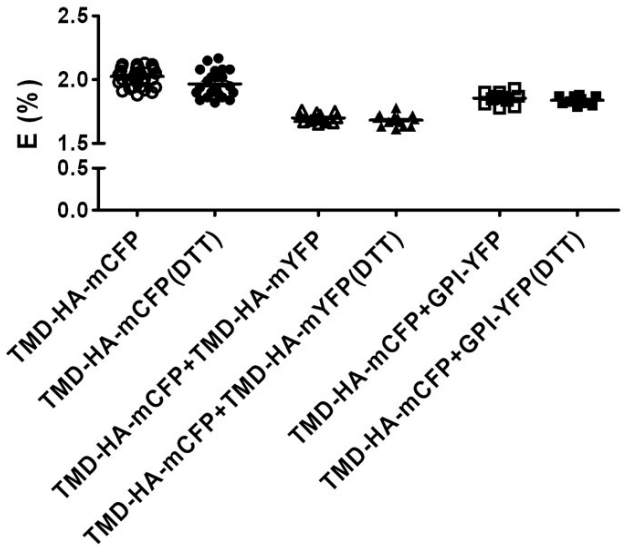

Figure 53: TMD-HA-mCFP lifetime is not affected by DTT treatment. Incubation of cells coexpressing TMD-HA-mCFP and TMD-HA-mYFP or GPI-YFP with a 10mM DTT solution did not affect mCFP lifetime. Each point refers to a single cell. Experiments were carried out at 25 °C.

Taken together all these observations strongly supported the hypothesis of a direct neighborhood of TMD-HA-constructs. Thus the measured FRET efficiency indicates lipid domain independent association of the constructs. To sustain this conclusion time resolved anisotropy measurements were performed (see below).

4.4.6 Time-resolved fluorescence spectroscopy of purified plasma membranes

To assess lateral organization of fluorescent GPI and TMD-HA constructs by an independent technique, we performed homoFRET measurements by measuring time-resolved anisotropy. I.e., in samples containing only donor (GPI-mCFP) or only acceptor (TMD-HA-mYFP), energy homotransfer could be assessed from picosecond resolution fluorescence anisotropy decays, which is translated to information on the aggregation state of the donor and the acceptor separately, an important knowledge to rationalize the heteroFRET data. This approach should give in principle equivalent results, since FRET efficiency is based on FLIM measurements where 1) a ROI was selected containing only the plasma membrane pixels; 2) the photons collected in those pixels were summed up to obtain a fluorescence intensity decay with a large number of counts (as in a cuvette experiment), and 3) the data from a large number of cells from several independent samples were used to compute the final values. For this purpose, plasma membranes of CHO-cell lysates expressing either GPI-mCFP or TMD-HA-mYFP, or coexpressing GPI-mCFP and TMD-HA-mYFP were purified by Nycodenz step-gradient. As shown (**Figure 54**) top fractions used for

measurements are enriched of TMD-HA and GPI- fluorescent proteins and contain only minor amounts of ER and Golgi membranes as proven by Western Blot analysis (**Figure 54**).

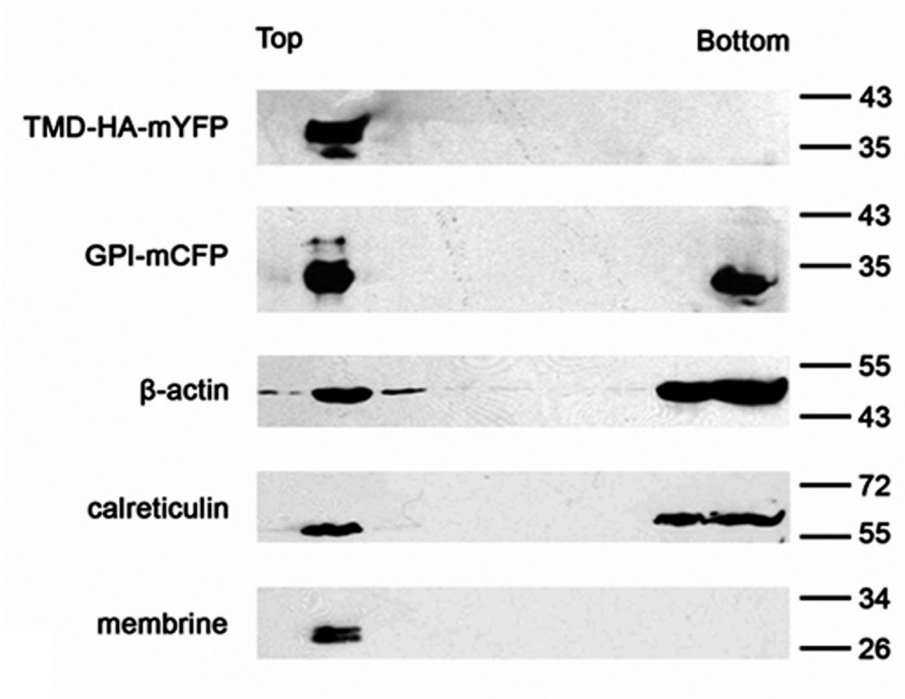

Figure 54: Plasma membrane purification. Fractions collected after fractionation in Nycodenz gradient were subjected to TCA precipitation and Western Blot analysis. TMD-HA-mYFP as well as GPI-mCFP was found almost exclusively at the top of the gradient. Those fractions were subsequently used in time-resolved fluorescence measurements. As a control for purity, antibodies against β-actin (cytoskeleton marker), calreticulin (ER marker) and membrine (Golgi apparatus marker) were used.

For each sample, due to the amount required, plasma membrane from a very large number of cells was obtained. Nevertheless, as in the case of FLIM, independent samples were analysed. In **Table 11**, the values of the lifetime components, their amplitudes, the average lifetimes, the steady-state anisotropy and the rotational correlation times (obtained from the fluorescence anisotropy decays) are given for GPI-CFP and GPI-mCFP samples without and with MβCD pre-treatment of cells (GPI-CFP and GPI-mCFP are indicated in **Table 11** simply as CFP and mCFP). The fluorescence intensity decays are described by three exponentials, where a short component contributes very little to the average lifetimes. This component is usually not detected, and in the present case it was probably due to scattering. The two main components were similar to those previously published by others [116] and to those recovered from the FLIM data analysis obtained from *in vivo* measurements. In addition, the amplitude weighted lifetime (2,4-2,5 ns) was also coincident with the FLIM results, validating the FLIM data analysis. Also in agreement with the FLIM studies, the average fluorescence lifetime of GPI-CFP and GPI-mCFP (in the absence of acceptor) does not change with addition of MβCD, and thus the shortening observed in the presence of acceptor (see below) can be directly related to FRET.

Table 11: Time resolved anisotropy decay. Parameters describing the fluorescence intensity decays of purified plasma membrane suspensions from CHO cells expressing either GPI-CFP (CFP) or GPI-mCFP (mCFP), untreated (-MβCD) or treated (+ MβCD) with MβCD to extract cholesterol. α_n- amplitude; τ_n- lifetime; τ_{AV}- amplitude-averaged fluorescence lifetime; <τ>- fluorescence lifetime; χ^2- chi square; χ^2_{tot}- global chi square. The rotational correlation times (ϕ_1 and ϕ_2) retrieved from the fluorescence anisotropy decays and the steady-state fluorescence anisotropy <r> are also shown.

Sample	α_1	τ_1 (ns)	α_2	τ_2 (ns)	α_3	τ_3 (ns)	τ_{AV} (ns)	<τ> (ns)	χ^2	ϕ_1 (ns)	ϕ_2 (ns)	χ^2_{tot}	<r>
CFP	0,17	0,45	0,36	1,70	0,47	3,75	2,45	3,14	1,25	n.d.	n.d.	n.d.	n.d.
CFP	0,16	0,34	0,34	1,51	0,50	3,68	2,43	3,15	1,21	n.d.	n.d.	n.d.	n.d.
CFP	0,14	0,65	0,32	1,66	0,53	3,49	2,49	2,99	1,14	0,80	34,9	1,06	0,33
CFP	0,13	0,49	0,31	1,66	0,56	3,52	2,54	3,06	1,08	0,75	34,8	1,13	0,33
CFP + MβCD	0,12	0,55	0,32	1,57	0,57	3,48	2,53	3,03	1,16	1,09	36,6	1,19	0,33
mCFP	0,19	0,42	0,33	1,80	0,48	3,90	2,54	3,30	1,27	1,93	31,1	1,17	0,31
mCFP	0,19	0,63	0,33	1,92	0,48	3,65	2,50	3,06	1,09	1,16	33,3	1,20	0,33
mCFP	0,15	0,50	0,33	1,71	0,53	3,57	2,51	3,07	1,11	1,15	33,3	1,17	0,32
mCFP +MβCD	0,16	0,58	0,35	1,84	0,49	3,63	2,51	3,06	1,17	----	32,4	1,23	0,34

The steady-state anisotropy <r> values are very similar in all samples studied, ranging from 0,31 to 0,34 (Table 11). However, among the rotational correlation times ϕ_1 (short rotational correlation time) and ϕ_2 (long rotational correlation time), significant differences were found. The long rotational correlation time can be interpreted as the wobbling of the GPI-linked (m)CFP moiety. It is around 34 ± 3 ns. Since it depends only on the size and shape of the fluorophore and viscosity of the medium, it is not surprising that no significant changes were detected. Regarding the short rotational correlation time, however, it cannot be related to the movement of a large chromophore such as (m)CFP, but it is rather due to a process of energy homotransfer or energy migration (homoFRET, see e.g. [106]). In the case of mCFP, it has a value of 1,2-1,9 ns, indicative of proximity of the chromophores corresponding to a distance between two GPI-mCFP of about 33 Å (for calculation see 3.2.5.4). Pretreatment of cells with MβCD led to a loss of homoFRET and, hence, of the short compontent ϕ_1 of the fluorescence anisotropy decay, showing that the average distance between GPI-mCFP increased and that the large majority of the chromophores are no longer within FRET distance. As expected, the ϕ_1 value in case of CFP was shorter (0.80-0.75) and treatment with MβCD led only to an increase of the short rotational parameter. This behaviour can be related to dimer formation of the fluorophores lacking the A206K mutation. Therefore, CFP proteins are in closer proximity reflected in a short ϕ_1 value, which does not totally disappear upon extraction of cholesterol simply because fluorophores are in an oligomeric state. The above results are in agreement with previous homoFRET studies, [106] confirming the cholesterol sensitive lateral

organization of raft marker GPI-mCFP. Purified plasma membranes of cells coexpressing GPI-mCFP and TMD-HA-mYFP were also employed. As for FLIM-FRET experiments, also in suspension samples of plasma membrane vesicles, GPI-mCFP fluorescence lifetime decreased in the presence of TMD-HA-mYFP. In **Table 12**, the parameters describing the fluorescence intensity decays of GPI-mCFP in the presence of acceptor and the corresponding average lifetimes for a typical sample are given.

Table 12: FLIM-FRET in GPI-mCFP and TMD-HA-mYFP containing- plasma membranes. The results obtained from measurements carried out in cuvette with plasma membrane suspentions of cells coexpressing GPI-mCFP (mCFP) and TMD-HA-mYFP (mYFP) were in agreement with the ones measured in living cells (FLIM), thus confirming previous results. α_n- amplitude; τ_n- lifetime; τ_{AV}- amplitude-averaged fluorescence lifetime; $<\tau>$- fluorescence lifetime; χ^2- chi square; χ^2_{tot}- global chi square

Sample	α_1	τ_1 (ns)	α_2	τ_2 (ns)	α_3	τ_3 (ns)	τ_{AV}(ns)	$<\tau>$ (ns)	χ_{tot}^2
mCFP + mYFP	0,24	0,41	0,31	1,51	0,25	3,79	2,27	3,17	1,21

The calculated FRET efficiency was about 10%, a value similar to those obtained from living cells by FLIM (for the same FRET pair). To confirm the close proximity of TMD-HA-constructs, the steady-state and time resolved fluorescence anisotropy (in Figure 55 anisotropy decays of GPI-mCFP and TMD-HA-mYFP are compared) of purified CHO plasma membrane suspensions containing TMD-HA-mYFP, were investigated.

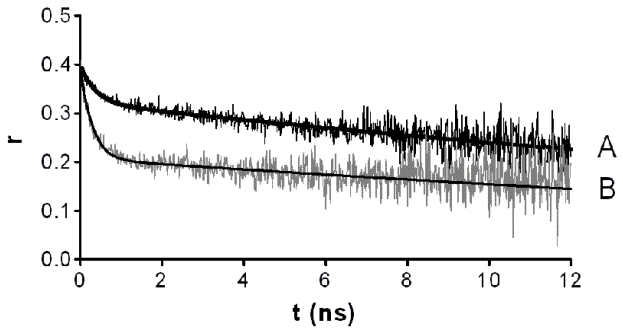

Figure 55: Fluorescence Anisotropy decays. Typical anisotropy decay curves of GPI-mCFP (A) and TMD-HA-mYFP (B) proteins are reported in the graph. As can be seen, the curves can be divided into two components, one referred to as fast, characterized by a small slope, which correspond to the ϕ1 parameter and the other component much slower corresponding to the ϕ2 parameter (see Table 11 and Table 13). Experiments were carried out at 25 °C.

In this case, it is clear first that the long rotational correlation time is similar to the one observed for GPI-mCFP (**Table 11**), which is expected, because the size and shape of the two chromophores is identical; and second that the short rotational correlation time is below 0,5 ns, pointing also to a close proximity. Indeed, the intermolecular distance can be estimated to about 40 Å (see 3.2.5.4). The TMD-HA-mYFP amplitude weighted lifetime measured in plasma membrane extracts was about 2,87 ± 0,11 ns (average calculated on a number of 6 experiments), highly comparable to the one measured *in vivo* (2,86 ± 0,12 ns, average calculated on a number of 15 cells) Notably, the

homoFRET contribution to the integrated steady-state anisotropy is larger in comparison to GPI-mCFP. Furthermore, the steady-state anisotropy is essentially independent of the surface density (c_F) of TMD-HA-mYFP (**Table 13**). Both observations are in agreement with a stable association between TMD-HA-mYFP molecules. Furthermore, as reported in **Table 13**, pre-incubation with MβCD did not lead to any significant change in the ϕ_1 and ϕ_2 values.

Table 13: TMD-HA-mYFP time resolved anisotropy parameters. Rotational correlation times retrieved from the fluorescence anisotropy decays, chi-square of the fitting, and steady-state fluorescence anisotropy of purified plasma membrane suspensions from CHO cells expressing TMD-HA-mYFP, untreated (- MβCD) or treated with MβCD (+ MβCD) to extract cholesterol. The total protein concentration c_P, the fluorescence intensity I_F (indicative of fluorescent protein amount) and $c_F = I_F / c_P$ indicative of fluorescent protein concentration are given. The rotational correlation times (ϕ_1 and ϕ_2) retrieved from the fluorescence anisotropy decays and the steady-state fluorescence anisotropy <r> are also shown.

Sample	c_P (μg/ml)	I_F (a.u.)	c_F (I_F/c_P)	ϕ_1	ϕ_2	χ_{tot}	<r>
- MβCD	50	1000	20,4	0,29	43	1,17	0,33
- MβCD	565	940	1,7	0,32	34	1,22	0,32
+ MβCD	227	540	2,4	0,41	24	1,23	0,32
+ MβCD	216	507	2,3	0,21	43	1,28	0,32

4.4.7 Lateral organization of TMD-HA- and GPI- fusion proteins in GPMVs

As a complementary approach, lateral organization of TMD-HA- and GPI- fusion proteins was studied in giant plasma membrane vesicles (GPMVs) or "blebs". Since blebs derive from chemically induced vesiculation of the cell plasma membrane, they provide a suitable biological system for studying partitioning of lipids and proteins. Indeed, in contrast to lipid domains of mammalian plasma membranes, which are of submicroscopic size [76] and cannot be visualized directly *in vivo*, GPMVs separate in micrometer-scale phases at temperatures below ~ 25 °C [101]. Blebs were formed from CHO-K1 cells stably transfected either with GPI-mCFP or with TMD-HA-mYFP. As a control, blebs obtained from CHO-K1 cells transfected with HA-mCer (kindly provided by Stephanie Engel, Free University, Berlin), were used. R18 was employed as marker for liquid disordered (ld) domains since it preferentially partitions in the ld-like phase in GPMVs [119]. A micrometer-scale separation of fluid phase domains was induced in GPMVs by lowering the temperature (10 °C). In **Figure 56** typical pictures of blebs are reported. As can be clearly seen, while both TMD-HA-mYFP and TMD-HA-mCer show the same fluorescence distribution as R18, the full length HA-mCer presents a preferential but not exclusive partition into ld domains. In contrast, GPI-mCFP localized exclusively into lo domains as shown by the distribution of the raft marker complementary to the one of R18. These results might seem in contrast with the previous FLIM-FRET experiments demonstrating lipid raft partitioning of TMD-HA fusion proteins.

However it has to be reminded that GPMVs extrude from the cell plasma membrane and although they maintain the lipid composition, they might not preserve the lipid bilayer architecture.

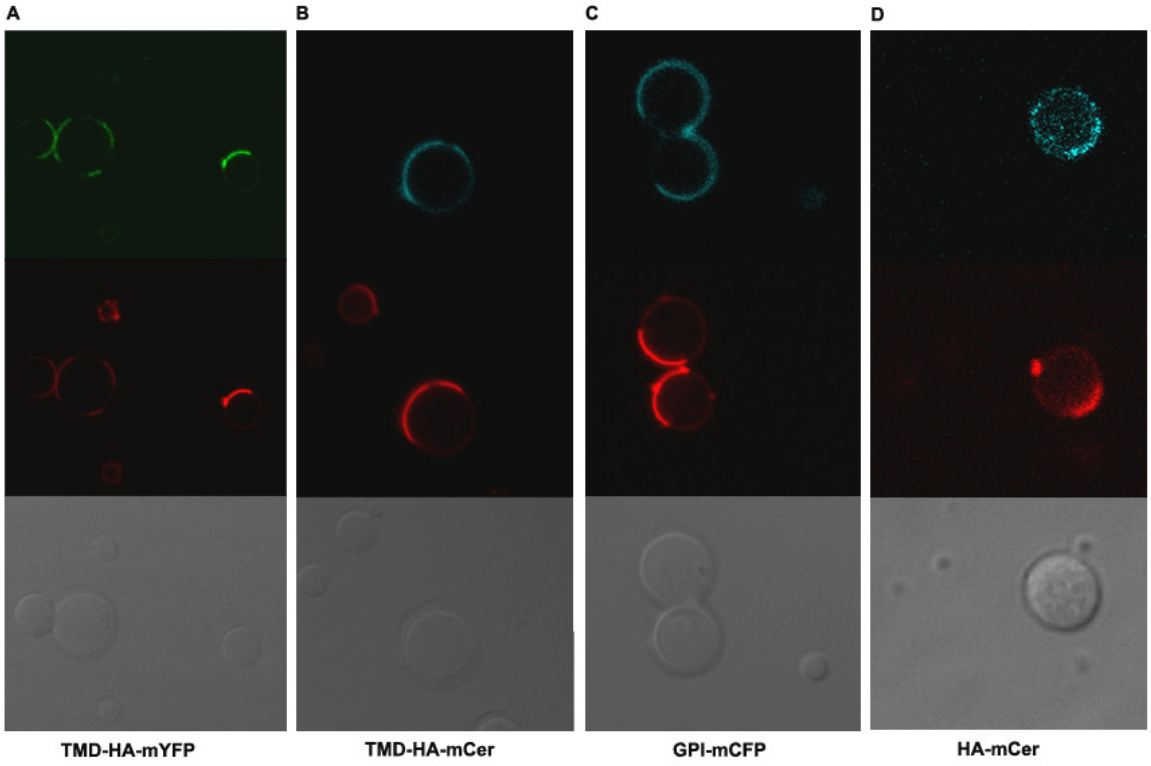

Figure 56: Lateral organization of TMD-HA- and GPI- constructs in GPMVs. Giant plasma membrane vesicles formed from CHO-K1 cells transfected with different proteins. A and B correspond to GPMV expressing TMD-HA-mYFP or TMD-HA-mCer. These proteins show the same lateral organization as R18, which preferentially enriches in ld domains. In contrast, GPI-mCFP (C) shows complementary localization to that shown by R18. Finally, HA-mCer (D) despite of presenting enrichment into ld domains, it also partially localizes into lo domains. Measurements were done at 10 °C.

5 DISCUSSION

In the present study the lateral organization of the transmembrane domain (TMD) and cytoplasmic tail (CT) of HA (TMD-HA constructs) in the plasma membrane of living mammalian cells was investigated. To date, essentially biochemical assays based on detergent insolubility and immunoelectron microscopy [40,88] have provided evidences that HA is localized to lipid domains enriched in cholesterol, saturated phospholipids and/or glycosphingolipids, so-called rafts. To enable measurement on living cells the TMD-HA constructs and the well established raft marker GPI were tagged with the fluorescent proteins YFP and CFP, respectively and their interaction was assessed by FLIM-FRET. While previous approaches [91] tagged the CT of HA with variants of fluorescent proteins, here the HA ectodomain was replaced by a fluorescent protein. Thereby, any interference of the fluorophore with a role of the CT in lateral organization of HA is avoided. Indeed, previous studies indicated that mutations in the TMD and the CT of HA reduce association with detergent-resistant fractions [38,87,88,120]

HeteroFRET can be assessed in living cells by FLIM or by steady-state measurements of the donor intensity. In the latter case bleaching of the acceptor which is required to investigate FRET may be incomplete or even affect the stability of the donor. For example, previous studies on GPI linked fluorescent proteins using acceptor bleaching did not detect any significant heteroFRET beyond noise [103,106,121]. In contrast, homoFRET measurements revealed clustering of GPI constructs [106]. In line with the latter, significant heteroFRET between GPI-CFP and GPI-YFP by FLIM was measured in this work, indicating that this technique is superior to acceptor bleaching based experiments. HeteroFRET studies also revealed a cholesterol dependent arrangement of GPI-CFP and TMD-HA-YFP constructs in mammalian cells. As a complementary approach to extract information on lipid domain organization of TMD-HA, time resolved anisotropy measurements were also carried out. In particular, strong homoFRET between TMD-HA proteins was observed, in agreement with a tight association of constructs. This is also corroborated by heteroFRET observed between TMD-HA-CFP and TMD-HA-YFP, and by the absence of any effect of cholesterol depletion on FRET efficiency. Furthermore the very low FRET efficiency between TMD-HA and the SFV-E2 constructs strongly indicate that TMD-HA forms specifically homodimers, but not heterodimers.

5.1 CHARACTERISATION OF TMD-HA CONSTRUCTS

TMD-HA fluorescent constructs were generated fusing the HA transmembrane and cytoplasmic domain to the C-terminus of YFP. However the subsequent addition of the HA signal peptide to the N-terminus of the fluorophore was found to be essential for the delivery of the proteins to the plasma membrane, otherwise accumulating into the cytosol (see **Figure 19**). Indeed, it was previously

demonstrated that HA mutants lacking this sequence were retained in the cytoplasm [17]. Thus, since in general this signal peptide mediates the cotranslational insertion of the nascent protein into the ER membrane [122], it is likely that due to its absence the polypeptide synthesis is redirected from ER bound ribosomes to free ribosomes. In contrast, TMD-HA proteins, fused to the signal peptide (SpHA), were palmitoylated and transported to the plasma membrane (see Figures 22, 23 and 26). In a similar manner, except for palmitoylation, the mutant TMD-HAC3S was processed and delivered to the cell surface (see **Figure 25** and **Figure 26**). Upon Triton X-100 extraction and sucrose gradient centrifugation, TMD-HA but not TMD-HAC3S, was partially enriched in the DRM fractions, in agreement with what observed for full length HA ([87] and Engel et al., unpublished data). Although nowadays this biochemical approach is considered to generate controversial results, it assured that the artificial TMD-HA variants maintained in principle the characteristics of the full length HA. Furthermore, it was also investigated whether TMD-HA constructs form oligomers. Indeed the HA native structure is homotrimeric and recent studies reported that synthetic TMD-HA peptides form heat stable oligomers [32,123,124]. However, whether *in vivo* the three TMD of a single HA form a coiled coil structure in the membrane, still remains unclear. Radioactive labelling of TMD-HA proteins and subsequent polyacrylamide gel electrophoresis under reducing and non reducing conditions revealed that the constructs form disulfide linked dimers and, in a minor extent, trimers (**Figure 28** and**Figure 29**). Finally treatment of the proteins with EndoH probed that TMD-HA constructs are transported to the plasma membrane exclusively in a dimeric or trimeric form (**Figure 34** and **Figure 36**). This is in agreement with previous results showing that only HA trimers are transported to the plasma membrane but not monomers [20,125].

5.1.1 Investigation of TMD-HA oligomerization

The TMD-HA-YFP sequence contains seven cysteines: C22 in the signal peptide, C49 and C71 in the fluorophore, C537 in the transmembrane domain and the three palmitoylation sites, C551, C559 and C562, one at the border between transmembrane domain and cytoplasmic tail and two in the cytoplasmic tail. In order to elucidate which of these cysteines are involved in the disulfide bond-mediated oligomerization, several different mutants were produced. In every case, cysteines were substituted with serines. A priori, it was excluded that the palmitoylation sites are responsible for dimerization, since the protein TMD-HAC3S forms oligomers (**Figure 36** B). Thus, proteins carrying the C537S mutation in the transmembrane domain were generated as well as mutants with the C22S mutation in the signal peptide, although this sequence should be cleaved upon translocation into the ER lumen. Finally, the C49S and C71S point mutations were inserted in the fluorophore. The C22S mutation placed either alone or together with the mutation in the transmembrane domain, abolished trimerization, but not dimerization (**Figure 36** A and B). The mutation C537S in the transmembrane domain affected only partially the assembly of trimers.

Interestingly, the mutant lacking the cysteine in the signal peptide, in the transmembrane domain and the three palmitoylation sites, forms dimers. Hence, it was hypothesized that TMD-HA dimerization was due to disulfide bond formation between C49 and C71 in the fluorophore. Indeed it was reported that secretory forms of GFP produce, prior to complete folding, disulfide linked oligomers in endocrine cells [113]. Surprisingly, when the C49S and C71S mutations were inserted into the TMD-HA-mYFP protein, dimers and trimers were still visible even though none of the species was EndoH resistant (**Figure 35**) and no fluorescence was detected upon transfection in CHO cells. This result, reported also by Jain et al. [113], is probably the consequence of the misfolding of the fluorophore, due to the double point mutation. Taken together these results led to the hypothesis that TMD-HA oligomer formation is a process in which at least two to four of the seven cysteines are involved. Formation of dimers results from the cooperation of at least two cysteines, while trimers are formed from the association of a dimer with a monomer, mediated by C22. In absence of C22 and C537, the cysteines in the fluorophore are likely to be the responsible for formation of stable dimers. However, when residues C49 and C71 in the fluorophore were mutated, dimers and trimers were probably due to disulfide bonds between the other two cysteines, i.e. in the signal peptide and in the transmembrane domain. Disulfide linked dimers and trimers are likely to form in the ER, nevertheless it is not clear whether dimer and trimer formation follows the same kinetcs. Infact, pulse chase experiments have shown that while monomeric and dimeric TMD-HA proteins are equally synthesized, and dimers acquire EndoH resistance about 27 hours post-transfection (**Figure 37**), trimers appear to be generated only subsequently to the export of the proteins from the ER, since they start to be visible only after 1 hour of chasing (**Figure 37**, t_1). This indicates that trimers might be assembled during the transport to the Golgi apparatus, e.g. from the association of dimers with monomers. In general, monomers never acquire EndoH resistance hence they are not delivered to the cell surface. This indicates that the organization of TMD-HA constructs in oligomers is a prerequisite for the transport to the plasma membrane. In support to this conclusion is the observation that the full length HA trimerizes shortly after synthesis, before the transfer of HA_0 to the Golgi apparatus, and that no monomers have been detected at the cell surface [20]. In contrast, the monomeric form of TMD-HA proteins carrying the C22S mutation was found to be partially EndoH resistant (**Figure 36**). It could be hypothesized that these monomers originate from the dissociation of oligomers that might occur subsequently to the delivery of the proteins to the plasma membrane.

Finally, it has to be stressed that oligomer formation between SFV and HA transmembrane domains was not observed. This result (discussed in details in 5.2.1) indicates that oligomerization of TMD-HA proteins reflects specific properties, e.g. the presence in the TMD of particular amino acidic sequences, that induce the specific interaction between TMD-HA molecules. Hence, we surmise that

disulfide bond formation is simply a consequence of the close proximity driven by the strong affinity of the transmembrane domain fragments.

Oligomerization of TMD-HA constructs was investigated in parallel by FLIM-FRET imaging and time resolved anisotropy. Energy transfer was measured for different TMD-HA donor-acceptor pairs, e.g. TMD-HA-CFP was coexpressed either with TMD-HA-YFP or with TMD-HAC3S-YFP, mutant lacking the palmitoylation sites, or viceversa TMD-HAC3S-CFP was coexpressed either with TMD-HA-YFP or TMD-HAC3S-YFP. Significant FRET was detected for every couple, indicating that TMD-HA protein interaction is mainly driven by disulfide bond formation. In addition, fluorescence anisotropy measurements carried out on plasma membrane preparations, revealed strong homoFRET between TMD-HA-constructs. Indeed the very short rotational correlation time (ϕ_1) obtained from the anisotropy decay, is the result of the close proximity between fluorophores, suggesting tightly association between TMD-HA proteins. Based on the distance of about 39 Å between the fluorescent proteins of two associated TMD-HA constructs (calculated as described in 3.2.5.4) revealed by homoFRET, and the Förster radius of 49 Å for a CFP-YFP pair [107], the FRET efficiency E should be in the order of 60 to 70%. Nevertheless, one has to keep in mind that apart from heterodimeric TMD-HA constructs also homodimeric constructs (TMD-HA-CFP/TMD-HA-CFP and TMD-HA-YFP/TMD-HA-YFP) are formed and homodimers by itself do not contribute to heteroFRET. Therefore, the expected FRET efficiency, in the order of about 20% is in agreement with the values measured for TMD-HA wild type constructs (**Table 9**). However, it has to be outlined that preincubation of transfected cells with the cholesterol extracting agent, MβCD, led to an increase of FRET efficiency. Based on these results it was hypothesized that extraction of cholesterol might eliminate physical boundaries between TMD-HA wild type proteins, leading to the formation of large aggregates. Palmitoylation might play a central role in this mechanism. Indeed it was reported that palmitic acid residues attached to the HA transmembrane domain and cytoplasmic tail, might interact with each other and with residues attached to other neighboring HA molecules. Furthermore palmitoylation might also modulate the HA cytoplasmic tail conformation in order to support the interaction of the glycoproteins with other viral proteins [23], a fundamental step in viral assembly. Therefore, due to cholesterol extraction, the palmitic acid residues might drive the association of several TMD-HA molecules, reflected in an increased FRET efficiency. In agreement with this hypothesis is also the observation that cholesterol extraction from cell cotransfected with mutants lacking palmitoylation did not have any effect on FRET efficiency (**Table 9**).

At last, it has to be pointed out that CFP lifetime was significantly shorter when the fluorophore was fused to TMD-HA rather than to GPI. This effect, referred to as “pseudo-homoFRET”, is due to the oligomerization of the HA transmembrane domain, which brings the CFP molecules in close proximity, so that energy is transferred from one fluorophore to the other. However, in general

homoFRET has no effect on lifetimes and it is normally detected by anisotropy measurements. Nevertheless, due to the oligomerization, the chromophores might assume new conformations associated to slightly different emission spectra and thus to diverse populations of CFP, some acting as donors and some as acceptors. In this situation energy is transferred from one population of donors (blue shifted) to the other (red shifted) resulting in a decrease of the CFP fluorescence lifetime [115].

5.2 Recruitment of TMD-HA proteins to raft domains

FLIM-FRET was used to investigate *in vivo* the lateral organization of TMD-HA and GPI constructs. Control experiments with the GPI-(m)CFP/GPI-YFP donor-acceptor pair (where "m" stands for monomeric, see 4.4.3) were first carried out in order to establish the sensitivity of the method. The calculated FRET efficiency (E) was in the order of 12% (**Figure 42**). This magnitude of E has been also reported for other membrane proteins recruited to rafts [126]. As expected, preincubation of cells with MβCD led to a significant decrease of FRET efficiency, indicating cholesterol dependent organization of GPI fluorescent proteins (**Figure 42**). In agreement with these results, Sharma et al. [106] have shown that in the plasma membrane of CHO-K1 cells cholesterol sensitive clusters of GPI-GFP and other GPI-linked protein are present. The typical size of these clusters is only about 5 nm, and they contain about 4 to 5 GPI linked protein molecules. Significant energy transfer was measured for the donor-acceptor pair GPI-(m)CFP/TMD-HA-(m)YFP (where "m" stands for monomeric, see 4.4.3). Although FRET efficiencies were slightly lower than for GPI-protein pairs, they substantially decrease upon extraction of cholesterol (**Figure 44**). This is consistent with the recruitment of TMD-HA-(m)YFP to rafts since the association is abolished upon disintegration of rafts by cholesterol depletion. FRET efficiencies were also plotted against the acceptor intensities (**Figure 50**). These graphs showed that increasing the amount of acceptor, does not significantly increase the FRET efficiency and that the dependence of the latter from the acceptor concentration becomes more punctuated upon extraction of cholesterol. This acknowledges that energy transfer between TMD-HA and GPI-proteins arise from the clustering of the molecules in lipid microdomains and it is not just the result of overexpression or random interactions. Based on the above observation of cholesterol sensitive FRET between GPI-(m)CFP and TMD-HA-(m)YFP it is speculated that TMD-HA constructs recruit to those nanoclusters. Since the fraction of those clusters has been found to be less than 30% [106] a large pool of GPI-linked fluorescent proteins and TMD-HA constructs is outside of these clusters explaining the limited FRET efficiency.

Similar FRET efficiencies for the GPI-mCFP/TMD-HA-mYFP pair in the plasma membrane of intact cells and in plasma membrane extracts used in time resolved anisotropy measurements, were obtained (see 4.4.6). Very likely, plasma membrane purification perturbs the cytoskeleton of cells. Hence, this result would indicate that the cytoskeleton has no major influence on association of

TMD-HA constructs with cholesterol sensitive lipid domains, at least with those of the exoplasmic leaflet. This is also supported by the observation that pre-treatment of cells with the cytoskeleton disrupting agent cytochalasin D did not affect the FRET efficiency between GPI-CFP and TMD-HA-YFP (**Figure 45** B), although cytoskeleton was indeed perturbed by the treatment (**Figure 46**). Interestingly, it has been reported that the HA cytoplasmic tail does not contain signals known to interact with the intracellular structures and that it might be too short to associate with the cytoskeleton [127,128].

When employing GPI-YFP as an acceptor and TMD-HA-CFP as a donor, a lower but significant FRET efficiency, in comparison to the pair GPI-CFP and TMD-HA-YFP, was observed. This might be related to fact that in the former case the donor is organized as a dimer while in the latter the donor is organized as a monomer. Aggregation of TMD-HA proteins might confine GPI molecules at the border of the cluster, causing a virtual decrease of GPI-YFP available for energy transfer. Indeed it has been suggested that the HA transmembrane domain might promote the accumulation of HA molecules in order to increase the affinity for lipid rafts [88]. Hence, since FRET efficiency depends essentially on the concentration of acceptor available for the donor, FRET is lower when TMD-HA serves as a donor. In that case donors organized as dimers are shielded somewhat from the acceptor (**Figure 57** B).

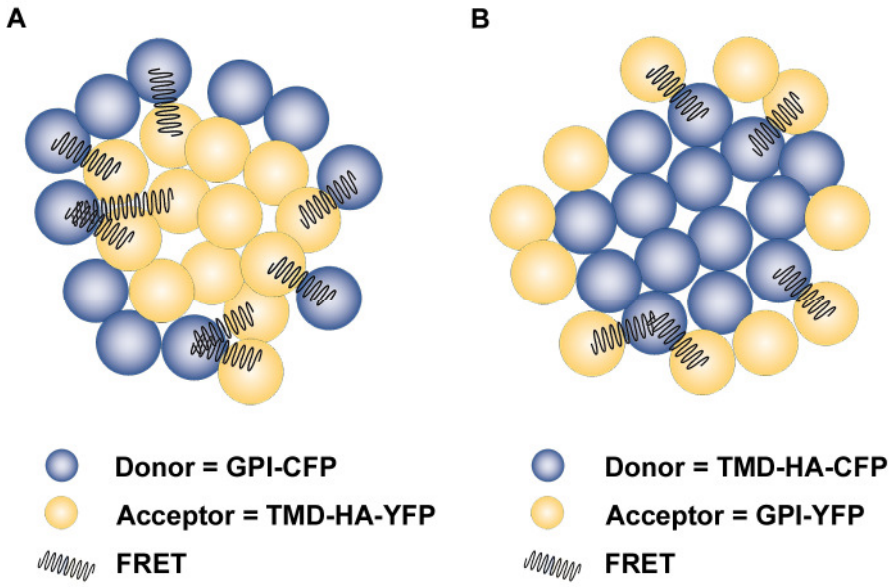

Figure 57: FRET between different donor-acceptor pairs. FRET efficiency between GPI-CFP and TMD-HA-YFP (A) is higher compared to that calculated for the TMD-HA-CFP and GPI-YFP couple (B). This situation is probably related to the oligomerization and clustering of TMD-HA proteins. Indeed, while GPI-CFP molecules are all equally available for the acceptors (A), only a part of TMD-HA-CFP proteins are in contact to GPI-YFP (B). In addition while GPI-CFP molecules surround a cluster of acceptors, the restriction of GPI-YFP proteins to the periphery of the TMD-HA-CFP bunch, lower the amount of acceptors available for FRET.

5.2.1 TMD-HA and SFV-E2 clustering

Very low energy transfer was measured upon coexpression of SFV-E2-mCFP and TMD-HA-mYFP or GPI-YFP. This result not only confirms the different localization of the proteins in the plasma membrane, but also indicates that oligomerization between SFV-E2 and TMD-HA does not occur. Thus, it is possible that formation of TMD-HA oligomers might be driven by specific properties of the transmembrane fragment that brings the proteins in close proximity. In case of full length HA this process would allow non-covalent homotrimer production, while for TMD-HA proteins this mechanism favours disulfide bond formation. In support to this hypothesis is the observation that anchor-free HA molecules do not require trimer formation for efficient cell surface transport [129], while full length HA trimerization shortly after synthesis is a prerequisite for the subsequent transport to the Golgi apparatus and then to the plasma membrane [130].

Finally, this experiments also assures that the reduction of lifetime observed when TMD-HA is coexpressed with GPI raft marker has to be related to FRET due to close proximity of the molecules and thus due to clustering into lipid raft domains.

5.3 Recruitment of TMD-HA mutants to raft domains

Support for the localization of TMD-HA in rafts is also given by the observation that the non-palmitoylated variant of TMD-HA (TMD-HAC3S-YFP) shows a much lower FRET efficiency. Palmitoylation is considered to be important for association of HA with cholesterol enriched lipid domains [38,131,132]. The low affinity of TMD-HAC3S-YFP to rafts is also corroborated by the observation that cholesterol depletion did not affect the FRET behaviour between GPI-CFP and TMD-HAC3S-YFP (**Figure 48** B). The different affinity of TMD-HA-YFP and TMD-HAC3S-YFP for rafts is also reflected by the difference in DRM partitioning (**Figure 27**). These results confirm that palmitoylation contributes to raft targeting. Beside palmitoylation, other residues in the HA transmembrane domain might play a critical role in lipid raft targeting, e.g. the first three aminoacids of the HA transmembrane domain might represent an important raft signal [88]. Indeed when TMD-HA-AAA and TMD-HAC3S-AAA mutants were coexpressed with the raft marker, no significant energy transfer was detected (**Figure 49**), thus confirming the importance of these sequence for the lateral organization of HA molecules. It has to be pointed out that the TMD-HA mutants lacking the raft signals have a tendency to accumulate intracellularly, although they follow the same kinetics as the wild type (**Figure 37**) and they are still efficiently transported to the plasma membrane (**Figure 25**). It has been observed that the same mutation inserted in the full length HA not only diminished the affinity of the glycoprotein for lipid rafts, but it also resulted in a remittal surface transport of the proteins (Stephanie Engel, unpublished data). In particular, the substitution of the amino acids VIL with three small, less hydrophobic alanines decreased the hydrophobicity and caused the physical

shortening of the HA transmembrane domain. The change in the transmembrane length might lead to a reduced affinity for lipid microdomains (Stephanie Engel, unpublished data), supposed to form in the Golgi apparatus [93] and functioning as platform for the delivery of different proteins to the apical membrane [133,134]. Thus, the lack of raft association might explain why TMD-HA-AAA and TMD-HAC3S-AAA mutants accumulate in the cytosol, enforcing the hypothesis that rafts might function as transport platforms for the accumulation of HA at the budding site and that the HA transmembrane domain length might be critical for this to occur.

5.4 Lateral distribution of TMD-HA proteins in GPMVs

Controversial to what shown *in vivo*, TMD-HA fusion proteins localize exclusively in ld domains in GPMVs (**Figure 56**). However one has to keep in mind that very likely the lateral organization of the plasma membrane in blebs is altered. Furthermore, GPMVs undergo domain formation at temperature far below from physiological or room temperature [101]. Therefore, assuming that TMD-HA proteins have a weak affinity for lipid microdomains, or even, that they are placed at the border of rafts, the tight lipid packaging induced by lowering the temperature would result in the total exclusion of the proteins from lo domains. In agreement with this hypothesis is the observation that TMD-HA molecules are only slightly enriched in DRMs upon Triton X-100 extraction (**Figure 27**). Notably, the raft marker, GPI-CFP, partitions almost exclusively in DRM fractions (**Figure 27**) and shows lo preference in GPMVs (**Figure 56**). Finally, the full length HA protein seems to distribute both in lo and ld domains, although it accumulates preferentially in ld phase (**Figure 56**). As well as for TMD-HA and GPI-CFP the distribution of HA in blebs resembles its partitioning in DRMs (**Figure 27**). Indeed a higher amount of full length HA is localized in DRM fractions with respect to TMD-HA. We surmise that the different behaviour of the two proteins might be related to the different association between the transmembrane domains. As previously discussed, TMD-HA oligomers are disulfide linked, whereas trimerization of full length HA is mediated by electrostatic interactions between the ectodomains [30]. Thus, the non-covalently bound transmembrane domains might have more flexibility, feature that might not only confer more stability to the protein, but it may also allow to adapt to different lipid packing properties and, hence, to increase the affinity for lipid rafts.

6 CONCLUSION

Influenza virus spike protein hemagglutinin (HA) is one of the best characterized viral glycoproteins with respect to its structure and function. However, still little is known about the role of its transmembrane domain and cytoplasmic tail. Several studies indicate that this fragment is far from acting simply as an anchor for the ectodomain, indeed it is critical for complete fusion to occur [25,135] and it might also be responsible for the lateral organization of HA in the host cell plasma membrane [87]. In this study we have shown that the membrane anchor of HA can be recruited to previously characterized [106] cholesterol-sensitive nanoclusters in the plasma membrane of CHO-K1 cells and that palmitoylation might be critical not only for the association to lipid rafts, but also for the association of HA molecules with each other, a mechanism supposed to guide viral assembly. In support of this observation, Polozov et al. [136] proposed that palmitic acid residues might induce the accumulation of HA molecules and cholesterol in order to increase viral stability. Whether clusters of similar size exist in the plasma membrane of native host cells of influenza virus still remains to be elucidated. If so, such small clusters have to be merged in order to form a virus budding site. This can be accomplished by interaction of the viral matrix protein M1 with the cytoplasmic tails of HA and of NA [42,137] on one side, and by the polymerization of M1 [138] on the other. The initial small size of clusters and, hence, the low number of proteins in such a cluster, as well as the specific interaction of M1 with viral proteins, might provide a mechanism to specifically enrich viral proteins in merged clusters and expel non-viral membrane proteins. In addition, we demonstrated that association of few HA molecules in lipid microdomains might occur already in the Golgi apparatus and that further coalescence in large aggregates might be mediated by the merging of several HA-lipid domains. Indeed rafts seem to function as carriers for transporting TMD-HA proteins to the cell surface, since mutants lacking palmitoylation or specific sequences in the transmembrane domain (referred to as raft signals) are either slowly transported or even intracellularly retained. However, although important, association to lipid microdomains does not seem to be fundamental for transport of TMD-HA proteins to the plasma membrane. Nevertheless, while TMD-HA wild type proteins exploit both raft-mediated and non-raft mediated transport, HA molecules lacking the raft signals (i.e. VIL sequence in the TMD and palmitoylation sites) cannot take advantage of the former system. We hypothesize that, subsequent to the fusion of the raft domain carrying TMD-HA molecules with the membrane bilayer, neighboring TMD-HA proteins form large aggregates due to the interaction between palmitic acid residues and between the cytoplasmic tails of the molecules. This process involves all proximal TMD-HA, either raft- or non-raft associated. Indeed it was demonstrated that clustering of HA occurs at all accessible length scales [91]. This is also supported by the observation that extraction of cholesterol in cells expressing TMD-HA proteins leads to an increase of FRET efficiency, indicating enhanced

aggregation. We further propose that TMD-HA molecules might be simply displaced at the border of lipid rafts. This organization might explain the limited FRET efficiency measured when TMD-HA-YFP is coexpressed with the raft marker GPI-CFP. We have observed that GPI-anchored fluorophores accumulate preferentially in lipid rafts or in liquid ordered domains as indicated not only by their enrichment in DRMs, but also by the absolute exclusion from ld in GPMVs. Therefore, according to the above proposed hypothesis, the decrease of FRET efficiency observed upon extraction of cholesterol may not be due to the displacement of both TMD-HA- and GPI- molecules from rafts, but it might be only related to the dispersion of GPI-CFP proteins. The different affinity of TMD-HA for lipid rafts is also reflected in the behaviour of this protein in GPMVs. While at physiological temperature HA might be distributed at the border of rafts, at 10 ºC, temperature in which lo domains are induced, lipids become too tightly packed, thus excluding TMD-HA proteins. Furthermore, it has to be underlined that while *in vivo* lipid rafts are a mixture between lo and ld, in GPMVs these two domains are strictly separated. Finally, the limited FRET efficiency detected for GPI donor-acceptor couples might be related to two factors. First, it is likely that GPI proteins are not the exclusive inhabitants of lipid rafts, second it was demonstrated that not more than 40% of GPI anchored proteins are organized in lipid microdomains [106].

We also surmise that TMD-HA mutants lacking the raft signals may be simply spread in the plasma membrane and that neither they distribute at the border of lipid microdomains, nor they aggregate. This assumption is supported by two important observations. First, FRET efficiency between TMD-HA mutants and the raft marker was very low; second, the extraction of cholesterol from cells coexpressing TMD-HAC3S proteins as donor-acceptor couple did not have any effect on FRET efficiencies.

Collectively, our results suggest the following model for assembly and budding of influenza virus (Figure 58).

1. HA molecules associate with lipid rafts in the Golgi apparatus and they are transported to the plasma membrane. Lipid rafts function as carriers mediating the fast delivery of the spike proteins to the plasma membrane.
2. Raft transporting HA fuses with the lipid bilayer. Subsequently HA proteins form large aggregates by dint of the association between palmitic acid residues of molecules localized inside or outside of rafts. Cholesterol and raft lipids are entrapped into these complexes, but their role in HA clustering becomes marginal. As a consequence, HA complexes might be displaced from membrane rafts and they may create new domains showing characteristics of rafts and non-raft domains.
3. The very bulky ectodomain of the spike proteins induces the bending of the plasma membrane and the subsequent fission and budding of the new particles.

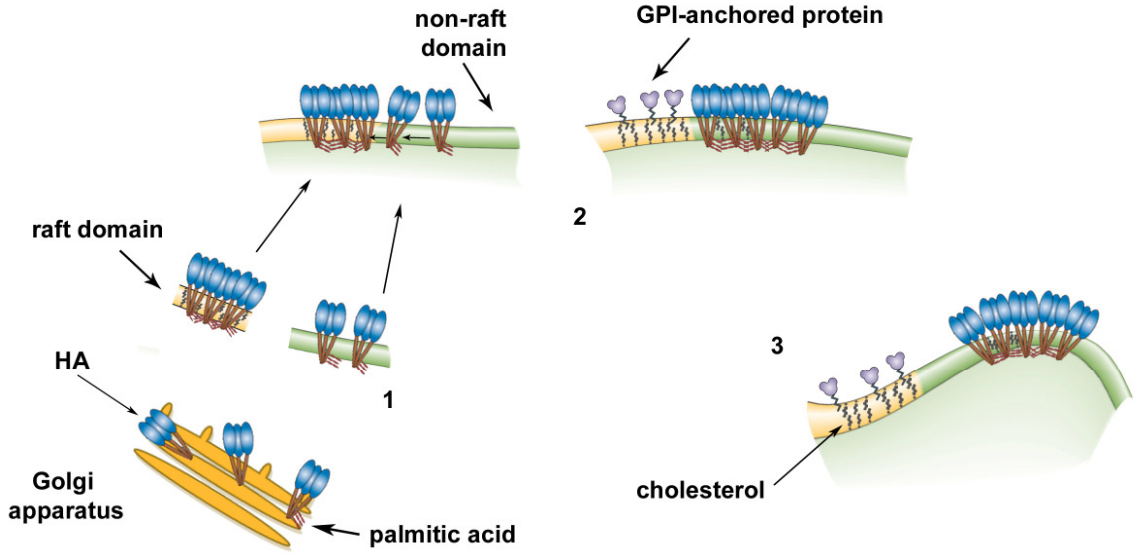

Figure 58: Model of influenza virus assembly. Association of HA proteins with lipid rafts occurs in the Golgi apparatus. Membrane microdomains mediate the delivery of HA to the plasma membrane, although association of HA with rafts is not essential for the transport (1). Once in the plasma membrane, HA molecules aggregate by means of the interaction between palmitic acid residues (2). Finally, the very bulky HA ectodomain induces the bending of the membrane (3). For simplicity, palmitic acid residues have been designed only on some molecules.

Cholesterol in the viral envelope may be used by the virus to reduce the high packaging induced by the spike proteins, which might form a structure similar to solid domains (so). As suggested by Polozov et al. [136], cholesterol might disrupt so domains rather than inducing the formation of lo domains from ld domains, thus maintaining fluidity in the viral envelope. The presence of lo-like domains in the envelope may be important for the formation of HA fusion complexes during viral infection as demonstrated by the reduced infectivity of viral particles formed from cholesterol depleted cells [139]. Nevertheless at late stages of assembly, the role of lipid domains might become marginal as shown by enhanced budding of influenza virus from cholesterol depleted cells [140].

In summary, the above presented model is one possible way to interpret our data. However we are aware that much uncertainty arises from such a new assumption and that further investigation and more experiments are needed to support this hypothesis. Therefore, the TMD-HA-constructs may be used in the future as a basis to elucidate the proposed role of HA in recruiting the viral components to the viral budding site. In particular coexpression of TMD-HA constructs with other labelled viral components, e.g. vRNPs, might unravel important functions of the HA cytoplasmic tail.

BIBLIOGRAPHY

[1] Oxford, J. S. (2000): Influenza A pandemics of the 20th century with special reference to 1918: virology, pathology and epidemiology, Rev Med Virol 10 [2], pp. 119-33.

[2] Whittaker, G. R. (2001): Intracellular trafficking of influenza virus: clinical implications for molecular medicine, Expert Rev Mol Med 2001, pp. 1-13.

[3] Betakova, T. and Hay, A. J. (2007): Evidence that the CM2 protein of influenza C virus can modify the pH of the exocytic pathway of transfected cells, J Gen Virol 88 [Pt 8], pp. 2291-6.

[4] Sunstrom, N. A.; Premkumar, L. S.; Premkumar, A.; Ewart, G.; Cox, G. B. and Gage, P. W. (1996): Ion channels formed by NB, an influenza B virus protein, J Membr Biol 150 [2], pp. 127-32.

[5] Aragon, T.; de la Luna, S.; Novoa, I.; Carrasco, L.; Ortin, J. and Nieto, A. (2000): Eukaryotic translation initiation factor 4GI is a cellular target for NS1 protein, a translational activator of influenza virus, Mol Cell Biol 20 [17], pp. 6259-68.

[6] Watanabe, K.; Takizawa, N.; Katoh, M.; Hoshida, K.; Kobayashi, N. and Nagata, K. (2001): Inhibition of nuclear export of ribonucleoprotein complexes of influenza virus by leptomycin B, Virus Res 77 [1], pp. 31-42.

[7] Karlsson Hedestam, G. B.; Fouchier, R. A.; Phogat, S.; Burton, D. R.; Sodroski, J. and Wyatt, R. T. (2008): The challenges of eliciting neutralizing antibodies to HIV-1 and to influenza virus, Nat Rev Microbiol 6 [2], pp. 143-55.

[8] Ibricevic, A.; Pekosz, A.; Walter, M. J.; Newby, C.; Battaile, J. T.; Brown, E. G.; Holtzman, M. J. and Brody, S. L. (2006): Influenza virus receptor specificity and cell tropism in mouse and human airway epithelial cells, J Virol 80 [15], pp. 7469-80.

[9] Whittaker, G. R.; Kann, M. and Helenius, A. (2000): Viral entry into the nucleus, Annu Rev Cell Dev Biol 16, pp. 627-51.

[10] Whittaker, G. R. and Helenius, A. (1998): Nuclear import and export of viruses and virus genomes, Virology 246 [1], pp. 1-23.

[11] Steinhauer, D. A. and Skehel, J. J. (2002): Genetics of influenza viruses, Annu Rev Genet 36, pp. 305-32.

[12] von Itzstein, M. (2007): The war against influenza: discovery and development of sialidase inhibitors, Nat Rev Drug Discov 6 [12], pp. 967-74.

[13] Colman, P. M. (1994): Influenza virus neuraminidase: structure, antibodies, and inhibitors, Protein Sci 3 [10], pp. 1687-96.

[14] Wilson, I. A.; Skehel, J. J. and Wiley, D. C. (1981): Structure of the haemagglutinin membrane glycoprotein of influenza virus at 3 A resolution, Nature 289 [5796], pp. 366-73.

[15] Skehel, J. J. and Wiley, D. C. (2000): Receptor binding and membrane fusion in virus entry: the influenza hemagglutinin, Annu Rev Biochem 69, pp. 531-69.

[16] Garten, W. and Klenk, H. D. (1999): Understanding influenza virus pathogenicity, Trends Microbiol 7 [3], pp. 99-100.

[17] Sekikawa, K. and Lai, C. J. (1983): Defects in functional expression of an influenza virus hemagglutinin lacking the signal peptide sequences, Proc Natl Acad Sci U S A 80 [12], pp. 3563-7.

[18] Roberts, P. C.; Garten, W. and Klenk, H. D. (1993): Role of conserved glycosylation sites in maturation and transport of influenza A virus hemagglutinin, J Virol 67 [6], pp. 3048-60.

[19] Wagner, R.; Heuer, D.; Wolff, T.; Herwig, A. and Klenk, H. D. (2002): N-Glycans attached to the stem domain of haemagglutinin efficiently regulate influenza A virus replication, J Gen Virol 83 [Pt 3], pp. 601-9.

[20] Copeland, C. S.; Doms, R. W.; Bolzau, E. M.; Webster, R. G. and Helenius, A. (1986): Assembly of influenza hemagglutinin trimers and its role in intracellular transport, J Cell Biol 103 [4], pp. 1179-91.

[21] Braakman, I.; Hoover-Litty, H.; Wagner, K. R. and Helenius, A. (1991): Folding of influenza hemagglutinin in the endoplasmic reticulum, J Cell Biol 114 [3], pp. 401-11.

[22] Veit, M. and Schmidt, M. F. (2006): Palmitoylation of influenza virus proteins, Berl Munch Tierarztl Wochenschr 119 [3-4], pp. 112-22.

[23] Veit, M.; Kretzschmar, E.; Kuroda, K.; Garten, W.; Schmidt, M. F.; Klenk, H. D. and Rott, R. (1991): Site-specific mutagenesis identifies three cysteine residues in the cytoplasmic tail as acylation sites of influenza virus hemagglutinin, J Virol 65 [5], pp. 2491-500.

[24] Armstrong, R. T.; Kushnir, A. S. and White, J. M. (2000): The transmembrane domain of influenza hemagglutinin exhibits a stringent length requirement to support the hemifusion to fusion transition, J Cell Biol 151 [2], pp. 425-37.

[25] Kemble, G. W.; Danieli, T. and White, J. M. (1994): Lipid-anchored influenza hemagglutinin promotes hemifusion, not complete fusion, Cell 76 [2], pp. 383-91.

[26] Martens, S. and McMahon, H. T. (2008): Mechanisms of membrane fusion: disparate players and common principles, Nat Rev Mol Cell Biol 9 [7], pp. 543-56.

[27] Connor, R. J.; Kawaoka, Y.; Webster, R. G. and Paulson, J. C. (1994): Receptor specificity in human, avian, and equine H2 and H3 influenza virus isolates, Virology 205 [1], pp. 17-23.

[28] Wiley, D. C. and Skehel, J. J. (1987): The structure and function of the hemagglutinin membrane glycoprotein of influenza virus, Annu Rev Biochem 56, pp. 365-94.

[29] Huang, Q.; Opitz, R.; Knapp, E. W. and Herrmann, A. (2002): Protonation and stability of the globular domain of influenza virus hemagglutinin, Biophys J 82 [2], pp. 1050-8.

[30] Huang, Q.; Sivaramakrishna, R. P.; Ludwig, K.; Korte, T.; Bottcher, C. and Herrmann, A. (2003): Early steps of the conformational change of influenza virus hemagglutinin to a fusion active state: stability and energetics of the hemagglutinin, Biochim Biophys Acta 1614 [1], pp. 3-13.

[31] Carr, C. M. and Kim, P. S. (1993): A spring-loaded mechanism for the conformational change of influenza hemagglutinin, Cell 73 [4], pp. 823-32.

[32] Chang, D. K.; Cheng, S. F.; Kantchev, E. A.; Lin, C. H. and Liu, Y. T. (2008): Membrane interaction and structure of the transmembrane domain of influenza hemagglutinin and its fusion peptide complex, BMC Biol 6, p. 2.

[33] Hernandez, L. D.; Hoffman, L. R.; Wolfsberg, T. G. and White, J. M. (1996): Virus-cell and cell-cell fusion, Annu Rev Cell Dev Biol 12, pp. 627-61.

[34] Blumenthal, R.; Sarkar, D. P.; Durell, S.; Howard, D. E. and Morris, S. J. (1996): Dilation of the influenza hemagglutinin fusion pore revealed by the kinetics of individual cell-cell fusion events, J Cell Biol 135 [1], pp. 63-71.

[35] Harrison, Stephen C (2008): Viral Membrane Fusion, nature structural and molecular biology 15 [7], pp. 690-698.

[36] Elton, D.; Simpson-Holley, M.; Archer, K.; Medcalf, L.; Hallam, R.; McCauley, J. and Digard, P. (2001): Interaction of the influenza virus nucleoprotein with the cellular CRM1-mediated nuclear export pathway, J Virol 75 [1], pp. 408-19.

[37] Ma, K.; Roy, A. M. and Whittaker, G. R. (2001): Nuclear export of influenza virus ribonucleoproteins: identification of an export intermediate at the nuclear periphery, Virology 282 [2], pp. 215-20.

[38] Zhang, J.; Pekosz, A. and Lamb, R. A. (2000): Influenza virus assembly and lipid raft microdomains: a role for the cytoplasmic tails of the spike glycoproteins, J Virol 74 [10], pp. 4634-44.

[39] Barman, S.; Ali, A.; Hui, E. K.; Adhikary, L. and Nayak, D. P. (2001): Transport of viral proteins to the apical membranes and interaction of matrix protein with glycoproteins in the assembly of influenza viruses, Virus Res 77 [1], pp. 61-9.

[40] Scheiffele, P.; Rietveld, A.; Wilk, T. and Simons, K. (1999): Influenza viruses select ordered lipid domains during budding from the plasma membrane, J Biol Chem 274 [4], pp. 2038-44.

[41] Bancroft, C. T. and Parslow, T. G. (2002): Evidence for segment-nonspecific packaging of the influenza a virus genome, J Virol 76 [14], pp. 7133-9.

[42] Gomez-Puertas, P.; Albo, C.; Perez-Pastrana, E.; Vivo, A. and Portela, A. (2000): Influenza virus matrix protein is the major driving force in virus budding, J Virol 74 [24], pp. 11538-47.

[43] Nayak, D. P.; Hui, E. K. and Barman, S. (2004): Assembly and budding of influenza virus, Virus Res 106 [2], pp. 147-65.

[44] De Clercq, E. (2006): Antiviral agents active against influenza A viruses, Nat Rev Drug Discov 5 [12], pp. 1015-25.

[45] Metzner, C.; Salmons, B.; Gunzburg, W. H. and Dangerfield, J. A. (2008): Rafts, anchors and viruses--a role for glycosylphosphatidylinositol anchored proteins in the modification of enveloped viruses and viral vectors, Virology 382 [2], pp. 125-31.

[46] Dalley, J. A. and Bulleid, N. J. (2003): How does the translocon differentiate between hydrophobic sequences that form part of either a GPI (glycosylphosphatidylinositol)-anchor signal or a stop transfer sequence? Biochem Soc Trans 31 [Pt 6], pp. 1257-9.

[47] Muniz, M. and Riezman, H. (2000): Intracellular transport of GPI-anchored proteins, Embo J 19 [1], pp. 10-5.

[48] Ikezawa, H. (2002): Glycosylphosphatidylinositol (GPI)-anchored proteins, Biol Pharm Bull 25 [4], pp. 409-17.

[49] Orlean, P. and Menon, A. K. (2007): Thematic review series: lipid posttranslational modifications. GPI anchoring of protein in yeast and mammalian cells, or: how we learned to stop worrying and love glycophospholipids, J Lipid Res 48 [5], pp. 993-1011.

[50] Lisanti, M. P.; Caras, I. W.; Davitz, M. A. and Rodriguez-Boulan, E. (1989): A glycophospholipid membrane anchor acts as an apical targeting signal in polarized epithelial cells, J Cell Biol 109 [5], pp. 2145-56.

[51] Singer, S. J. and Nicolson, G. L. (1972): The fluid mosaic model of the structure of cell membranes, Science 175 [23], pp. 720-31.

[52] Zachowski, A. (1993): Phospholipids in animal eukaryotic membranes: transverse asymmetry and movement, Biochem J 294 (Pt 1), pp. 1-14.

[53] Pomorski, T.; Hrafnsdottir, S.; Devaux, P. F. and van Meer, G. (2001): Lipid distribution and transport across cellular membranes, Semin Cell Dev Biol 12 [2], pp. 139-48.

[54] Simons, K. and van Meer, G. (1988): Lipid sorting in epithelial cells, Biochemistry 27 [17], pp. 6197-202.

[55] Simons, K. and Ikonen, E. (1997): Functional rafts in cell membranes, Nature 387 [6633], pp. 569-72.

[56] Pike, L. J. (2006): Rafts defined: a report on the Keystone Symposium on Lipid Rafts and Cell Function, J Lipid Res 47 [7], pp. 1597-8.

[57] Morris, R.; Cox, H.; Mombelli, E. and Quinn, P. J. (2004): Rafts, little caves and large potholes: how lipid structure interacts with membrane proteins to create functionally diverse membrane environments, Subcell Biochem 37, pp. 35-118.

[58] Devaux, P. F. and Morris, R. (2004): Transmembrane asymmetry and lateral domains in biological membranes, Traffic 5 [4], pp. 241-6.

[59] Subczynski, W. K. and Kusumi, A. (2003): Dynamics of raft molecules in the cell and artificial membranes: approaches by pulse EPR spin labeling and single molecule optical microscopy, Biochim Biophys Acta 1610 [2], pp. 231-43.

[60] de Almeida, R. F.; Fedorov, A. and Prieto, M. (2003): Sphingomyelin/phosphatidylcholine/cholesterol phase diagram: boundaries and composition of lipid rafts, Biophys J 85 [4], pp. 2406-16.

[61] London, E. (2005): How principles of domain formation in model membranes may explain ambiguities concerning lipid raft formation in cells, Biochim Biophys Acta 1746 [3], pp. 203-20.

[62] Hancock, J. F. (2006): Lipid rafts: contentious only from simplistic standpoints, Nat Rev Mol Cell Biol 7 [6], pp. 456-62.

[63] Munro, S. (2003): Lipid rafts: elusive or illusive? Cell 115 [4], pp. 377-88.

[64] London, E. and Brown, D. A. (2000): Insolubility of lipids in triton X-100: physical origin and relationship to sphingolipid/cholesterol membrane domains (rafts), Biochim Biophys Acta 1508 [1-2], pp. 182-95.

[65] Lenne, P. F.; Wawrezinieck, L.; Conchonaud, F.; Wurtz, O.; Boned, A.; Guo, X. J.; Rigneault, H.; He, H. T. and Marguet, D. (2006): Dynamic molecular confinement in the plasma membrane by microdomains and the cytoskeleton meshwork, Embo J 25 [14], pp. 3245-56.

[66] Chichili, G. R. and Rodgers, W. (2007): Clustering of membrane raft proteins by the actin cytoskeleton, J Biol Chem 282 [50], pp. 36682-91.

[67] Sheets, E. D.; Holowka, D. and Baird, B. (1999): Membrane organization in immunoglobulin E receptor signaling, Curr Opin Chem Biol 3 [1], pp. 95-9.

[68] Danielsen, E. M. and van Deurs, B. (1995): A transferrin-like GPI-linked iron-binding protein in detergent-insoluble noncaveolar microdomains at the apical surface of fetal intestinal epithelial cells, J Cell Biol 131 [4], pp. 939-50.

[69] Simons, K. and Ehehalt, R. (2002): Cholesterol, lipid rafts, and disease, J Clin Invest 110 [5], pp. 597-603.

[70] Mukherjee, S. and Maxfield, F. R. (2004): Membrane domains, Annu Rev Cell Dev Biol 20, pp. 839-66.

[71] Skibbens, J. E.; Roth, M. G. and Matlin, K. S. (1989): Differential extractability of influenza virus hemagglutinin during intracellular transport in polarized epithelial cells and nonpolar fibroblasts, J Cell Biol 108 [3], pp. 821-32.

[72] Heerklotz, H. (2002): Triton promotes domain formation in lipid raft mixtures, Biophys J 83 [5], pp. 2693-701.

[73] Shogomori, H. and Brown, D. A. (2003): Use of detergents to study membrane rafts: the good, the bad, and the ugly, Biol Chem 384 [9], pp. 1259-63.

[74] Dietrich, C.; Yang, B.; Fujiwara, T.; Kusumi, A. and Jacobson, K. (2002): Relationship of lipid rafts to transient confinement zones detected by single particle tracking, Biophys J 82 [1 Pt 1], pp. 274-84.

[75] Wawrezinieck, L.; Rigneault, H.; Marguet, D. and Lenne, P. F. (2005): Fluorescence correlation spectroscopy diffusion laws to probe the submicron cell membrane organization, Biophys J 89 [6], pp. 4029-42.

[76] Varma, R. and Mayor, S. (1998): GPI-anchored proteins are organized in submicron domains at the cell surface, Nature 394 [6695], pp. 798-801.

[77] Mayor, S. and Riezman, H. (2004): Sorting GPI-anchored proteins, Nat Rev Mol Cell Biol 5 [2], pp. 110-20.

[78] Lackowicz (2006): Principles of Fluorescence Spectroscopy, Third Edition. ed., Springer Science+Business Media, New York.

[79] Chen, Y.; Mills, J. D. and Periasamy, A. (2003): Protein localization in living cells and tissues using FRET and FLIM, Differentiation 71 [9-10], pp. 528-41.

[80] de Almeida, R. F.; Loura, L. M. and Prieto, M. (2009): Membrane lipid domains and rafts: current applications of fluorescence lifetime spectroscopy and imaging, Chem Phys Lipids 157 [2], pp. 61-77.

[81] Vogel, S. S.; Thaler, C. and Koushik, S. V. (2006): Fanciful FRET, Sci STKE 2006 [331], p. re2.

[82] Rao, M. and Mayor, S. (2005): Use of Forster's resonance energy transfer microscopy to study lipid rafts, Biochim Biophys Acta 1746 [3], pp. 221-33.

[83] Wallrabe, H. and Periasamy, A. (2005): Imaging protein molecules using FRET and FLIM microscopy, Curr Opin Biotechnol 16 [1], pp. 19-27.

[84] Yasuda, R. (2006): Imaging spatiotemporal dynamics of neuronal signaling using fluorescence resonance energy transfer and fluorescence lifetime imaging microscopy, Curr Opin Neurobiol 16 [5], pp. 551-61.

[85] Gautier, I.; Tramier, M.; Durieux, C.; Coppey, J.; Pansu, R. B.; Nicolas, J. C.; Kemnitz, K. and Coppey-Moisan, M. (2001): Homo-FRET microscopy in living cells to measure monomer-dimer transition of GFP-tagged proteins, Biophys J 80 [6], pp. 3000-8.

[86] White, J.; Helenius, A. and Gething, M. J. (1982): Haemagglutinin of influenza virus expressed from a cloned gene promotes membrane fusion, Nature 300 [5893], pp. 658-9.

[87] Scheiffele, P.; Roth, M. G. and Simons, K. (1997): Interaction of influenza virus haemagglutinin with sphingolipid-cholesterol membrane domains via its transmembrane domain, Embo J 16 [18], pp. 5501-8.

[88] Takeda, M.; Leser, G. P.; Russell, C. J. and Lamb, R. A. (2003): Influenza virus hemagglutinin concentrates in lipid raft microdomains for efficient viral fusion, Proc Natl Acad Sci U S A 100 [25], pp. 14610-7.

[89] de Almeida, R. F.; Loura, L. M.; Fedorov, A. and Prieto, M. (2005): Lipid rafts have different sizes depending on membrane composition: a time-resolved fluorescence resonance energy transfer study, J Mol Biol 346 [4], pp. 1109-20.

[90] Hess, S. T.; Kumar, M.; Verma, A.; Farrington, J.; Kenworthy, A. and Zimmerberg, J. (2005): Quantitative electron microscopy and fluorescence spectroscopy of the membrane distribution of influenza hemagglutinin, J Cell Biol 169 [6], pp. 965-76.

[91] Hess, S. T.; Gould, T. J.; Gudheti, M. V.; Maas, S. A.; Mills, K. D. and Zimmerberg, J. (2007): Dynamic clustered distribution of hemagglutinin resolved at 40 nm in living cell membranes discriminates between raft theories, Proc Natl Acad Sci U S A 104 [44], pp. 17370-5.

[92] Silvius, J. R. (2005): Partitioning of membrane molecules between raft and non-raft domains: insights from model-membrane studies, Biochim Biophys Acta 1746 [3], pp. 193-202.

[93] Brown, D. A. and Rose, J. K. (1992): Sorting of GPI-anchored proteins to glycolipid-enriched membrane subdomains during transport to the apical cell surface, Cell 68 [3], pp. 533-44.

[94] Rizzo, M. A.; Springer, G. H.; Granada, B. and Piston, D. W. (2004): An improved cyan fluorescent protein variant useful for FRET, Nat Biotechnol 22 [4], pp. 445-9.

[95] Keller, P.; Toomre, D.; Diaz, E.; White, J. and Simons, K. (2001): Multicolour imaging of post-Golgi sorting and trafficking in live cells, Nat Cell Biol 3 [2], pp. 140-9.

[96] Zacharias, D. A.; Violin, J. D.; Newton, A. C. and Tsien, R. Y. (2002): Partitioning of lipid-modified monomeric GFPs into membrane microdomains of live cells, Science 296 [5569], pp. 913-6.

[97] Urban, A.; Neukirchen, S. and Jaeger, K. E. (1997): A rapid and efficient method for site-directed mutagenesis using one-step overlap extension PCR, Nucleic Acids Res 25 [11], pp. 2227-8.

[98] Veit, M.; Ponimaskin, E. and Schmidt, M. F. (2002): Analysis of S-acylation of proteins, Methods Mol Biol 194, pp. 159-78.

[99] Cooper, J. A. (1987): Effects of cytochalasin and phalloidin on actin, J Cell Biol 105 [4], pp. 1473-8.

[100] Landry, Y. D.; Denis, M.; Nandi, S.; Bell, S.; Vaughan, A. M. and Zha, X. (2006): ATP-binding cassette transporter A1 expression disrupts raft membrane microdomains through its ATPase-related functions, J Biol Chem 281 [47], pp. 36091-101.

[101] Baumgart, T.; Hammond, A. T.; Sengupta, P.; Hess, S. T.; Holowka, D. A.; Baird, B. A. and Webb, W. W. (2007): Large-scale fluid/fluid phase separation of proteins and lipids in giant plasma membrane vesicles, Proc Natl Acad Sci U S A 104 [9], pp. 3165-70.

[102] Sengupta, P.; Hammond, A.; Holowka, D. and Baird, B. (2008): Structural determinants for partitioning of lipids and proteins between coexisting fluid phases in giant plasma membrane vesicles, Biochim Biophys Acta 1778 [1], pp. 20-32.

[103] Kenworthy, A. K. and Edidin, M. (1998): Distribution of a glycosylphosphatidylinositol-anchored protein at the apical surface of MDCK cells examined at a resolution of <100 A using imaging fluorescence resonance energy transfer, J Cell Biol 142 [1], pp. 69-84.

[104] De Almeida, R. F.; Loura, L. M.; Prieto, M.; Watts, A.; Fedorov, A. and Barrantes, F. J. (2006): Structure and dynamics of the gammaM4 transmembrane domain of the acetylcholine receptor in lipid bilayers: insights into receptor assembly and function, Mol Membr Biol 23 [4], pp. 305-15.

[105] Tanaka, F., Mataga N. (1979): Theory of time dependent photoselection in interacting fixed systems, Photochemistry Photobiology 29 [6], pp. 1091-97.

[106] Sharma, P.; Varma, R.; Sarasij, R. C.; Ira; Gousset, K.; Krishnamoorthy, G.; Rao, M. and Mayor, S. (2004): Nanoscale organization of multiple GPI-anchored proteins in living cell membranes, Cell 116 [4], pp. 577-89.

[107] Patterson, G. H.; Piston, D. W. and Barisas, B. G. (2000): Forster distances between green fluorescent protein pairs, Anal Biochem 284 [2], pp. 438-40.

[108] Harrison, P. T.; Hutchinson, M. J. and Allen, J. M. (1994): A convenient method for the construction and expression of GPI-anchored proteins, Nucleic Acids Res 22 [18], pp. 3813-4.

[109] Legler, D. F.; Doucey, M. A.; Schneider, P.; Chapatte, L.; Bender, F. C. and Bron, C. (2005): Differential insertion of GPI-anchored GFPs into lipid rafts of live cells, Faseb J 19 [1], pp. 73-5.

[110] Kornfeld, R. and Kornfeld, S. (1985): Assembly of asparagine-linked oligosaccharides, Annu Rev Biochem 54, pp. 631-64.

[111] Tall, R. D.; Alonso, M. A. and Roth, M. G. (2003): Features of influenza HA required for apical sorting differ from those required for association with DRMs or MAL, Traffic 4 [12], pp. 838-49.

[112] Ceriotti, A. and Colman, A. (1990): Trimer formation determines the rate of influenza virus haemagglutinin transport in the early stages of secretion in Xenopus oocytes, J Cell Biol 111 [2], pp. 409-20.

[113] Jain, R. K.; Joyce, P. B.; Molinete, M.; Halban, P. A. and Gorr, S. U. (2001): Oligomerization of green fluorescent protein in the secretory pathway of endocrine cells, Biochem J 360 [Pt 3], pp. 645-9.

[114] Brown, D. A. and London, E. (2000): Structure and function of sphingolipid- and cholesterol-rich membrane rafts, J Biol Chem 275 [23], pp. 17221-4.

[115] Grailhe, R.; Merola, F.; Ridard, J.; Couvignou, S.; Le Poupon, C.; Changeux, J. P. and Laguitton-Pasquier, H. (2006): Monitoring protein interactions in the living cell through the fluorescence decays of the cyan fluorescent protein, Chemphyschem 7 [7], pp. 1442-54.

[116] Borst, J. W.; Hink, M. A.; van Hoek, A. and Visser, A. J. (2005): Effects of refractive index and viscosity on fluorescence and anisotropy decays of enhanced cyan and yellow fluorescent proteins, J Fluoresc 15 [2], pp. 153-60.

[117] Briggs, J. A.; Wilk, T. and Fuller, S. D. (2003): Do lipid rafts mediate virus assembly and pseudotyping? J Gen Virol 84 [Pt 4], pp. 757-68.

[118] Lu, Y. E. and Kielian, M. (2000): Semliki forest virus budding: assay, mechanisms, and cholesterol requirement, J Virol 74 [17], pp. 7708-19.

[119] Baumgart, T.; Hunt, G.; Farkas, E. R.; Webb, W. W. and Feigenson, G. W. (2007): Fluorescence probe partitioning between Lo/Ld phases in lipid membranes, Biochim Biophys Acta 1768 [9], pp. 2182-94.

[120] Lin, S.; Naim, H. Y.; Rodriguez, A. C. and Roth, M. G. (1998): Mutations in the middle of the transmembrane domain reverse the polarity of transport of the influenza virus hemagglutinin in MDCK epithelial cells, J Cell Biol 142 [1], pp. 51-7.

[121] Kenworthy, A. K.; Petranova, N. and Edidin, M. (2000): High-resolution FRET microscopy of cholera toxin B-subunit and GPI-anchored proteins in cell plasma membranes, Mol Biol Cell 11 [5], pp. 1645-55.

[122] Finidori, J.; Rizzolo, L.; Gonzalez, A.; Kreibich, G.; Adesnik, M. and Sabatini, D. D. (1987): The influenza hemagglutinin insertion signal is not cleaved and does not halt translocation when presented to the endoplasmic reticulum membrane as part of a translocating polypeptide, J Cell Biol 104 [6], pp. 1705-14.

[123] Tamm, L. K. (2003): Hypothesis: spring-loaded boomerang mechanism of influenza hemagglutinin-mediated membrane fusion, Biochim Biophys Acta 1614 [1], pp. 14-23.

[124] Tatulian, S. A. and Tamm, L. K. (2000): Secondary structure, orientation, oligomerization, and lipid interactions of the transmembrane domain of influenza hemagglutinin, Biochemistry 39 [3], pp. 496-507.

[125] Doms, R. W.; Lamb, R. A.; Rose, J. K. and Helenius, A. (1993): Folding and assembly of viral membrane proteins, Virology 193 [2], pp. 545-62.

[126] Hofman, E. G.; Ruonala, M. O.; Bader, A. N.; van den Heuvel, D.; Voortman, J.; Roovers, R. C.; Verkleij, A. J.; Gerritsen, H. C. and van Bergen En Henegouwen, P. M. (2008): EGF induces coalescence of different lipid rafts, J Cell Sci 121 [Pt 15], pp. 2519-28.

[127] Kusumi, A. and Sako, Y. (1996): Cell surface organization by the membrane skeleton, Curr Opin Cell Biol 8 [4], pp. 566-74.

[128] Shvartsman, D. E.; Kotler, M.; Tall, R. D.; Roth, M. G. and Henis, Y. I. (2003): Differently anchored influenza hemagglutinin mutants display distinct interaction dynamics with mutual rafts, J Cell Biol 163 [4], pp. 879-88.

[129] Singh, I.; Doms, R. W.; Wagner, K. R. and Helenius, A. (1990): Intracellular transport of soluble and membrane-bound glycoproteins: folding, assembly and secretion of anchor-free influenza hemagglutinin, Embo J 9 [3], pp. 631-9.

[130] Tatu, U.; Hammond, C. and Helenius, A. (1995): Folding and oligomerization of influenza hemagglutinin in the ER and the intermediate compartment, Embo J 14 [7], pp. 1340-8.

[131] Melkonian, K. A.; Ostermeyer, A. G.; Chen, J. Z.; Roth, M. G. and Brown, D. A. (1999): Role of lipid modifications in targeting proteins to detergent-resistant membrane rafts. Many raft proteins are acylated, while few are prenylated, J Biol Chem 274 [6], pp. 3910-7.

[132] Zhang, J.; Leser, G. P.; Pekosz, A. and Lamb, R. A. (2000): The cytoplasmic tails of the influenza virus spike glycoproteins are required for normal genome packaging, Virology 269 [2], pp. 325-34.

[133] Nichols, B. J.; Kenworthy, A. K.; Polishchuk, R. S.; Lodge, R.; Roberts, T. H.; Hirschberg, K.; Phair, R. D. and Lippincott-Schwartz, J. (2001): Rapid cycling of lipid raft markers between the cell surface and Golgi complex, J Cell Biol 153 [3], pp. 529-41.

[134] Nichols, B. J. and Lippincott-Schwartz, J. (2001): Endocytosis without clathrin coats, Trends Cell Biol 11 [10], pp. 406-12.

[135] Schroth-Diez, B.; Ludwig, K.; Baljinnyam, B.; Kozerski, C.; Huang, Q. and Herrmann, A. (2000): The role of the transmembrane and of the intraviral domain of glycoproteins in membrane fusion of enveloped viruses, Biosci Rep 20 [6], pp. 571-95.

[136] Polozov, I. V.; Bezrukov, L.; Gawrisch, K. and Zimmerberg, J. (2008): Progressive ordering with decreasing temperature of the phospholipids of influenza virus, Nat Chem Biol 4 [4], pp. 248-55.

[137] Enami, M. and Enami, K. (1996): Influenza virus hemagglutinin and neuraminidase glycoproteins stimulate the membrane association of the matrix protein, J Virol 70 [10], pp. 6653-7.

[138] Baudin, F.; Petit, I.; Weissenhorn, W. and Ruigrok, R. W. (2001): In vitro dissection of the membrane and RNP binding activities of influenza virus M1 protein, Virology 281 [1], pp. 102-8.

[139] Sun, X. and Whittaker, G. R. (2003): Role for influenza virus envelope cholesterol in virus entry and infection, J Virol 77 [23], pp. 12543-51.

[140] Barman, S. and Nayak, D. P. (2007): Lipid raft disruption by cholesterol depletion enhances influenza A virus budding from MDCK cells, J Virol 81 [22], pp. 12169-78.

Acknowledgement

My greatest thanks go to Prof. Dr. Andreas Herrmann, for introducing and driving me in this fascinating world, for always inciting me and supporting my decisions, for fighting against my stubborness and never let my motivation fall.

My sincere appreciation is for PD Dr. Veit, for welcoming me in his laboratory and for always giving me precious advices and fundamental teachings.

I am grateful to Prof. Dr. Manuel Prieto, for his hospitality, for sharing his vast knowdlege and for dividing his office with me. It was “my pleasure”.

My deepest gratitude is for Stephanie Engel, for accompanying me in this experience, for always pushing me and never letting me alone.

Thanks to Anna and Gabi for all the help and the smiles they gave me in these three years.

I want to thank Rodrigo and Bruno for making me feeling at home during my stay in Lisbon.

I am obliged to Dr. Martin Stöckl and Dr. Thomas Korte, for always rescuing me from “microscopic” and “informatic” problems.

I want to thank Nils and Julia for guiding me in the fantastic world of physics.

Particular thanks go to Susann who always accepted my chaos and to Roland who friendly shared his desk with my papers.

I am indebt with the “Veit laboratory”, in particular with Bastian Thaa for the long discussions, for the exchanged protocols and proteins and with Frau Poese for teaching me with her great experience.

At last I want to thank my mum and my dad for their love and for always being present in my life, even from so far away. Thanks to my brother Stefano and Tommaso, for all the support and faith they had in me. I am greatful to Francesca and Francesca for their absolute friendship. Finally, I want to thank Emilio for the calmness and the confidence he constantly gives me.

Publications

Talks

"Sorting of Influenza Virus proteins in membranes", Annual Meeting Marie Curie EST project *Biomem*, Utrecht, The Netherlands (18.06.06 - 21.06.06)

"Sorting of Influenza A Virus Hemagglutinin in membranes", Annual Meeting Marie Curie EST project *Biomem*, Berlin, Germany (13.09.07 - 15.09.07)

"Lateral sorting of Influenza Hemmaglutinin in membranes", 51st Annual Meeting of the US Biophysical Society, Long Beach, California (02.02.08 – 06.02.08)

"Lateral distribution of the transmembrane domain and cytoplasmic tail of Influenza Virus Hemagglutinin. A FLIM-FRET and energy migration study", Annual Meeting Marie Curie EST project *Biomem*, Madrid, Spain (01.10.08 – 05.10.08)

Posters

Scolari, S., Korte, T., Veit, M. and Herrmann, A. "Sorting of Influenza A Virus proteins in membranes". 58. Mosbacher Kolloquium "Protein and lipid sorting in health and disease", Mosbach, Germany (29.03.07 – 31.03.07)

Scolari, S., Engel, S., Krebs, N., De Almeida R. F., Prieto, M., Veit, M. and Herrmann, A. "Lateral sorting of Influenza Virus Hemagglutinin in membranes". German Biophysical Society Meeting, Berlin, Germany (28.09.08 – 01.10.08)

Manuscripts

Scolari, S., Engel, S., Krebs, N., Plazzo, A.P., De Almeida, R.F., Prieto, M., Veit, M., Herrmann, A (2009). Lateral distribution of the transmembrane domain of influenza virus hemagglutinin revealed by time-resolved fluorescence imaging. J Biol. Chem. in press

Engel, S., Scolari, S., Sieben, C., Thaa, B., Krebs, N., Korte, T., Herrmann, A., Veit, M. (2008). FLIM-FRET study on influenza virus hemagglutinin: Conversion to the post-fusion conformation reduces raft association. Submitted to Traffic

Patent

European Patent "Fluorescent labeled artificial Hemmaglutinin and Raft-markers for drug development" (2007)

Eidesstattliche Erklärung

Hiermit erkläre ich, die vorliegende Arbeit selbständig ohne fremde Hilfe verfasst und nur die angegebene Literatur verwendet zu haben.

Ich besitze keinen entsprechenden Doktorgrad und habe mich anderwärts nicht um einen solchen beworben.

Die dem Promotionsverfahren zugrunde liegende Promotionsordnung ist mir bekannt.

Silvia Scolari